

NIKHEF/96-027

ITP-SB-96-66

DESY 96-258

INLO-PUB-22/96

## Charm electroproduction viewed in the variable-flavour number scheme versus fixed-order perturbation theory

M. BUZA <sup>1</sup>

NIKHEF/UVA,  
POB 41882, NL-1009 DB Amsterdam,  
The Netherlands.

Y. MATIOUNINE

Institute for Theoretical Physics,  
State University of New York at Stony Brook,  
New York 11794-3840, USA.

J. SMITH <sup>2</sup>

Deutsches Elektronen-Synchrotron DESY  
Notkestrasse 85, D-22603, Hamburg  
Germany

W.L. VAN NEERVEN

Instituut-Lorentz,  
University of Leiden,  
PO Box 9506, 2300 RA Leiden,  
The Netherlands.

December 1996

### Abstract

Starting from fixed-order perturbation theory (FOPT) we derive expressions for the heavy-flavour components of the deep-inelastic structure functions ( $F_{i,H}(x, Q^2, m_H^2)$ ,  $i = 2, L$ ;  $H = c, b, t$ ) in the variable-flavour number scheme (VFNS). These expressions are valid in all orders of perturbation theory. This derivation establishes a relation between the parton densities

---

<sup>1</sup>supported by the Foundation for Fundamental Research on Matter (FOM)

<sup>2</sup>on leave from ITP, SUNY at Stony Brook, New York 11794-3840, USA

parametrized at  $n_f$  and  $n_f + 1$  light flavours. The consequences for the existing parametrizations of the parton densities are discussed. Further we show that in charm electroproduction the exact and asymptotic expressions for the heavy-quark coefficient functions yield identical results for  $F_{2,c}(x, Q^2, m_c^2)$  when  $Q^2 \geq 20$  (GeV/c)<sup>2</sup>. We also study the differences between the FOPT and the VFNS descriptions for  $F_{2,c}(x, Q^2, m_c^2)$ . It turns out that the charm structure function in the VFNS is larger than the one obtained in FOPT over the whole  $Q^2$ -range. Furthermore inspection of the perturbation series reveals that the higher order corrections in the VFNS are smaller than those present in FOPT for  $Q^2 \geq 10$  (GeV/c)<sup>2</sup>. Therefore the VFNS gives a better prediction for the charm structure function at large  $Q^2$ -values than FOPT.

# 1 Introduction

The study of charm production in deep-inelastic electron-proton scattering and in photon-proton scattering provides us with important information about heavy-quark-production mechanisms. In particular, we can distinguish between intrinsic- and extrinsic-charm production. In the latter case the charm quark only appears in the final state so the dominant subprocess is given by (virtual) photon-gluon fusion, which is the only reaction present on the Born level [1]. Hence one can measure the  $x$ -dependence of the gluon density  $G(x, \mu^2)$ , where  $x$  denotes the Bjorken scaling variable and  $\mu$  stands for the factorization and renormalization scales. Next-to-leading (NLO) corrections [2], [3], to which also other processes contribute, reveal that this picture remains unaltered.

Besides extrinsic-charm production one can also consider intrinsic-charm production [4], which is given by the flavour-excitation process. In this case the charm quark also appears in the initial state and it is considered to be a part of the hadronic wave function. Hence this quark is described by a parton density in the hadron, as in the cases of the other light flavours (u,d,s) and the gluon (g). Notice that in the context of perturbative QCD the flavour-excitation mechanism is always accompanied by the photon-gluon fusion process. However the latter can occur without the presence of intrinsic-charm production because one can always assume that the probability to find a charm quark inside the proton is equal to zero without violating the principles of perturbative QCD. The difference between both production mechanisms becomes very clear when one looks at differential distributions. In the case of extrinsic-charm production the photon-gluon-fusion subprocess predicts that both the charm quark and the charm anti-quark appear back-to-back in the final state. For intrinsic-charm production, where the flavour-excitation mechanism dominates, it turns out that either the charm quark or the charm anti-quark appears in the final state. Hence the transverse momentum of this heavy quark is not balanced by that of its antiparticle, in contrast to the situation in the photon-gluon fusion process. Recent experiments carried out at HERA at  $Q^2 = 0$  [5] (photoproduction) or at  $10 < Q^2 < 100$  (GeV/c)<sup>2</sup> [6] (electroproduction), where  $Q^2$  denotes the virtual photon mass squared, give strong evidence for extrinsic-charm production. Therefore we only concentrate on the latter production mechanism in this paper.

As has been mentioned above the extrinsic-charm mechanism can be stud-

ied in photoproduction ( $Q^2 = 0$ ) and in electroproduction ( $Q^2 > 0$ ). The photoproduction reaction has the advantage that the production rate is much larger than in the case of electroproduction because the latter rate is suppressed by the photon propagator, which decreases when  $Q^2$  gets larger. In the context of perturbative QCD, however, the description of electroproduction is easier due to the absence of the hadronic (resolved) photon component which contributes in photoproduction (for a discussion see [7]). Moreover electroproduction enables us to study the charm contribution to the deep-inelastic structure functions  $F_2(x, Q^2)$  and  $F_L(x, Q^2)$ .

For the treatment of the charm component of the structure functions  $F_{k,c}(x, Q^2, m_c^2)$  ( $k = 2, L$ ) one has adopted two different prescriptions for extrinsic-charm production in the literature. The first one is advocated in [8] where the charm quark is treated as a heavy quark and its contribution is given by fixed-order perturbation theory (FOPT). This involves the computation of the photon-gluon-fusion process mentioned above and its higher order corrections. The second approach is the so-called variable-flavour number scheme (VFNS) [9]. Here charm is treated in a similar way to a massless quark and its contribution is described by a parton density in the hadron, denoted by  $f_c^{\text{VFNS}}(x, \mu^2)$ . At first sight this looks similar to intrinsic-charm production. However there is one important difference. This becomes clear when one looks at eq.(10) of [9] where there exists a relation between  $f_c^{\text{VFNS}}$  and the gluon density originally appearing in the photon-gluon process. In this way there is an intimate relation between FOPT and the VFNS which imposes some conditions on the charm-quark density. These conditions do not exist in the intrinsic-charm approach, where this density is just an arbitrary function fitted to experimental data. It is clear that the VFNS-procedure is not very well suited to describe charm production in the threshold region because the photon-gluon fusion process requires that the charm component of the structure function vanishes above  $x = Q^2/(Q^2 + 4 m_c^2)$ , while this threshold condition gets lost in the  $x$ -behaviour of  $f_c^{\text{VFNS}}(x, \mu^2)$ . On the other hand FOPT also has its drawbacks when  $Q^2$  gets very large. The reason is that the heavy-quark coefficient functions calculated up to NLO in [3] are dominated by large logarithms of the type  $\ln^i(Q^2/m_c^2) \ln^j(\mu^2/m_c^2)$  when  $Q^2 \gg m_c^2$  [10]. Although it was shown in NLO [11] that these logarithms lead to rather stable charm structure functions  $F_{i,c}(x, Q^2, m_c^2)$  with respect to variations in the factorization and renormalization scales  $\mu$ , their size still warrants some special treatment (for a discussion of the scale dependence of the charm con-

tribution in the FOPT and VFNS approaches see also [12],[13],[14]). However as we will show in this paper the above criterion is not sufficient to decide about the rate of convergence of the perturbation series. It still may happen that these large logarithms vitiate the perturbation series, in particular when corrections beyond NLO are included. Hence these logarithms have to be resummed using the standard techniques of the renormalization group.

This resummation proceeds as follows. First one has to add the light-parton component of the structure functions  $F_k(x, Q^2)$ ,  $k = 2, L$  to the charm contributions  $F_{k,c}(x, Q^2, m_c^2)$  both presented with three light flavours. The light component consists of the light-parton (u,d,s,g) densities convoluted with the light-parton coefficient functions. The same densities are used for the charm component where they are convoluted with the heavy-quark coefficient functions. Then one takes the limit  $Q^2 \rightarrow \infty$  and performs mass factorization in order to remove the above mass singular logarithms in  $m_c$  from the asymptotic heavy-quark coefficient functions. The latter can be written as a convolution of the heavy-quark operator-matrix elements (OME's), containing these mass-singular logarithms, and the light-parton coefficient functions which are finite in the limit  $m_c \rightarrow 0$ . The light-parton densities are then modified by multiplying the original u,d,s and g densities by the heavy-quark OME's, where one has to introduce a new parton density to represent the charm quark. Notice that the latter is not an arbitrary function since, via the heavy-quark OME's, it depends on the original densities represented by the three light flavours (u,d,s) and the gluon (g) in the three-flavour scheme. The whole procedure leads to the structure functions  $F_i$  and  $F_{i,c}$  which are now represented in the four-flavour scheme. The latter are expressed into four light-flavour densities (including charm) and the gluon density convoluted with the light-parton coefficient functions. Further the heavy-quark coefficient functions due to the charm have completely disappeared. Although these formulae are similar to those obtained for intrinsic-charm production their origin is completely different. Here we want to emphasize again that the VFNS is derived from FOPT, where, in the large- $Q^2$  limit, one has resummed the large logarithmic terms in the heavy-quark coefficient functions in all orders of perturbation theory. This procedure, which is only described up to leading order (LO) in [9], will be generalized to all orders in QCD perturbation theory in Section 2.

In Section 3 we will study at which  $Q^2$  the large logarithms in the heavy-quark coefficient functions actually dominate the charm component of the

structure functions. We will investigate the  $x$ - and  $\mu^2$ -dependence of the charm density in the VFNS approach and compare it with the existing charm densities in the literature. We will also study the differences between the FOPT approach and the VFNS approach for the charm component of the deep-inelastic structure functions in the  $x$ - and  $Q^2$ -range explored by present experiments. Further we investigate which approach is more stable with respect to higher order corrections to the charm structure functions. In Appendix A we present some heavy-quark OME's which were not previously calculated in the literature. In Appendix B we list all renormalized heavy-quark OME's which are needed for our analysis in Section 3.

## 2 Derivation of the VFNS representation of the structure functions

In this section we present the variable-flavour number scheme (VFNS) representation of the structure functions  $F_k(x, Q^2)$  in all orders of perturbation theory. Our results hold for any species of heavy quark although at present collider energies the VFNS is only interesting for the charm quark. As mentioned in the previous section logarithms of the type  $\ln^i(Q^2/m^2) \ln^j(\mu^2/m^2)$  arise in the heavy-quark coefficient functions when  $Q^2 \gg m^2$  and we work in fixed-order perturbation theory (FOPT). Here  $m$  stands for the mass of the heavy quark, denoted by H in the subsequent part of this section. When going from the FOPT representation for the structure functions to that of the VFNS one has to remove these mass-singular logarithms from the heavy-quark coefficient functions. This is achieved using the technique of mass factorization, which is a generalization to all orders in perturbation theory of the procedure carried out up to lowest order (LO) in Sections II D and II E in [9]. Although this procedure resembles the usual mass factorization of the collinear singularities, which appear in the partonic structure functions or partonic cross sections, it is actually much more complicated. This is due to the presence of the light (u,d,s and g) partons, as well as of the heavy (c,b and t) quarks, in the Feynman diagrams describing heavy-flavour production.

In the calculations of the heavy-flavour cross sections the light partons are usually taken to be massless, whereas the heavy quarks get a mass  $m \neq 0$ . Note that the mass is defined by on-mass-shell renormalization. When  $Q^2 \gg m^2$  two types of collinear singularities appear in the partonic contributions. One type can be attributed to the light partons. In this case the collinear divergences can be regularized using various techniques. The most well-known among them is  $n$ -dimensional regularization. The second type can be traced back to the heavy quark and the singularity manifests itself as  $m \rightarrow 0$  in the large logarithmic terms mentioned above. Beyond order  $\alpha_s$  both types of singularities appear in the partonic cross sections and in the heavy-quark operator matrix elements (OME's). The latter show up in the mass-factorization formulae, and they are needed to remove the mass-singular terms (as  $m \rightarrow 0$ ) from the heavy-quark coefficient functions. Hence the mass factorization becomes much more complicated than when we only have to deal with collinear divergences due to massless partons. Therefore we first

present the mass factorization with respect to the latter before we apply this technique to the mass singularities related to the heavy-quark mass  $m$ .

Consider first deep-inelastic electron-proton scattering in which only light-partons show up in the calculation of the QCD corrections. The deep-inelastic structure function  $F_i(n_f, Q^2)$  can be expressed as follows

$$F_i(n_f, Q^2) = \frac{1}{n_f} \sum_{k=1}^{n_f} e_k^2 \left[ \hat{\Sigma}(n_f) \otimes \hat{\mathcal{F}}_{i,q}^S(n_f, \frac{Q^2}{p^2}, \mu^2) + \hat{G}(n_f) \otimes \hat{\mathcal{F}}_{i,g}^S(n_f, \frac{Q^2}{p^2}, \mu^2) + n_f \hat{\Delta}_k(n_f) \otimes \hat{\mathcal{F}}_{i,q}^{NS}(n_f, \frac{Q^2}{p^2}, \mu^2) \right]. \quad (2.1)$$

In this equation the charge of the light quark is represented by  $e_k$  and  $n_f$  denotes the number of light flavours. Further  $\otimes$  denotes the convolution symbol and, for convenience, the dependence of all the above quantities on the hadronic scaling variable  $x$  and the partonic scaling variable  $z$  is suppressed. The bare quantities in (2.1) are indicated by a hat in order to distinguish them from their finite analogues, which emerge after mass factorization. Starting with the parton densities,  $\hat{\Sigma}(n_f)$  and  $\hat{G}(n_f)$  denote the singlet combination of light-quark densities and the gluon density respectively, with  $n_f$  light flavours. The former is given by

$$\hat{\Sigma}(n_f) = \sum_{l=1}^{n_f} [\hat{f}_l(n_f) + \hat{f}_{\bar{l}}(n_f)], \quad (2.2)$$

where  $\hat{f}_l(n_f)$  and  $\hat{f}_{\bar{l}}(n_f)$  stand for the light-quark and light-anti-quark densities respectively. The non-singlet combination of light-quark densities is given by

$$\hat{\Delta}_k(n_f) = \hat{f}_k(n_f) + \hat{f}_{\bar{k}}(n_f) - \frac{1}{n_f} \hat{\Sigma}(n_f). \quad (2.3)$$

The QCD radiative corrections due to the (virtual) photon light-parton subprocesses are described by the partonic structure functions  $\hat{\mathcal{F}}_{i,l}(n_f)$  ( $i = 2, L; l = q, g$ ) where  $l$  stands for the parton which appears in the initial state. As with the parton densities they can also be classified into singlet, non-singlet and gluonic parts. Furthermore we assume that coupling-constant renormalization has been performed on the partonic (bare) structure functions, which is indicated by their dependence on the renormalization scale  $\mu$ . However they still contain collinear divergences which, for convenience,



are regularized by taking the external momentum  $p$  of the incoming parton off-mass-shell ( $p^2 < 0$ ). Notice that these divergences do not show up in the final state because the deep-inelastic structure functions are totally-inclusive quantities.

The reason we choose off-shell regularization is that it allows us to distinguish between the collinear divergences coming from the massless partons and from the heavy quarks. The former divergences are the  $\ln^i(-\mu^2/p^2)$  terms in the perturbative expansion, whereas the latter are the  $\ln^i(\mu^2/m^2)$  terms.

We can now also reexpress Eq. (2.1) in finite quantities so that the collinear divergences are absent. This is achieved via mass factorization which proceeds as follows

$$\hat{\mathcal{F}}_{i,q}^{\text{NS}}\left(n_f, \frac{Q^2}{p^2}, \mu^2\right) = A_{qq}^{\text{NS}}\left(n_f, \frac{\mu^2}{p^2}\right) \otimes \mathcal{C}_{i,q}^{\text{NS}}\left(n_f, \frac{Q^2}{\mu^2}\right), \quad (2.4)$$

and

$$\hat{\mathcal{F}}_{i,k}^{\text{S}}\left(n_f, \frac{Q^2}{p^2}, \mu^2\right) = \sum_{l=q,g} A_{lk}^{\text{S}}\left(n_f, \frac{\mu^2}{p^2}\right) \otimes \mathcal{C}_{i,l}^{\text{S}}\left(n_f, \frac{Q^2}{\mu^2}\right). \quad (2.5)$$

In the above expressions  $\mathcal{C}_{i,k}$  ( $i = 2, L; k = q, g$ ) denote the light-parton coefficient functions and the  $A_{lk}$  represent the renormalized operator-matrix elements (OME's) which are defined by

$$A_{lk}\left(n_f, \frac{\mu^2}{p^2}\right) = \langle k(p) | O_l(0) | k(p) \rangle, \quad (l, k = q, g). \quad (2.6)$$

Here  $O_l$  are the renormalized operators which appear in the operator-product expansion of two electromagnetic currents near the light cone. The product of these two currents is sandwiched between proton states and its Fourier transform into momentum space defines the structure functions in (2.1). Like the other quantities  $\mathcal{C}_{i,k}$  and  $A_{lk}$  can be divided into singlet and non-singlet parts. The scale  $\mu$  appearing in Eqs. (2.4)-(2.6) originates from operator renormalization as well as from coupling-constant renormalization. Notice that the operator-renormalization scale is identical to the mass-factorization scale. Using the mass-factorization relations in Eqs. (2.4),(2.5) we can cast the hadronic structure functions  $F_i(n_f, Q^2)$  (2.1) into the form

$$F_i(n_f, Q^2) = \frac{1}{n_f} \sum_{k=1}^{n_f} e_k^2 \left[ \Sigma(n_f, \mu^2) \otimes \mathcal{C}_{i,q}^{\text{S}}\left(n_f, \frac{Q^2}{\mu^2}\right) + G(n_f, \mu^2) \otimes \mathcal{C}_{i,g}^{\text{S}}\left(n_f, \frac{Q^2}{\mu^2}\right) \right]$$

$$+n_f \Delta_k(n_f, \mu^2) \otimes \mathcal{C}_{i,q}^{\text{NS}}\left(n_f, \frac{Q^2}{\mu^2}\right) \Big], \quad (2.7)$$

where the finite (renormalized) parton densities  $\Sigma$ ,  $\Delta$  and  $G$  are expressed in the bare ones  $\hat{\Sigma}$ ,  $\hat{\Delta}$  and  $\hat{G}$  in the following way

$$\Delta_k(n_f, \mu^2) = A_{qq}^{\text{NS}}\left(n_f, \frac{\mu^2}{p^2}\right) \otimes \hat{\Delta}_k(n_f), \quad (2.8)$$

$$\Sigma(n_f, \mu^2) = A_{qq}^{\text{S}}\left(n_f, \frac{\mu^2}{p^2}\right) \otimes \hat{\Sigma}(n_f) + A_{gg}^{\text{S}}\left(n_f, \frac{\mu^2}{p^2}\right) \otimes \hat{G}(n_f), \quad (2.9)$$

and

$$G(n_f, \mu^2) = A_{qq}^{\text{S}}\left(n_f, \frac{\mu^2}{p^2}\right) \otimes \hat{\Sigma}(n_f) + A_{gg}^{\text{S}}\left(n_f, \frac{\mu^2}{p^2}\right) \otimes \hat{G}(n_f). \quad (2.10)$$

All quantities given above satisfy renormalization group equations (RGE's). Here we are only interested in those RGE's for the OME's and the parton densities. Define the differential operator  $D$  as

$$D = \mu \frac{\partial}{\partial \mu} + \beta(n_f, g) \frac{\partial}{\partial g}, \quad g \equiv g(n_f, \mu^2), \quad (2.11)$$

where  $\alpha_s = g^2/(4\pi)$ , then the OME's satisfy the following RGE's

$$DA_{qq}^{\text{NS}}\left(n_f, \frac{\mu^2}{p^2}\right) = -\gamma_{qq}^{\text{NS}}(n_f) \otimes A_{qq}^{\text{NS}}\left(n_f, \frac{\mu^2}{p^2}\right), \quad (2.12)$$

$$DA_{ij}^{\text{S}}\left(n_f, \frac{\mu^2}{p^2}\right) = -\sum_{k=q,g} \gamma_{ik}^{\text{S}}(n_f) \otimes A_{kj}^{\text{S}}\left(n_f, \frac{\mu^2}{p^2}\right). \quad (2.13)$$

Here  $\gamma_{ij}$  denote the anomalous dimensions corresponding to the operators  $O_i$ . They can be expanded as a perturbation series in  $\alpha_s$ . In Bjorken  $x$ -space there exists a relation between the anomalous dimensions  $\gamma_{ij}$  and the DGLAP splitting functions, denoted by  $P_{ij}$ , which is given by

$$\gamma_{ij}(n_f) = -P_{ij}(n_f). \quad (2.14)$$

Notice that this relation only holds for twist-two operators. From the above equation one infers that the  $\gamma_{ij}$ , which are the residues of the ultraviolet

divergences in the unrenormalized OME's, have just the opposite signs to those of the  $P_{ij}$ . The latter show up in the partonic quantities  $\hat{\mathcal{F}}_{i,l}(n_f)$  in (2.1) and they represent the residues of the collinear divergences. We will return to this relation (2.14) when we discuss the heavy-quark OME's. The finite (renormalized) parton densities satisfy the RGE's

$$D\Delta_k(n_f, \mu^2) = -\gamma_{qq}^{\text{NS}}(n_f) \otimes \Delta_k(n_f, \mu^2), \quad (2.15)$$

$$D\Sigma(n_f, \mu^2) = -\gamma_{qq}^{\text{S}}(n_f) \otimes \Sigma(n_f, \mu^2) - \gamma_{gq}^{\text{S}}(n_f) \otimes G(n_f, \mu^2), \quad (2.16)$$

and

$$DG(n_f, \mu^2) = -\gamma_{gq}^{\text{S}}(n_f) \otimes \Sigma(n_f, \mu^2) - \gamma_{gg}^{\text{S}}(n_f) \otimes G(n_f, \mu^2). \quad (2.17)$$

From these equations we can derive the Altarelli-Parisi equations.

Before we add the heavy-quark contributions to the deep-inelastic structure functions (2.7) it is convenient to split the singlet quantities  $\hat{\mathcal{F}}_{i,q}^{\text{S}}$ ,  $\mathcal{C}_{i,q}^{\text{S}}$  and  $A_{qq}^{\text{S}}$  into non-singlet and purely-singlet parts, namely

$$\hat{\mathcal{F}}_{i,q}^{\text{S}} = \hat{\mathcal{F}}_{i,q}^{\text{NS}} + \hat{\mathcal{F}}_{i,q}^{\text{PS}}, \quad (2.18)$$

$$\mathcal{C}_{i,q}^{\text{S}} = \mathcal{C}_{i,q}^{\text{NS}} + \mathcal{C}_{i,q}^{\text{PS}}, \quad (2.19)$$

and

$$A_{qq}^{\text{S}} = A_{qq}^{\text{NS}} + A_{qq}^{\text{PS}}. \quad (2.20)$$

This decomposition facilitates the mass factorization of the heavy-quark coefficient functions and can be explained as follows. If we calculate the diagrams contributing to the parton subprocesses with a quark in the initial state, the resulting expressions have to be projected on the singlet and non-singlet channels with respect to the flavour group. The latter projection leads to  $\hat{\mathcal{F}}_{i,q}^{\text{NS}}$ . However the singlet part i.e.  $\hat{\mathcal{F}}_{i,q}^{\text{S}}$  can be split into two types of contributions. The first one is equal to  $\hat{\mathcal{F}}_{i,q}^{\text{NS}}$  whereas the second one is represented by  $\hat{\mathcal{F}}_{i,q}^{\text{PS}}$ . The purely-singlet partonic structure function arises from the Feynman graphs where the projection on the non-singlet channel yields zero, so that only singlet contributions remain. They are characterized by those Feynman graphs in which only gluons are exchanged in the  $t$ -channel. Such graphs show up for the first time in two-loop order. An example is given in Fig. 1. The same characteristics also hold for  $A_{qq}^{\text{PS}}$  (see Fig. 2) and the resulting

coefficient function  $\mathcal{C}_{i,q}^{\text{PS}}$ . Another important feature is that the purely-singlet quantities are proportional to the number of light flavours  $n_f$ . This property is shared by the gluonic quantities  $\hat{\mathcal{F}}_{i,g}^{\text{S}}$ ,  $\mathcal{C}_{i,g}^{\text{S}}$  and  $A_{qq}^{\text{S}}$ . The proportionality to  $n_f$  can be traced back to the fact that in the case of  $\hat{\mathcal{F}}_{i,q}^{\text{PS}}$ ,  $\hat{\mathcal{F}}_{i,g}^{\text{S}}$  the virtual photon is attached to the light-quark loop (see e.g. Fig. 1) and one has to sum over all light flavours. In the case of  $A_{qq}^{\text{PS}}$  and  $A_{qq}^{\text{S}}$  this is due to the insertion of the operator vertex into the light-quark loop where also a sum over all light flavours has to be carried out. Because of the mass-factorization relation (2.5) the proportionality to  $n_f$  is transferred to the coefficient functions  $\mathcal{C}_{i,q}^{\text{PS}}$ ,  $\mathcal{C}_{i,g}^{\text{S}}$  and the anomalous dimensions  $\gamma_{qq}^{\text{PS}}$ ,  $\gamma_{qq}^{\text{S}}$ . To facilitate the mass factorization of the heavy-quark coefficient functions it is very convenient to extract this overall factor of  $n_f$  from the quantities above so we define

$$T_{i,k} = n_f \tilde{T}_{i,k}, \quad (2.21)$$

where

$$T_{i,q} = \hat{\mathcal{F}}_{i,q}^{\text{PS}}, \mathcal{C}_{i,q}^{\text{PS}}; \quad T_{i,g} = \hat{\mathcal{F}}_{i,g}^{\text{S}}, \mathcal{C}_{i,g}^{\text{S}}; \quad (2.22)$$

and

$$R_{ij} = n_f \tilde{R}_{ij}, \quad (2.23)$$

where

$$R_{qq} = A_{qq}^{\text{PS}}, \gamma_{qq}^{\text{PS}}; \quad R_{qg} = A_{qg}^{\text{S}}, \gamma_{qg}^{\text{S}}. \quad (2.24)$$

Besides the overall dependence on  $n_f$ , which we have extracted from the quantities defined by  $T_{i,k}$  and  $R_{ij}$  above, there still remains a residual dependence on  $n_f$  in  $\tilde{T}_{i,k}$  and  $\tilde{R}_{ij}$ . The latter dependence originates from internal light-flavour loops which are neither attached to the virtual photon nor to the operator-vertex insertions. Since there are more contributions to  $\tilde{T}_{i,k}$  and  $\tilde{R}_{ij}$  which are not due to these light flavour-loops it is impossible to extract an overall factor  $n_f$  anymore from the quantities indicated by a tilde. Therefore the dependence of the latter on  $n_f$  means that it can be only attributed to internal light-flavour loops. Using the above definitions one can now rewrite Eqs. (2.1) and (2.7) and the results become

$$F_i(n_f, Q^2) = \sum_{k=1}^{n_f} e_k^2 \left[ \hat{\Sigma}(n_f) \otimes \tilde{\mathcal{F}}_{i,q}^{\text{PS}}\left(n_f, \frac{Q^2}{p^2}, \mu^2\right) + \hat{G}(n_f) \otimes \tilde{\mathcal{F}}_{i,g}^{\text{S}}\left(n_f, \frac{Q^2}{p^2}, \mu^2\right) + \left\{ \hat{f}_k(n_f) + \hat{f}_{\bar{k}}(n_f) \right\} \otimes \hat{\mathcal{F}}_{i,q}^{\text{NS}}\left(n_f, \frac{Q^2}{p^2}, \mu^2\right) \right], \quad (2.25)$$

$$\begin{aligned}
F_i(n_f, Q^2) = & \sum_{k=1}^{n_f} e_k^2 \left[ \Sigma(n_f, \mu^2) \otimes \tilde{\mathcal{C}}_{i,q}^{\text{PS}}\left(n_f, \frac{Q^2}{\mu^2}\right) + G(n_f, \mu^2) \otimes \tilde{\mathcal{C}}_{i,g}^{\text{S}}\left(n_f, \frac{Q^2}{\mu^2}\right) \right. \\
& \left. + \{f_k(n_f, \mu^2) + f_{\bar{k}}(n_f, \mu^2)\} \otimes \mathcal{C}_{i,q}^{\text{NS}}\left(n_f, \frac{Q^2}{\mu^2}\right) \right], \quad (2.26)
\end{aligned}$$

with the relation

$$\begin{aligned}
f_k(n_f, \mu^2) + f_{\bar{k}}(n_f, \mu^2) = & A_{qq}^{\text{NS}}\left(n_f, \frac{\mu^2}{p^2}\right) \otimes \{f_k(n_f) + f_{\bar{k}}(n_f)\} \\
& + \tilde{A}_{qq}^{\text{PS}}\left(n_f, \frac{\mu^2}{p^2}\right) \otimes \hat{\Sigma}(n_f) + \tilde{A}_{qg}^{\text{S}}\left(n_f, \frac{\mu^2}{p^2}\right) \otimes \hat{G}(n_f). \quad (2.27)
\end{aligned}$$

Using Eqs. (2.5),(2.9) and (2.10) one can now write the mass factorization relations for the quantities indicated by  $\tilde{T}_{i,k}$  and  $\tilde{R}_{ij}$  in (2.21)-(2.24). The same can be done for the RGE's which can be derived from (2.13),(2.16) and (2.17). Since this derivation is easy it is left to the reader. Here we only want to report the RGE for the left-hand-side of (2.27) which follows from (2.15) and (2.16). It is given by

$$\begin{aligned}
D[f_k(n_f, \mu^2) + f_{\bar{k}}(n_f, \mu^2)] = & -\gamma_{qq}^{\text{NS}}(n_f) \otimes [f_k(n_f, \mu^2) + f_{\bar{k}}(n_f, \mu^2)] \\
& -\tilde{\gamma}_{qq}^{\text{PS}}(n_f) \otimes \Sigma(n_f, \mu^2) - \tilde{\gamma}_{qg}^{\text{S}}(n_f) \otimes G(n_f, \mu^2). \quad (2.28)
\end{aligned}$$

After having presented the formulae needed for the mass factorization of the light-parton structure functions  $\hat{\mathcal{F}}_{i,l}$  with the corresponding RGE's we want to deal in a similar way with the asymptotic heavy-quark coefficient functions where the large logarithmic terms depending on the heavy-quark mass  $m$  have to be removed. For that purpose we have to add the heavy-quark contribution to the deep-inelastic structure function  $F_i(n_f, Q^2)$  (2.26) which is equal to

$$\begin{aligned}
F_{i,H}(n_f, Q^2, m^2) = & \\
& \sum_{k=1}^{n_f} e_k^2 \left[ \Sigma(n_f, \mu^2) \otimes \tilde{L}_{i,q}^{\text{PS}}\left(n_f, \frac{Q^2}{m^2}, \frac{m^2}{\mu^2}\right) + G(n_f, \mu^2) \otimes \tilde{L}_{i,g}^{\text{S}}\left(n_f, \frac{Q^2}{m^2}, \frac{m^2}{\mu^2}\right) \right. \\
& \left. + \{f_k(n_f, \mu^2) + f_{\bar{k}}(n_f, \mu^2)\} \otimes L_{i,q}^{\text{NS}}\left(n_f, \frac{Q^2}{m^2}, \frac{m^2}{\mu^2}\right) \right]
\end{aligned}$$

$$+e_H^2 \left[ \Sigma(n_f, \mu^2) \otimes H_{i,q}^{\text{PS}}\left(n_f, \frac{Q^2}{m^2}, \frac{m^2}{\mu^2}\right) + G(n_f, \mu^2) \otimes H_{i,g}^{\text{S}}\left(n_f, \frac{Q^2}{m^2}, \frac{m^2}{\mu^2}\right) \right], \quad (2.29)$$

where  $e_H$  stands for the charge of the heavy quark denoted by H. Further  $L_{i,k}$  and  $H_{i,k}$  ( $i = 2, L; k = q, g$ ) represent the heavy-quark coefficient functions. Like in the case of the light-parton coefficient functions  $\mathcal{C}_{i,k}$  they can be split into singlet and non-singlet parts. The former can be decomposed into non-singlet and purely-singlet pieces in a similar way as given in (2.19). The distinction between  $L_{i,k}$  and  $H_{i,k}$  can be traced back to the different (virtual) photon-parton heavy-quark production mechanisms from which they originate. The functions  $L_{i,k}$  are attributed to the reactions where the virtual photon couples to the light quarks (u, d, and s), whereas the  $H_{i,k}$  describe the interactions between the virtual photon and the heavy quark. Hence  $L_{i,k}$  and  $H_{i,k}$  in (2.29) are multiplied by  $e_k^2$  and  $e_H^2$  respectively. Moreover, when the reaction where the photon couples to the heavy quark contains a light quark in the initial state, then it can only proceed via the exchange of a gluon in the  $t$ -channel (see Fig. 1). Therefore  $H_{i,q}$  is purely-singlet and a non-singlet contribution does not exist. This is in contrast with  $L_{i,q}$  which has both purely-singlet and non-singlet contributions.

For  $Q^2 \gg m^2$  the heavy-quark coefficient functions take their asymptotic forms, which are dominated by the large logarithms mentioned at the beginning of this section. If these terms become too large they vitiate the perturbation series so that a resummation via the RGE is necessary. Before this resummation can be carried out we have first to perform mass factorization to remove the mass-singular terms  $\ln^i(\mu^2/m^2)$  from the asymptotic heavy-quark coefficient functions. This can be done in a similar way as shown for the partonic structure functions in Eqs. (2.4),(2.5), where now  $\ln^i(-\mu^2/p^2)$  are replaced by  $\ln^i(\mu^2/m^2)$ . In the VFNS approach we require that the following relation holds

$$F_i(n_f, Q^2) + \lim_{Q^2 \gg m^2} \left[ F_{i,H}(n_f, Q^2, m^2) \right] = F_i^{\text{VFNS}}(n_f + 1, Q^2). \quad (2.30)$$

The above formula implies that, at large  $Q^2$ , the left-hand-side can be written as a structure function containing densities and coefficient functions corresponding to only light partons, in which the number of light flavours is enhanced by one. In  $F_i^{\text{VFNS}}(n_f + 1, Q^2)$  the light-parton densities are mod-

ified with respect to those appearing in  $F_i(n_f, Q^2)$  in (2.26) and the heavy-flavour component  $F_{i,H}(Q^2, m^2)$  in (2.29) because the former have absorbed the logarithms  $\ln^i(\mu^2/m^2)$  coming from the heavy-quark coefficient functions. Moreover a new parton density appears in  $F_i^{\text{VFNS}}$  corresponding to the heavy quark H which is now treated as a light quark.

If relation (2.30) holds one has to impose the following mass-factorization relations for the heavy-quark coefficient functions. In the case of the coefficient functions  $L_{i,k}$  we get for  $Q^2 \gg m^2$

$$\mathcal{C}_{i,q}^{\text{NS}}(n_f) + L_{i,q}^{\text{NS}}(n_f) = A_{qq,H}^{\text{NS}}(n_f) \otimes \mathcal{C}_{i,q}^{\text{NS}}(n_f + 1), \quad (2.31)$$

$$\begin{aligned} \tilde{\mathcal{C}}_{i,q}^{\text{PS}}(n_f) + \tilde{L}_{i,q}^{\text{PS}}(n_f) &= \left[ A_{qq,H}^{\text{NS}}(n_f) + n_f \tilde{A}_{qq,H}^{\text{PS}}(n_f) + \tilde{A}_{Hq}^{\text{PS}}(n_f) \right] \otimes \tilde{\mathcal{C}}_{i,q}^{\text{PS}}(n_f + 1) \\ &+ \tilde{A}_{qq,H}^{\text{PS}}(n_f) \otimes \mathcal{C}_{i,q}^{\text{NS}}(n_f + 1) + A_{gg,H}^{\text{S}}(n_f) \otimes \tilde{\mathcal{C}}_{i,g}^{\text{S}}(n_f + 1), \end{aligned} \quad (2.32)$$

and

$$\begin{aligned} \tilde{\mathcal{C}}_{i,g}^{\text{S}}(n_f) + \tilde{L}_{i,g}^{\text{S}}(n_f) &= \tilde{A}_{gg,H}^{\text{S}}(n_f) \otimes \mathcal{C}_{i,q}^{\text{NS}}(n_f + 1) + A_{gg,H}^{\text{S}}(n_f) \otimes \tilde{\mathcal{C}}_{i,g}^{\text{S}}(n_f + 1) \\ &+ \left[ n_f \tilde{A}_{gg,H}^{\text{S}}(n_f) + \tilde{A}_{Hg}^{\text{S}}(n_f) \right] \otimes \tilde{\mathcal{C}}_{i,q}^{\text{PS}}(n_f + 1). \end{aligned} \quad (2.33)$$

For the heavy quark coefficient functions  $H_{i,k}$  we obtain for  $Q^2 \gg m^2$

$$\begin{aligned} H_{i,q}^{\text{PS}}(n_f) &= \tilde{A}_{Hq}^{\text{PS}}(n_f) \otimes \left[ \mathcal{C}_{i,q}^{\text{NS}}(n_f + 1) + \tilde{\mathcal{C}}_{i,q}^{\text{PS}}(n_f + 1) \right] \\ &+ \left[ A_{qq,H}^{\text{NS}}(n_f) + n_f \tilde{A}_{qq,H}^{\text{PS}}(n_f) \right] \otimes \tilde{\mathcal{C}}_{i,q}^{\text{PS}}(n_f + 1) \\ &+ A_{gg,H}^{\text{S}}(n_f) \otimes \tilde{\mathcal{C}}_{i,g}^{\text{S}}(n_f + 1), \end{aligned} \quad (2.34)$$

and

$$\begin{aligned} H_{i,g}^{\text{S}}(n_f) &= A_{gg,H}^{\text{S}}(n_f) \otimes \tilde{\mathcal{C}}_{i,g}^{\text{S}}(n_f + 1) + n_f \tilde{A}_{gg,H}^{\text{S}}(n_f) \otimes \tilde{\mathcal{C}}_{i,q}^{\text{PS}}(n_f + 1) \\ &+ \tilde{A}_{Hg}^{\text{S}}(n_f) \otimes \left[ \mathcal{C}_{i,q}^{\text{NS}}(n_f + 1) + \tilde{\mathcal{C}}_{i,q}^{\text{PS}}(n_f + 1) \right]. \end{aligned} \quad (2.35)$$

In the above equations  $A_{Hk}$  denotes the heavy-quark OME defined by

$$A_{Hk}\left(n_f, \frac{\mu^2}{m^2}\right) = \langle k(p) | O_H(0) | k(p) \rangle, \quad (2.36)$$

which is the analogue of the light-quark OME's in (2.6). The quantities  $A_{lk,H}(n_f, \mu^2/m^2)$ , which also appear above, represent the heavy-quark-loop contributions to the light-quark and gluon OME's defined in (2.6).

Although there exists some similarity between the mass factorization of  $\hat{\mathcal{F}}_{i,l}$  in (2.4),(2.5) and the ones given for the heavy-quark coefficient functions above we also observe a striking difference which makes the proof of Eqs. (2.31)-(2.35) and consequently of Eq. (2.30) much harder. The main difference is that the light partons appear in the initial as well as in the final state of the subprocesses contributing to  $\hat{\mathcal{F}}_{i,l}$  whereas the heavy quark only shows up in the final state of the reactions leading to  $L_{i,l}, H_{i,l}$  (2.29). This implies that there is no analogue for  $\hat{\mathcal{F}}_{i,H}$  in Eq. (2.29) meaning that the coefficient functions  $L_{i,H}$  and  $H_{i,H}$  do not appear in the latter equation. The same holds for the bare heavy-quark density  $\hat{f}_H$  which has no counter part in (2.26) and (2.27) either. Hence the mass factorization relations in (2.31)-(2.35) are much more cumbersome than those presented in (2.4),(2.5). Therefore the proofs of the former relations and implicitly of Eq. (2.30) become more involved. We have explicitly checked that the above relations hold up to order  $\alpha_s^2$  using the asymptotic heavy-quark coefficient functions in [10] and the heavy quark OME's in Appendix B.

Yet another complication arises when we consider the OME's  $A_{Hk}$  and  $A_{lk,H}$  defined above. Contrary to the light-parton OME's in (2.6) which only depend, apart from  $\mu^2$ , on one mass scale  $p^2$  the former also depend on the mass scale  $m^2$  due to the presence of the heavy quark. Therefore the unrenormalized expressions of  $A_{Hk}$  and  $A_{lk,H}$  contain besides ultraviolet (UV) divergences two types of collinear divergences which are represented by  $\ln^i(\mu^2/p^2)$  (light partons) and  $\ln^i(\mu^2/m^2)$  (heavy quark) respectively. The singularity at  $p^2 = 0$  shows up because external massless lines represented by  $k = q, g$  in (2.36) are coupled to internal massless quanta. This phenomenon shows up for the first time in order  $\alpha_s^2$  see [10]. Notice that the singularities at  $p^2 = 0$  also appear in the partonic quantities leading to the heavy-quark coefficient functions before they are removed by mass factorization as outlined in the beginning of this section. Therefore we also have to subtract the collinear singularities in  $p^2 = 0$  from the unrenormalized OME's  $A_{Hk}, A_{lk,H}$  in addition to the UV divergences. This twofold subtraction leads to two different scales in the renormalized OME's in (2.31)-(2.36) which are called the operator-renormalization scale and mass-factorization scale respectively.



Usually these two scales are set to be equal and they are denoted by one parameter  $\mu^2$ . However the appearance of these two scales results in more complicated RGE's for the heavy-quark OME's in comparison with those presented for the light-parton OME's in (2.12),(2.13) as we will see below. In the actual calculations of  $A_{Hk}, A_{lk,H}$  in [10] we have put  $p^2 = 0$  in (2.36) because we did the same for the partonic quantities computed in [3] leading to the heavy-quark coefficient functions  $L_{i,l}, H_{i,l}$ . Hence we had to adopt  $n$ -dimensional regularization for the UV as well as the collinear singularities in  $p^2 = 0$ . In this way both are represented by pole terms of the type  $1/(n-4)^j$ . If the latter are removed in the  $\overline{\text{MS}}$ -scheme the OME's  $A_{Hk}$  and  $A_{lk,H}$  automatically depend on one scale  $\mu$ .

Another comment we want to make is that  $\alpha_s$  appearing in the heavy-quark coefficient functions is renormalized at  $n_f$  flavours. This means that the renormalization of the coupling constant is carried out in such a way that all quarks equal to H and heavier than H decouple in the quark loops contributing to  $\alpha_s$ . In the right-hand-side of Eqs. (2.31)-(2.35) the decoupling of the heavy quark H has been undone so that here  $\alpha_s$  depends on  $n_f + 1$  flavours. This decoupling gives rise to additional logarithms of the type  $\ln^i(\mu^2/m^2)$ , which are cancelled by the OME's of the type  $A_{kl,H}$ . However explicit indication of this procedure further complicates our mass factorization relations above, which we want to avoid, so we have to bear in mind that this decoupling is implicitly understood.

If we now substitute Eqs. (2.31)-(2.35) into the left-hand-side of (2.29) and rearrange some terms then we obtain the expression for  $F_k^{\text{VFNS}}$  as presented in (2.26), where  $n_f \rightarrow n_f + 1$ . This implies that the new parton densities taken at  $n_f + 1$  light flavours can be expressed in terms of those given for  $n_f$  flavours. The original  $n_f$  light-flavour densities get modified so that for  $k = 1, \dots, n_f$

$$\begin{aligned}
f_k(n_f+1, \mu^2) + f_{\bar{k}}(n_f+1, \mu^2) &= A_{qq,H}^{\text{NS}}\left(n_f, \frac{\mu^2}{m^2}\right) \otimes [f_k(n_f, \mu^2) + f_{\bar{k}}(n_f, \mu^2)] \\
&+ \tilde{A}_{qq,H}^{\text{PS}}\left(n_f, \frac{\mu^2}{m^2}\right) \otimes \Sigma(n_f, \mu^2) \\
&+ \tilde{A}_{qq,H}^{\text{S}}\left(n_f, \frac{\mu^2}{m^2}\right) \otimes G(n_f, \mu^2), \quad (2.37)
\end{aligned}$$

whereas the parton density of the heavy quark can be expressed in the original

light flavours in the following way

$$\begin{aligned}
f_{H+\bar{H}}(n_f+1, \mu^2) &\equiv f_{n_f+1}(n_f+1, \mu^2) + f_{\overline{n_f+1}}(n_f+1, \mu^2) \\
&= \tilde{A}_{Hq}^{\text{PS}}\left(n_f, \frac{\mu^2}{m^2}\right) \otimes \Sigma(n_f, \mu^2) + \tilde{A}_{Hg}^{\text{S}}\left(n_f, \frac{\mu^2}{m^2}\right) \otimes G(n_f, \mu^2).
\end{aligned} \tag{2.38}$$

Comparing the above expression with Eq. (2.27) we observe that the first term in (2.27) has no counter part in (2.38). This is because we have no bare heavy-quark density unless one assumes that there already exists an intrinsic heavy-quark component of the proton wave function. The singlet combination of the quark densities becomes

$$\begin{aligned}
\Sigma(n_f+1, \mu^2) &= \sum_{k=1}^{n_f+1} \left[ f_k(n_f+1, \mu^2) + f_{\bar{k}}(n_f+1, \mu^2) \right] \\
&= \left[ A_{qq,H}^{\text{NS}}\left(n_f, \frac{\mu^2}{m^2}\right) + n_f \tilde{A}_{qq,H}^{\text{PS}}\left(n_f, \frac{\mu^2}{m^2}\right) + \tilde{A}_{Hq}^{\text{PS}}\left(n_f, \frac{\mu^2}{m^2}\right) \right] \otimes \Sigma(n_f, \mu^2) \\
&\quad + \left[ n_f \tilde{A}_{qg,H}^{\text{S}}\left(n_f, \frac{\mu^2}{m^2}\right) + \tilde{A}_{Hg}^{\text{S}}\left(n_f, \frac{\mu^2}{m^2}\right) \right] \otimes G(n_f, \mu^2).
\end{aligned} \tag{2.39}$$

The non-singlet combination  $\Delta_k(n_f+1)$  is defined in an analogous way as in (2.3) and it reads for  $k = 1, \dots, n_f+1$

$$\Delta_k(n_f+1, \mu^2) = f_k(n_f+1, \mu^2) + f_{\bar{k}}(n_f+1, \mu^2) - \frac{1}{n_f+1} \Sigma(n_f+1, \mu^2). \tag{2.40}$$

Finally the gluon density for  $n_f+1$  light flavours is

$$\begin{aligned}
G(n_f+1, \mu^2) &= A_{gq,H}^{\text{S}}(n_f, \mu^2) \otimes \Sigma(n_f, \mu^2) \\
&\quad + A_{gg,H}^{\text{S}}(n_f, \mu^2) \otimes G(n_f, \mu^2).
\end{aligned} \tag{2.41}$$

The old as well as the new parton densities have to satisfy the momentum sum rule

$$\int_0^1 dx x \left[ \Sigma(n_f, x, \mu^2) + G(n_f, x, \mu^2) \right] = 1, \tag{2.42}$$

for any  $n_f$ . This implies that the OME's  $A_{Hk}$ ,  $A_{kl,H}$  have to satisfy two relations

$$\int_0^1 dx x \left[ A_{qq,H}^{\text{NS}}\left(n_f, x, \frac{\mu^2}{m^2}\right) + n_f \tilde{A}_{qq,H}^{\text{PS}}\left(n_f, x, \frac{\mu^2}{m^2}\right) + \tilde{A}_{Hq}^{\text{PS}}\left(n_f, x, \frac{\mu^2}{m^2}\right) + A_{gg,H}^{\text{S}}\left(n_f, x, \frac{\mu^2}{m^2}\right) \right] = 1, \quad (2.43)$$

and

$$\int_0^1 dx x \left[ n_f \tilde{A}_{qq,H}^{\text{S}}\left(n_f, x, \frac{\mu^2}{m^2}\right) + \tilde{A}_{Hg}^{\text{S}}\left(n_f, x, \frac{\mu^2}{m^2}\right) + A_{gg,H}^{\text{S}}\left(n_f, x, \frac{\mu^2}{m^2}\right) \right] = 1, \quad (2.44)$$

which can be checked up to second order using the results in Appendix B.

The OME's  $A_{Hk}$  and  $A_{kl,H}$  satisfy the following RGE's

$$\begin{aligned} D\tilde{A}_{Hq}^{\text{PS}} &= \left( \gamma_{qq}^{\text{NS}} + n_f \tilde{\gamma}_{qq}^{\text{PS}} \right) \otimes \tilde{A}_{Hq}^{\text{PS}} + \gamma_{gq}^{\text{S}} \otimes \tilde{A}_{Hg}^{\text{S}} \\ &\quad - \left( \gamma_{HH}^{\text{NS}} + \tilde{\gamma}_{HH}^{\text{PS}} \right) \otimes \tilde{A}_{Hq}^{\text{PS}} - \tilde{\gamma}_{Hg}^{\text{S}} \otimes A_{gg,H}^{\text{S}} \\ &\quad - \tilde{\gamma}_{Hq}^{\text{PS}} \otimes \left( A_{qq,H}^{\text{NS}} + n_f \tilde{A}_{qq,H}^{\text{PS}} \right), \end{aligned} \quad (2.45)$$

$$\begin{aligned} D\tilde{A}_{Hg}^{\text{S}} &= \gamma_{gg}^{\text{S}} \otimes \tilde{A}_{Hg}^{\text{S}} + n_f \tilde{\gamma}_{qq}^{\text{S}} \otimes \tilde{A}_{Hq}^{\text{PS}} - \left( \gamma_{HH}^{\text{NS}} + \tilde{\gamma}_{HH}^{\text{PS}} \right) \otimes \tilde{A}_{Hg}^{\text{S}} \\ &\quad - \tilde{\gamma}_{Hg}^{\text{S}} \otimes A_{gg,H}^{\text{S}} - n_f \tilde{\gamma}_{Hq}^{\text{PS}} \otimes \tilde{A}_{qq,H}^{\text{S}}, \end{aligned} \quad (2.46)$$

$$DA_{qq,H}^{\text{NS}} = -\gamma_{qq,H}^{\text{NS}} \otimes A_{qq,H}^{\text{NS}}, \quad (2.47)$$

$$\begin{aligned} D\tilde{A}_{qq,H}^{\text{PS}} &= \gamma_{gq}^{\text{S}} \otimes \tilde{A}_{qq,H}^{\text{S}} - \left( \gamma_{qq,H}^{\text{NS}} + n_f \tilde{\gamma}_{qq,H}^{\text{PS}} \right) \otimes \tilde{A}_{qq,H}^{\text{PS}} \\ &\quad - \tilde{\gamma}_{qq,H}^{\text{PS}} \otimes A_{qq,H}^{\text{NS}} - \left( \tilde{\gamma}_{qq,H}^{\text{S}} + \tilde{\gamma}_{qq}^{\text{S}} \right) \otimes A_{gg,H}^{\text{S}} \\ &\quad - \tilde{\gamma}_{qH}^{\text{PS}} \otimes \tilde{A}_{Hq}^{\text{PS}}, \end{aligned} \quad (2.48)$$

$$\begin{aligned} D\tilde{A}_{qq,H}^{\text{S}} &= \tilde{\gamma}_{qq}^{\text{S}} \otimes \left( A_{qq,H}^{\text{NS}} + n_f \tilde{A}_{qq,H}^{\text{PS}} \right) + \gamma_{gg}^{\text{S}} \otimes \tilde{A}_{qq,H}^{\text{S}} \\ &\quad - \left( \gamma_{qq,H}^{\text{NS}} + n_f \tilde{\gamma}_{qq,H}^{\text{PS}} + \gamma_{qq}^{\text{NS}} + n_f \tilde{\gamma}_{qq}^{\text{PS}} \right) \otimes \tilde{A}_{qq,H}^{\text{S}} \\ &\quad - \left( \tilde{\gamma}_{qq,H}^{\text{S}} + \tilde{\gamma}_{qq}^{\text{S}} \right) \otimes A_{gg,H}^{\text{S}} - \tilde{\gamma}_{qH}^{\text{PS}} \otimes \tilde{A}_{Hg}^{\text{S}}, \end{aligned} \quad (2.49)$$

$$\begin{aligned}
DA_{gq,H}^S &= (\gamma_{qq}^{\text{NS}} + n_f \tilde{\gamma}_{qq}^{\text{PS}}) \otimes A_{gq,H}^S + \gamma_{gq}^S \otimes A_{gg,H}^S \\
&\quad - (\gamma_{gq,H}^S + \gamma_{gq}^S) \otimes (A_{qq,H}^{\text{NS}} + n_f \tilde{A}_{qq,H}^{\text{PS}}) \\
&\quad - (\gamma_{gg,H}^S + \gamma_{gg}^S) \otimes A_{gq,H}^S - \gamma_{gH}^S \otimes \tilde{A}_{Hq}^{\text{PS}}, \tag{2.50}
\end{aligned}$$

and

$$\begin{aligned}
DA_{gg,H}^S &= n_f \tilde{\gamma}_{qg}^S \otimes A_{gq,H}^S - \gamma_{gg,H}^S \otimes A_{gg,H}^S \\
&\quad - n_f (\gamma_{gq,H}^S + \gamma_{gq}^S) \otimes \tilde{A}_{qg,H}^S - \gamma_{gH}^S \otimes \tilde{A}_{Hg}^S. \tag{2.51}
\end{aligned}$$

The above RGE's are much more complicated than those written for  $A_{kl}$  in Eqs. (2.12),(2.13). This is due to the fact already mentioned below (2.36) that  $\mu$  represents the operator-renormalization scale as well as the mass-factorization scale. In Eqs. (2.12),(2.13) it only stands for the operator-renormalization scale. The anomalous dimensions coming from operator renormalization carry a minus sign whereas those associated with mass factorization have a plus sign in front of them. This difference in sign can be traced back to Eq. (2.14) where it was stated that the residues of the ultraviolet divergences are just the opposite of the ones corresponding to the collinear divergences. Furthermore one has to bear in mind that the residues of the ultraviolet and collinear divergences are equal to the anomalous dimensions coming from operator renormalization and mass factorization respectively. In Eqs. (2.45)-(2.51) the anomalous dimensions  $\gamma_{kl}$  have a plus sign on account of the collinear divergences occurring in  $A_{kl}$ , where the partons indicated by  $k, l$  are massless. However the anomalous dimensions  $\gamma_{HH}, \gamma_{Hl}, \gamma_{lH}$  and  $\gamma_{kl,H}$  carry a minus sign because the mass of the heavy quark  $m$  prevents these OME's from being collinearly divergent so that we only have to deal with ultraviolet singularities.

Using the above equations and (2.15)-(2.17) one can derive the RGE's for the new parton densities appearing in  $F_i^{\text{VFNS}}$  (2.30). For  $k = 1, \dots, n_f + 1$ , including the heavy-quark flavour, the RGE reads

$$\begin{aligned}
D \left[ f_k(n_f + 1, \mu^2) + f_{\bar{k}}(n_f + 1, \mu^2) \right] &= \\
&\quad - \gamma_{qq}^{\text{NS}}(n_f + 1) \otimes \left[ f_k(n_f + 1, \mu^2) + f_{\bar{k}}(n_f + 1, \mu^2) \right] \\
&\quad - \tilde{\gamma}_{qq}^{\text{PS}}(n_f + 1) \otimes \Sigma(n_f + 1, \mu^2) - \tilde{\gamma}_{qg}^S(n_f + 1) \otimes G(n_f + 1, \mu^2). \tag{2.52}
\end{aligned}$$

The non-singlet combination of the quark densities satisfies the RGE

$$D\Delta_k(n_f + 1, \mu^2) = -\gamma_{qq}^{\text{NS}}(n_f + 1) \otimes \Delta_k(n_f + 1, \mu^2). \tag{2.53}$$

The singlet combination of the quark densities satisfies the RGE

$$\begin{aligned}
D\Sigma(n_f + 1, \mu^2) &= -\gamma_{qq}^S(n_f + 1) \otimes \Sigma(n_f + 1, \mu^2) \\
&\quad -\gamma_{gg}^S(n_f + 1) \otimes G(n_f + 1, \mu^2), \tag{2.54}
\end{aligned}$$

and the gluon density is given by

$$\begin{aligned}
DG(n_f + 1, \mu^2) &= -\gamma_{gq}^S(n_f + 1) \otimes \Sigma(n_f + 1, \mu^2) \\
&\quad -\gamma_{gg}^S(n_f + 1) \otimes G(n_f + 1, \mu^2). \tag{2.55}
\end{aligned}$$

In the above equations we have used the identities

$$\gamma_{ij}(n_f) + \gamma_{ij,H}(n_f) = \gamma_{ij}(n_f + 1), \tag{2.56}$$

$$\gamma_{HH}^{\text{NS}}(n_f + 1) = \gamma_{qq}^{\text{NS}}(n_f + 1); \quad \tilde{\gamma}_{HH}^{\text{PS}}(n_f + 1) = \tilde{\gamma}_{qq}^{\text{PS}}(n_f + 1), \tag{2.57}$$

$$\tilde{\gamma}_{qH}^{\text{PS}}(n_f + 1) = \tilde{\gamma}_{Hq}^{\text{PS}}(n_f + 1) = \tilde{\gamma}_{qq}^{\text{PS}}(n_f + 1), \tag{2.58}$$

$$\gamma_{gH}^S(n_f + 1) = \gamma_{gq}^S(n_f + 1); \quad \tilde{\gamma}_{Hg}^S(n_f + 1) = \tilde{\gamma}_{qg}^S(n_f + 1), \tag{2.59}$$

because the anomalous dimensions do not depend on the mass  $m$  of the heavy-quark  $H$ . A comparison of the above RGE's with those presented for the light-parton densities in Eqs. (2.15)-(2.17) reveals that they are exactly the same in spite of the fact that there is no counterpart of the bare heavy-quark density in the derivation of Eqs. (2.52)-(2.55).

All perturbative quantities which appear in this section are now available up to  $O(\alpha_s^2)$ . This holds for the anomalous dimensions  $\gamma_{kl}$  [15], the massless-parton coefficient functions  $\mathcal{C}_{i,k}$  [16] and the heavy-quark coefficient functions  $L_{i,k}$ ,  $H_{i,k}$  [3]. The OME's  $\tilde{A}_{Hq}^{\text{PS}}$ ,  $\tilde{A}_{Hg}^S$  and  $A_{qq,H}^{\text{NS}}$  are computed up to  $O(\alpha_s^2)$  and listed in unrenormalized form in Appendix C of [10]. We still require  $A_{gq,H}^S$  (Fig. 3) and  $A_{gg,H}^S$  (Fig. 4) which are calculated up to the same order in this paper. Exact expressions for the unrenormalized OME's can be found in Appendix A. Notice that up to second order in  $\alpha_s$  both  $\tilde{A}_{qg,H}^S$  and  $\tilde{A}_{qq,H}^{\text{PS}}$  are zero. The renormalized (finite) expressions for all these OME's, which we will use in the next section, are presented in Appendix B.

After having found the representation of the heavy-quark density  $f_{H+\bar{H}}$  in (2.38) and the RGE in (2.52) which determines its scale evolution we can write down the charm component of the deep-inelastic structure function in the VFNS representation. The latter is given by

$$\begin{aligned}
F_{i,H}^{\text{VFNS}}(n_f + 1, Q^2) &= e_H^2 \left[ f_{H+\bar{H}}(n_f + 1, \mu^2) \otimes \mathcal{C}_{i,q}^{\text{NS}}\left(n_f + 1, \frac{Q^2}{\mu^2}\right) \right. \\
&\quad + \Sigma(n_f + 1, \mu^2) \otimes \tilde{\mathcal{C}}_{i,q}^{\text{PS}}\left(n_f + 1, \frac{Q^2}{\mu^2}\right) \\
&\quad \left. + G(n_f + 1, \mu^2) \otimes \tilde{\mathcal{C}}_{i,g}^{\text{S}}\left(n_f + 1, \frac{Q^2}{\mu^2}\right) \right]. \quad (2.60)
\end{aligned}$$

The expression above satisfies  $DF_{i,H}^{\text{VFNS}} = 0$  (see (2.11)), so it is renormalization group invariant, which means that it is scheme independent and becomes a physical quantity. Notice that even though the form of  $F_{i,H}^{\text{VFNS}}$  is the same as the one presented for intrinsic heavy-quark production, their origins are completely different. The VFNS result, Eq. (2.60) is derived from FOPT when the exact heavy-quark coefficient functions are replaced by their asymptotic expressions taken at  $Q^2 \gg m^2$  (see (2.30)). Then we have performed mass factorization and absorbed the mass singularities with respect to the heavy-quark mass  $m$  into the light-parton densities taken at the original  $n_f$  light flavours (see Eqs. (2.37)-(2.41)). This procedure leads to relations between the parton densities in the  $n_f$  and  $n_f + 1$  flavour schemes. In particular this applies to the heavy-quark density  $f_{H+\bar{H}}$  in (2.38). For intrinsic heavy-quark production the origin of Eq. (2.60) is completely different. In this case it is not derived from perturbation theory and therefore there does not exist any relation between the heavy-quark density and the light-parton densities like in Eq. (2.38). Actually the intrinsic-charm density is determined by a simple fit to experimental data.

Furthermore we want to emphasize that the VFNS approach is only valid for totally inclusive quantities like structure functions since the logarithmic terms  $\ln^i(Q^2/m^2) \ln^j(\mu^2/m^2)$  only appear in the asymptotic form of the heavy-quark coefficient functions in this case. Hence expression (2.60) is just an alternative description for FOPT when the production of the heavy quarks occurs far above threshold where  $Q^2 \gg m^2$ . The only difference between the FOPT and the VFNS descriptions is that the large logarithms have been resummed in the latter approach so that one gets an improved expression with

respect to normal perturbation theory in the large  $Q^2$ -region. However on the level of differential distributions the large logarithms of the kind given above do not show up in the perturbation series. Therefore in this case the VFNS approach cannot be applied. As has been mentioned in the introduction one can only distinguish between intrinsic and extrinsic heavy-quark production.

Finally we want to comment about the work in [9] where one has proposed the idea of the VFNS approach. In particular we want to make some remarks about equation (9) in [9](ACOT) which is similar to our equation (2.60). Using the notations in the latter reference this equation reads

$$\sum_{\lambda} W_{BN}^{\lambda} = f_N^Q \otimes \sum_{\lambda} \omega_{BQ}^{\lambda(0)} - f_N^g \otimes f_g^{Q(1)} \otimes \sum_{\lambda} \omega_{BQ}^{\lambda(0)} + f_N^g \otimes \sum_{\lambda} \omega_{Bg}^{\lambda(1)}, \quad (2.61)$$

where we have summed over all helicities of the virtual photon denoted by  $\lambda$ . Further we have corrected a misprint because  $f_g^{Q(0)}$  in (9) should read  $f_g^{Q(1)}$ . To translate (2.61) into our language we have to make the following replacements

$$B \rightarrow \gamma^*; \quad Q \rightarrow H; \quad \sum_{\lambda} W_{BN}^{\lambda} \rightarrow F_{i,H}^{\text{ACOT}}, \quad (2.62)$$

$$\sum_{\lambda} \omega_{BQ}^{\lambda(0)} \rightarrow e_H^2 \mathcal{C}_{i,q}^{\text{NS},(0)} = e_H^2 \delta(1-z); \quad \sum_{\lambda} \omega_{Bg}^{\lambda(1)} \rightarrow e_H^2 H_{i,g}^{\text{S},(1)}, \quad (2.63)$$

$$f_g^{Q(1)} \rightarrow \tilde{A}_{Hg}^{\text{S},(1)}, \quad (2.64)$$

and

$$f_N^Q \rightarrow f_{H+\bar{H}}; \quad f_N^g \rightarrow G. \quad (2.65)$$

Hence Eq. (2.61) can be written in our notation as

$$\begin{aligned} F_{i,H}^{\text{ACOT}} &= e_H^2 \left[ f_{H+\bar{H}} \otimes \mathcal{C}_{i,q}^{\text{NS},(0)} + G \otimes \tilde{\mathcal{C}}_{i,g}^{\text{S},(1)} \right] \\ &+ e_H^2 \left[ G \otimes \{ H_{i,g}^{\text{S},(1)} - \tilde{\mathcal{C}}_{i,g}^{\text{S},(1)} - \tilde{A}_{Hg}^{\text{S},(1)} \otimes \mathcal{C}_{i,q}^{\text{NS},(0)} \} \right]. \end{aligned} \quad (2.66)$$

Comparing this expression with ours in (2.60) we notice the following differences. First Eq. (2.61) and therefore Eq. (2.66) in [9] was only derived in

lowest order (LO), whereas Eq. (2.60) is valid in all orders of perturbation theory. Second Eqs. (2.61) and (2.66) are not valid in next-to-leading order (NLO) but this can be repaired by replacing  $\mathcal{C}_{i,q}^{\text{NS},(0)}$  by  $\mathcal{C}_{i,q}^{\text{NS},(0)} + (\alpha_s/4\pi)\mathcal{C}_{i,q}^{\text{NS},(1)}$  in (2.66). However the most important difference is that the last term between the square brackets in (2.66) has no counter part in our expression (2.60). This is because we took the limit  $Q^2 \rightarrow \infty$  and dropped all terms proportional to  $(m^2/Q^2)^l$  in the asymptotic heavy-quark coefficient functions. This is revealed by the mass-factorization relation (2.35) for  $H_{i,g}^{\text{S}}$ , which only holds in the limit  $Q^2 \gg m^2$ . However the exact expressions for  $H_{i,g}^{\text{S},(1)}$ ,  $\tilde{\mathcal{C}}_{i,g}^{\text{S},(1)}$  and  $\tilde{A}_{Hg}^{\text{S},(1)}$  can be found in the literature (see [3], [16] and [10]). Expanding the latter in powers of  $m^2/Q^2$  we obtain

$$\begin{aligned} H_{i,g}^{\text{S},(1)} - \tilde{\mathcal{C}}_{i,g}^{\text{S},(1)} - \tilde{A}_{Hg}^{\text{S},(1)} \otimes \mathcal{C}_{i,q}^{\text{NS},(0)} \\ = \alpha_s(\mu^2) \sum_{l=1}^{\infty} \left(\frac{m^2}{Q^2}\right)^l \left[ a_i^{(l)} \ln\left(\frac{Q^2}{m^2}\right) + b_i^{(l)} \right]. \end{aligned} \quad (2.67)$$

When  $Q^2 \rightarrow \infty$  (2.67) vanishes, as was already expected from (2.35). The motivation for the above expression, included in [9], was to get a better stability of  $F_{i,H}^{\text{VFNS}}$  in the threshold region with respect to variations in the factorization scale. However we have dropped these type of contributions as shown in Eq. (2.67) in our representation for  $F_{i,H}^{\text{VFNS}}$  (2.60) for theoretical as well as practical reasons. The theoretical argument is that mass factorization does not apply to terms proportional to  $(m^2/Q^2)^l$  for  $l \geq 1$  so that Eq. (2.66) or (9) in [9] cannot be generalized to higher orders in  $\alpha_s$ . The practical reason is that the inclusion of higher order corrections automatically improves the stability of the perturbation series with respect to variations with respect to the factorization scale as is shown in [11], [12], [13].

Summarizing this section we have presented expressions for the total structure functions  $F_i^{\text{VFNS}}(n_f + 1, Q^2)$  (2.30) as well as for its heavy-quark component  $F_{i,H}^{\text{VFNS}}(n_f + 1, Q^2)$  (2.60) in the context of the variable-flavour-number scheme (VFNS), which are valid in all orders of perturbation theory. Starting from the structure functions  $F_i(n_f, Q^2)$ , expressed in the light-parton densities and coefficient functions, we could show that by adding the heavy-flavour contribution the sum can be written as  $F_i^{\text{VFNS}}(n_f + 1, Q^2)$ , provided  $Q^2 \gg m^2$  (see Eq. (2.30)). This procedure imposes relations between the parton densities appearing in  $F_i(n_f, Q^2)$  and the new ones showing up in



$F_i^{\text{VFNS}}(n_f + 1, Q^2)$ . These relations, given by (2.37)-(2.41), have to be satisfied in the VFNS approach. Unfortunately the existing parton-density sets in the literature do not satisfy these requirements. They do however satisfy the RGE's in (2.52)-(2.55). The consequences of the relations between the new parton densities taken at  $n_f + 1$  flavours and the old ones presented at  $n_f$  flavours will be discussed for charm production ( $n_f = 3$ ) in the next section.

### 3 Validity of FOPT and the VFNS

In this section we apply the findings of the last section to charm production. Here we want to investigate which of the two approaches i.e., FOPT or VFNS, is the most appropriate to describe the total structure function  $F_i(x, Q^2)$  and its charm component  $F_{i,c}(x, Q^2, m^2)$  in the different kinematical regimes. To do this we will study the following issues. The first one concerns the question at which values of  $x$  and  $Q^2$  the large logarithmic terms  $\ln^i(Q^2/m_c^2) \ln^j(\mu^2/m_c^2)$  in the heavy-quark coefficient functions constitute the bulk of the radiative corrections to the charm component of the structure functions. Further in the spirit of VFNS one should use the parton densities defined in (2.37)-(2.41) instead of the usual ones which are available in the literature. In the former there exist direct relations between the parton densities taken at  $n_f = 3$  (no charm-quark density) and the parton densities at  $n_f = 4$  (charm-quark density included). In the literature this relation is broken because in all parametrizations the charm-quark density is given by an arbitrary function in which the parameters are fitted to the data and there exists no direct relation between the charm density and the remaining u,d,s and g densities except that they have to satisfy the momentum sum rule. The effect of this difference on the charm structure function  $F_{2,c}(x, Q^2)$  will be investigated. Finally we study the difference in the behaviour of this function which occurs when going from the FOPT to the VFNS descriptions. In particular we focus on the visibility of the charm threshold which appears in FOPT but is absent in the case of the VFNS. We also study the rate of convergence of the perturbation series over a wide range of  $Q^2$ -values which will be different for these two approaches.

Before presenting our results we want to mention that all perturbative quantities like the operator-matrix elements (OME's), heavy-quark coefficient functions and light-parton coefficient functions are presented in the  $\overline{\text{MS}}$ -scheme. Therefore we have to use parton densities parametrized in the same scheme. Furthermore in FOPT the number of light flavours in the running coupling constant and the coefficient functions has to be equal to three ( $\Lambda_3 = 232$  MeV (LO);  $\Lambda_3 = 248$  MeV (NLO)) whereas in the VFNS this number should be equal to four ( $\Lambda_4 = 200$  MeV (LO and NLO)). For the mass of the charm quark and the factorization (renormalization) scale we have chosen  $m_c = 1.5$  GeV/ $c$  and  $\mu^2 = Q^2$  respectively because the same scale is usually adopted for the light-parton components of the structure

functions. Notice that in the literature [6], [9], [12] a different scale is chosen for the charm structure function in FOPT. However the results in NLO are rather independent of the scale as is shown in [11],[12] [13].

Starting with the first question about the dominance of the large logarithms we define the charm component in the FOPT approach by the function  $F_{i,c}(x, Q^2, m_c^2)$ . The latter is computed from (2.29) and contains the heavy-quark coefficient functions  $L_{i,k}$  and  $H_{i,k}$ , where  $i = 2, L$  and  $k = q, g$ . The above coefficient functions are exactly calculated up to  $O(\alpha_s^2)$  in [3]. Their asymptotic expressions, which contain the large logarithms above, as well as constant terms, are presented in [10]. The latter are strictly speaking only valid when  $Q^2 \gg m_c^2$ . Further let us denote by  $F_{i,c}^{\text{exact}}$  and  $F_{i,c}^{\text{asympt}}$  the charm structure functions computed by using the exact and asymptotic forms of the heavy-quark coefficient functions respectively. In order to determine the  $Q^2$  value above which  $F_{i,c}^{\text{exact}}$  and  $F_{i,c}^{\text{asympt}}$  coincide we plot the following ratios

$$R_i(x, Q^2, m_c^2) = \frac{F_{i,c}^{\text{asympt}}(x, Q^2, m_c^2)}{F_{i,c}^{\text{exact}}(x, Q^2, m_c^2)}. \quad (3.1)$$

For these plots we adopt the GRV94HO parton density set [17]. The reason that this set is chosen is because it is obtained from a fit to the deep-inelastic scattering data performed in the spirit of the FOPT approach, which means that the number of active flavours is chosen to be three and the charm component of the structure function is calculated from the photon-gluon fusion process and its higher order QCD corrections.

In Fig. 5 we plot  $R_2(NLO)$  as a function of  $Q^2$  for four different values of  $x$  i.e.  $x = 10^{-1}, 10^{-2}, 10^{-3}$  and  $10^{-4}$ . From this figure we infer that  $R_2$  tends to unity at  $Q^2$  values which are an order of magnitude larger than  $m_c^2$  ( $1 > R_2 > 0.9$  for  $Q^2 > 20$  (GeV/c) $^2$ ). This holds provided  $x < 10^{-2}$ , where the limit  $R_2 = 1$  is almost always approached from below. However for  $x > 10^{-1}$  the limit is reached from above and at a much bigger value of  $Q^2$  ( $1.1 > R_2 > 1$  for  $Q^2 > 300$  (GeV/c) $^2$ ), which is two orders of magnitude larger than  $m_c^2$ . The fact that the rate of convergence to  $R_2 = 1$  is much slower at large  $x$  is more clearly shown in Fig. 6. Here we plot  $R_2(NLO)$  as a function of  $x$  at  $Q^2 = 10, 50$  and  $100$  (GeV/c) $^2$ . At very large  $x$  all curves strongly deviate from  $R_2 = 1$ . When  $Q^2$  decreases the deviations occur at smaller  $x$ . This fact that  $R_2 \neq 1$  at large  $x$  and small  $Q^2$  can be wholly attributed to threshold terms, which are present in the exact heavy-quark coefficient functions, but which are absent in their asymptotic expressions.

In Fig. 7 we show the same plot for  $R_L(NLO)$  as presented for  $R_2(NLO)$  in Fig. 5. Here the approach to  $R_L = 1$  starts at a much larger value of  $Q^2$  than has been observed for  $R_2$ . One sees that  $0.9 < R_L < 1.1$  when  $Q^2 > 10^3$   $(\text{GeV}/c)^2$ . Again the rate of convergence is slower as  $x$  increases, which is the region where threshold effects become important. This becomes even more visible in Fig. 8. The reason that threshold effects are dominant at large  $x$  and small  $Q^2$  can be explained when one looks at the convolution

$$\int_x^{z_{\text{th}}} \frac{dz}{z} f_k\left(\frac{x}{z}, \mu^2\right) H_{i,k}\left(z, \frac{Q^2}{m^2}, \frac{m_c^2}{\mu^2}\right), \quad (3.2)$$

with a similar expression when  $H_{i,k}$  is replaced by  $L_{i,k}$ . Here  $f_k$  and  $H_{i,k}, L_{i,k}$  denote the parton densities and the heavy-quark coefficient functions respectively. The threshold value is given by

$$z_{\text{th}} = \frac{Q^2}{Q^2 + 4 m_c^2} \quad (3.3)$$

in the expression for the structure function (2.29). From the above equations one infers that when  $x$  is very large and  $Q^2$  is very small  $x \rightarrow z_{\text{th}}$  so that only threshold terms can contribute to the integral (3.2). We also would like to comment on the phenomenon that the approach to  $R_i(NLO) = 1$  is much slower for  $i = L$  than for  $i = 2$ . It originates from the fact that the power of the large logarithms appearing in the heavy-quark coefficient functions in the case of  $i = L$  is one unit smaller than that for  $i = 2$ . This phenomenon was also observed for heavy-flavour production in the Drell-Yan process [18]. It appears that the  $Q^2$  value for which the exact and asymptotic expressions of the physical quantities coincide is smaller when the powers of the large logarithmic terms increase. Notice that the Born contribution to the longitudinal coefficient function does not contain logarithms in the limit  $Q^2 \gg m_c^2$  so that it is independent of  $Q^2$  and  $m_c^2$ . In this case, as well as in some interference terms in the Drell-Yan process, the convergence to the asymptotic expressions takes place at an extremely large value of  $Q^2$ .

We have also studied  $R_i(LO)$  in the Born approximation to the charm structure functions in (3.1). Here it turns out that  $R_i(LO) \geq 1$  for all  $x$  and  $Q^2$  so that the limit is always approached from above. This behaviour is different from the one observed in NLO (see Figs. 5-8). Further  $R_i(LO)$  is closer to unity at small  $Q^2$  and large  $x$  than in the case of  $R_i(NLO)$  which

implies that threshold effects in leading order are smaller than in next-to-leading order. However the  $Q^2$  value at which  $R_i$  becomes equal to one is essentially the same in LO and NLO. In Section 5 of [10] we made the same study of  $R_i$  in (3.1) but on the level of the heavy-quark coefficient functions themselves. A comparison with the results from [10] reveals that the  $Q^2$  value for which the asymptotic and exact heavy-quark coefficient functions coincide is the same as the one obtained for the charm structure functions in (3.1). Hence the convolution with the parton densities in (3.2) hardly affects the  $Q^2$  value at which the exact and asymptotic expressions coincide.

Next we discuss the parton densities which emerge from the VFNS according to Eqs. (2.37)-(2.41). The most interesting among them is the charm-quark density which appears in the four-flavour scheme. It is derived from the formula in Eq. (2.38) where we choose  $n_f = 3$ . Up to  $O(\alpha_s^2)$  Eq. (2.38) becomes equal to

$$\begin{aligned}
f_{c+\bar{c}}^{\text{VFNS}}(4, x, \mu^2) &\equiv f_4(4, x, \mu^2) + f_{\bar{4}}(4, x, \mu^2) \\
&= \left(\frac{\alpha_s(\mu^2)}{4\pi}\right)^2 \int_x^1 \frac{dz}{z} \Sigma\left(3, \frac{x}{z}, \mu^2\right) \tilde{A}_{cq}^{\text{PS},(2)}\left(z, \frac{\mu^2}{m_c^2}\right) \\
&\quad + \int_x^1 \frac{dz}{z} G\left(3, \frac{x}{z}, \mu^2\right) \left[ \left(\frac{\alpha_s(\mu^2)}{4\pi}\right) \tilde{A}_{cg}^{\text{S},(1)}\left(z, \frac{\mu^2}{m_c^2}\right) + \left(\frac{\alpha_s(\mu^2)}{4\pi}\right)^2 \tilde{A}_{cg}^{\text{S},(2)}\left(z, \frac{\mu^2}{m_c^2}\right) \right],
\end{aligned} \tag{3.4}$$

where  $\tilde{A}_{Hq}^{\text{PS},(2)}$ ,  $\tilde{A}_{Hg}^{\text{S},(i)}$  ( $i = 1, 2$ ) with  $H = c$  are the OME's presented in (B.1)-(B.3) which are renormalized in such a way that  $\alpha_s$  in (3.4) depends on four flavours ( $\Lambda_4 = 200$  MeV). Further one has to put  $n_f = 3$  in the OME's above which up to order  $\alpha_s^2$  are independent of the number of flavours. The quantities  $\Sigma(3, \mu^2)$  and  $G(3, \mu^2)$  represent the singlet combination of parton densities and the gluon density in the three-flavour scheme respectively. Notice that the  $O(\alpha_s)$  term was already introduced in Eq. (10) of [9].

In order to make a comparison with the existing charm-quark densities present in the literature we now choose the GRV92HO set [19] to compute  $\Sigma(3, \mu^2)$  and  $G(3, \mu^2)$  in (3.4). The reason is that the GRV92 set contains a charm-quark density which is not included in the GRV94 set [17]. For a comparison between the charm-quark density  $f_{c+\bar{c}}^{\text{VFNS}}$  and the one presented by the GRV92 set we have to impose the same boundary conditions. Therefore we require  $f_{c+\bar{c}}^{\text{VFNS}}(4, x, m_c^2) = 0$  (3.4) since the same has been done for the charm-quark density in [19]. To that order the non-logarithmic terms in

$\tilde{A}_{cq}^{\text{PS},(2)}$  (B.1) and  $\tilde{A}_{cg}^{\text{S},(2)}$  (B.3) have to be removed, which is not needed for  $\tilde{A}_{cg}^{\text{S},(1)}$  (B.2) because the latter already vanishes at  $\mu^2 = m_c^2$ .

In Fig. 9 we plot the ratio

$$R_{\text{ch}} = \frac{f_{c+\bar{c}}^{\text{VFNS}}(4, x, \mu^2)}{f_{c+\bar{c}}^{\text{PDF}}(4, x, \mu^2)}, \quad (3.5)$$

as a function of  $\mu^2$  for the values  $x = 10^{-1}, 10^{-2}, 10^{-3}$  and  $10^{-4}$ . Here  $f_{c+\bar{c}}^{\text{VFNS}}$  is computed from (3.4) by choosing one of the parton density sets in the literature (here GRV92HO) for the determination of  $\Sigma(3, \mu^2)$  and  $G(3, \mu^2)$  while  $f_{c+\bar{c}}^{\text{PDF}}$  is the charm-quark density belonging to the same set. For  $x < 10^{-2}$  it turns out that  $1 > R_{\text{ch}} > 0.9$ . This is surprising because (3.4) is calculated up to finite order in perturbation theory whereas the GRV density is the NLO solution of RGE's in which all leading and next-to-leading logarithms are resummed. Hence we should expect a larger difference between the scale evolutions. However from the results in [20], [21] we anticipate that this difference is not so dramatic as long as  $\mu^2/m_c^2 < 10^3$ . Apparently the leading logarithms beyond  $O(\alpha_s^2)$ , which are neglected in (3.4), but not in the GRV charm density, do not play an important role provided  $\mu^2$  is not chosen to be too large. What is really striking is that the charm density depends on four-light-parton densities in the VFNS, whereas in the case of GRV this density is unconstrained except that it has to satisfy the momentum sum rule. Therefore it is unexpected that the ratio  $R_{\text{ch}}$  is so close to unity.

Besides the appearance of the charm-quark density, the four other light-parton densities representing u,d,s and g are modified while going from three to four active flavours. The modification for the light-quark densities is given by Eq. (2.37). Summing the latter over the three light flavours (u,d and s) one obtains the singlet density corrected up to  $O(\alpha_s^2)$  which is given by

$$\begin{aligned} \Sigma'(4, x, \mu^2) &= \int_x^1 \frac{dz}{z} \Sigma\left(3, \frac{x}{z}, \mu^2\right) \\ &\times \left[ \delta(1-z) + \left(\frac{\alpha_s(\mu^2)}{4\pi}\right)^2 A_{qq,c}^{\text{NS},(2)}\left(z, \frac{\mu^2}{m_c^2}\right) \right], \end{aligned} \quad (3.6)$$

where  $A_{qq,H}^{\text{NS},(2)}$  is given in (B.4) with  $H = c$ . Notice that  $\Sigma(4, x, \mu^2) = \Sigma'(4, x, \mu^2) + f_{c+\bar{c}}(4, x, \mu^2)$  in Eq. (2.39). Up to  $O(\alpha_s^2)$  the gluon density

in the four-flavour scheme (see Eq. (2.41)) is

$$\begin{aligned}
G(4, x, \mu^2) &= \left(\frac{\alpha_s(\mu^2)}{4\pi}\right)^2 \int_x^1 \frac{dz}{z} \Sigma\left(3, \frac{x}{z}, \mu^2\right) A_{gg,c}^{S,(2)}\left(z, \frac{\mu^2}{m_c^2}\right) \\
&+ \int_x^1 \frac{dz}{z} G\left(3, \frac{x}{z}, \mu^2\right) \left[\delta(1-z) + \left(\frac{\alpha_s(\mu^2)}{4\pi}\right) A_{gg,c}^{S,(1)}\left(z, \frac{\mu^2}{m_c^2}\right)\right. \\
&\left. + \left(\frac{\alpha_s(\mu^2)}{4\pi}\right)^2 A_{gg,c}^{S,(2)}\left(z, \frac{\mu^2}{m_c^2}\right)\right]. \tag{3.7}
\end{aligned}$$

The functions  $A_{gg,H}^{S,(2)}$  and  $A_{gg,H}^{S,(i)}$  ( $i = 1, 2$ ) with  $H = c$  are presented in Eqs. (B.5)-(B.7). Notice that up to  $O(\alpha_s^2)$  the above OME's are independent of the number of internal flavours  $n_f$ .

In the literature all parton density sets are presented either in the three-flavour scheme ( $n_f = 3$ ) e.g. GRV94 [17], GRV92 [19] or in the four-flavour scheme ( $n_f = 4$ ) e.g. CTEQ [22] and MRS [23]. This implies that  $n_f$ , which occurs in the anomalous dimensions and in the coefficient functions, is kept fixed above and below the charm threshold. In the case of GRV92 it means that even when  $Q^2 \gg m_c^2$  the light-parton densities evolve according to  $n_f = 3$  whereas in principle  $n_f = 4$  has to be chosen. In Fig. 10 we show the singlet combinations of parton densities  $\Sigma(3, \mu^2)$  and  $\Sigma'(4, \mu^2)$  (3.6) and, as the difference between them is  $O(\alpha_s^2)$ , it is essentially invisible. Therefore the error made in choosing  $\Sigma(3, \mu^2)$  instead of  $\Sigma'(4, \mu^2)$  above the charm threshold is extremely small. In Fig. 11 we make the same study for the gluon density where we compare  $G(3, \mu^2)$  with  $G(4, \mu^2)$ . Here the latter function yields the higher curves. In this case the difference is a larger than for the singlet-quark combination (3.6). This is no surprise because the difference already starts in  $O(\alpha_s)$  in the gluon case (see (3.7)). We also made a comparison with the parton densities of [22] (CTEQ) and [23] (MRS). In this case the parton-density sets are presented in the four-flavour scheme. Inverting Eqs. (3.6) and (3.7) one can easily get the corresponding densities for the three-flavour scheme and recompute  $f_{c+\bar{c}}^{\text{VFNS}}$  in (3.4). Like in the GRV92 case the fitted charm-quark density  $f_{c+\bar{c}}^{\text{PDF}}$  and the computed charm-quark density  $f_{c+\bar{c}}^{\text{VFNS}}$  show a remarkable agreement for each parton-density set separately. Since  $f_{c+\bar{c}}^{\text{VFNS}}$  is mainly determined by the gluon density in (3.4) the mutual differences between the charm-quark densities in the various parton-density sets may be attributed to the different parametrizations for the gluon.

Summarizing our findings above we can conclude that for the actual computation of the charm structure function  $F_{2,c}^{\text{VFNS}}$  in (2.60), it does not make much difference when the light-flavour densities in the VFNS, as given by Eqs. (3.4),(3.6) and (3.7) are replaced by those obtained from the various parton-density sets available in the literature.

Now we want to study the differences between the FOPT and VFNS approaches for the description of the charm structure function  $F_{2,c}$ . Using the set GRV92HO [19] we present plots for  $F_{2,c}^{\text{exact}}$  (2.29) in Figs. 12a-e (see also above (3.1)), which represents the FOPT. We do the same for  $F_{2,c}^{\text{VFNS}}$ , which is given by Eq. (2.60), using the densities in Eqs. (3.4),(3.6) and (3.7). Both are calculated in NLO. For  $Q^2 = 3 \text{ (GeV}/c)^2$  (see Fig. 12a) we observe the threshold effect in  $F_{2,c}^{\text{exact}}$  at large  $x$ . Here this function vanishes for  $x \geq 0.1$ . This effect does not show up in  $F_{2,c}^{\text{VFNS}}$  although the latter is so small in the large  $x$ -region that, in view of the low statistics of the data in that region, any distinction between the FOPT and the VFNS approaches will be invisible. The difference becomes even smaller when  $Q^2$  increases (see Figs. 12b-e). However at small  $x$  the difference between  $F_{2,c}^{\text{exact}}$  and  $F_{2,c}^{\text{VFNS}}$  becomes more conspicuous. It is in this region that data will appear from the HERA collider experiments. Although the difference is not that large at  $Q^2 = 3 \text{ (GeV}/c)^2$  it becomes big for  $5 < Q^2 < 10 \text{ (GeV}/c)^2$  (see Figs. 12b,c). Here  $F_{2,c}^{\text{VFNS}}$  exceeds  $F_{2,c}^{\text{exact}}$  by more than 60% with respect to the latter quantity at  $x = 10^{-4}$ . The difference becomes less when  $Q^2$  increases, e.g. at  $Q^2 = 100 \text{ (GeV}/c)^2$  (Fig. 12e) it is about 25%. The H1-collaboration has published data in [6] for  $Q^2 = 12, 25$  and  $45 \text{ (GeV}/c)^2$  which lie in the region  $x \leq 10^{-2}$ . From their analysis we infer that the predictions from FOPT lie below the data which means that, in view of our findings above, the predictions from VFNS are in better agreement with experiment. However one has to be cautious to draw too premature conclusions from the observations made above. First one has to bear in mind that  $F_{2,c}^{\text{VFNS}}$  is derived from  $F_{2,c}^{\text{asympt}}$  via mass factorization (see Section 2). Therefore the former is only reliable when the large logarithms mentioned in the beginning of this section dominate the corrections to the charm structure function. From Figs. 5,6 we infer that this happens for  $Q^2 > 20 \text{ (GeV}/c)^2$ . Another criterion is the perturbative stability of the various approaches, which will be discussed shortly, and from which we infer that the VFNS is better than FOPT for  $Q^2 > 10 \text{ (GeV}/c)^2$ . This implies that  $F_{2,c}^{\text{VFNS}}$  gives a more reliable



description of the data than  $F_{2,c}^{\text{exact}}$  for  $Q^2 > 20$  (GeV/c)<sup>2</sup>.

Further we have also plotted  $F_{2,c}^{\text{asympt}}$  (see above (3.1)). As expected from Figs. 5,6 this function approaches  $F_{2,c}^{\text{exact}}$  when  $Q^2$  gets very large. We did not plot  $F_{2,c}^{\text{asympt}}$  at  $Q^2 = 3$  (GeV/c)<sup>2</sup> (Fig. 12a) because here it becomes negative for  $x < 0.1$ . From Figs. 12b-e one observes a noticeable difference between  $F_{2,c}^{\text{asympt}}$  and  $F_{2,c}^{\text{VFNS}}$ , which is remarkable since the latter is derived from the former via mass factorization; a procedure which holds in all orders of perturbation theory. In our actual computations  $F_{2,c}^{\text{asympt}}$  has been computed up to order  $\alpha_s^2$  whereas  $F_{2,c}^{\text{VFNS}}$  involves  $\alpha_s^3$  contributions. The latter are due to the convolutions in Eq. (2.60) of the order  $\alpha_s^2$  corrected densities in (3.4),(3.6) and (3.7) with the order  $\alpha_s$  corrected light-parton coefficient functions. Due to the large logarithms these order  $\alpha_s^3$  contributions are quite appreciable and they survive in the region  $3 < Q^2 < 100$  (GeV/c)<sup>2</sup> covered by our plots. The corrections beyond order  $\alpha_s^2$  present in  $F_{2,c}^{\text{VFNS}}$  can be resummed using the RGE's in (2.52)-(2.55). This procedure has been applied to obtain the parton densities in the literature. If we substitute one of them (here we use GRV92HO [19]) in the expression for  $F_{2,c}^{\text{VFNS}}$  in Eq. (2.60) we call the corresponding charm structure function  $F_{2,c}^{\text{PDF}}$ . The results for this function are given in Figs. 12a-e. As can be expected from our discussions above  $F_{2,c}^{\text{PDF}}$  is slightly larger than  $F_{2,c}^{\text{VFNS}}$ . This is not surprising because the parton densities represent the resummation of the large logarithms in all orders of perturbation theory.

We also want to comment on the presentation of the charm structure function in (2.66) originating from (9) in [9] (ACOT). From (2.60) and the definitions for  $F_{i,c}^{\text{exact}}, F_{i,c}^{\text{asympt}}$  given above (3.1) one can easily derive that Eq. (2.66) is nothing but the  $O(\alpha_s)$  approximation to the following expression

$$F_{i,c}^{\text{ACOT}}(x, Q^2, m_c^2) = F_{i,c}^{\text{VFNS}}(x, Q^2) + F_{i,c}^{\text{exact}}(x, Q^2, m_c^2) - F_{i,c}^{\text{asympt}}(x, Q^2, m_c^2). \quad (3.8)$$

Up to  $O(\alpha_s)$ ,  $F_{i,c}^{\text{VFNS}}$  and  $F_{i,c}^{\text{exact}} - F_{i,c}^{\text{asympt}}$  correspond with the first and the last part of (2.66) respectively (for the last part see also (2.67)). In the previous figures we have seen that for  $Q^2 \geq 20$ (GeV/c)<sup>2</sup>,  $F_{i,c}^{\text{exact}}$  approaches  $F_{i,c}^{\text{asympt}}$  so that  $F_{i,c}^{\text{ACOT}}$  coincides with  $F_{i,c}^{\text{VFNS}}$ . Therefore  $F_{i,c}^{\text{ACOT}}$  gives a good description of the charm structure function at large  $Q^2$ -values. However at small  $Q^2$ ,  $F_{i,c}^{\text{VFNS}} \neq F_{i,c}^{\text{asympt}}$  (see Figs .12b-e) so that  $F_{i,c}^{\text{ACOT}}$  is not dominated by  $F_{i,c}^{\text{exact}}$ . Therefore  $F_{i,c}^{\text{ACOT}}$  (3.8) does not have the correct threshold behaviour

exhibited by  $F_{i,c}^{\text{exact}}$ . The inequality between  $F_{i,c}^{\text{VFNS}}$  and  $F_{i,c}^{\text{asympt}}$  is due to the large value of  $\alpha_s(Q^2)$  and the different ways that the corrections beyond  $O(\alpha_s)$  have been included in the latter two functions. In our case  $F_{i,c}^{\text{asympt}}$  is computed up  $O(\alpha_s^2)$  whereas  $F_{i,c}^{\text{VFNS}}$  contains even  $O(\alpha_s^3)$  contributions. If  $F_{i,c}^{\text{VFNS}}$  is replaced by  $F_{i,c}^{\text{PDF}}$  the above inequality becomes even larger since the latter includes all leading contributions in all orders of  $\alpha_s$ . Due to these considerations and the fact that the large logarithms only show up at large  $Q^2$  the expressions for  $F_{i,c}^{\text{VFNS}}$  and  $F_{i,c}^{\text{asympt}}$  have no physical meaning in the threshold region (low  $Q^2$ ). Hence they should be dropped in the latter region so that here the charm structure function is only represented by  $F_{i,c}^{\text{exact}}$ . In fact the EMC data on charm production were recently reexamined by [24] using the NLO results for  $F_{2,c}^{\text{exact}}(x, Q^2, m_c^2)$ . The theoretical results are in excellent agreement with the experimental data, except for one data point.

We have also studied the total structure function  $F_2(x, Q^2)$ , where the charm component is included. Since this structure function is dominated by the light-parton (u,d,s and g) contributions the differences between the various descriptions is much smaller than those observed for the charm component. At maximum these differences are of the order of 10%, which occurs in the region  $5 < Q^2 < 10$  (GeV/c)<sup>2</sup>.

To study the stability of the perturbation series for  $F_{i,c}$  one can proceed in two different ways. The first one is discussed in [9] and concerns the behaviour of the charm structure function with respect to variations in the factorization scale. It was found that near threshold (large  $x$  and small  $Q^2$ )  $F_{2,c}^{\text{exact}}$  shows a better stability than  $F_{2,c}^{\text{VFNS}}$  under variations of the factorization scale. Far above threshold it turns out that just the opposite happens, so that at large  $Q^2$  it is more preferable to use  $F_{2,c}^{\text{VFNS}}$  instead of  $F_{2,c}^{\text{exact}}$  (FOPT). However in the analysis of [9] the NLO corrections from [3] were not taken into account. In [11],[12] and [13] these corrections were included and one could show that far away from threshold  $F_{2,c}^{\text{exact}}$  is as stable as  $F_{2,c}^{\text{VFNS}}$  with respect to variations in the factorization scale. The second way to study the stability of the perturbation series is to look at the actual size of the higher order corrections. They have to decrease when the order in  $\alpha_s$  increases. To be more specific we study the following quantities

$$K_{i,c}^{(l)} = \frac{F_{i,c}^{(l)}(x, Q^2)}{F_{i,c}^{(l-1)}(x, Q^2)}, \quad (3.9)$$

where  $F_{i,c}^{(l)}$  denotes the  $O(\alpha_s^l)$  corrected charm structure function. Our criterion is that the perturbation series gets more stable if  $K_{i,c}^{(l)} \rightarrow 1$  for increasing  $l$ . Here we want to compare  $K_{2,c}^{(1),\text{exact}}$  (FOPT) with  $K_{2,c}^{(l),\text{VFNS}}$  ( $l = 1, 2$ ), which are derived from  $F_{2,c}^{\text{exact}}$  and  $F_{2,c}^{\text{VFNS}}$  respectively. In virtue of the observations made in Figs. 12a-e we replace the latter by  $F_{2,c}^{\text{PDF}}$  because this does not appreciably change the results which we now present. In Figs. 13a-g we plot  $K_{2,c}^{(1),\text{exact}}$ ,  $K_{2,c}^{(1),\text{PDF}}$  and  $K_{2,c}^{(2),\text{PDF}}$ . Here  $K_{2,c}^{(1),\text{exact}}$  is given by the ratio of the NLO over the LO charm structure functions in FOPT using the GRV92-set [19]. The same holds for  $K_{2,c}^{(1),\text{PDF}}$  which is obtained from the NLO over LO approximations to Eq. (2.60). Finally  $K_{2,c}^{(2),\text{PDF}}$  stands for the ratio of the next-to-next-to-leading-order (NNLO) and NLO corrected charm structure functions, where in NNLO only the light-parton coefficient functions of [16] have been included. Notice that the NNLO parton densities are not known yet because the three-loop splitting functions (anomalous dimensions) have not been calculated. From Fig. 13a we infer that for  $Q^2 = 3 \text{ (GeV}/c)^2$ ,  $K_{2,c}^{(1),\text{exact}}$  is rather close to unity over the whole  $x$ -range contrary to  $K_{2,c}^{(l),\text{PDF}}$  ( $l = 1, 2$ ) which deviate from unity in spectacular ways. This shows that one should use FOPT instead of VFNS at small  $Q^2$ . At  $Q^2 = 5 \text{ (GeV}/c)^2$  (see Fig. 13b) the deviation from unity becomes the same for  $K_{2,c}^{(1),\text{exact}}$  and  $K_{2,c}^{(1),\text{PDF}}$  in the small  $x$ -region. However at large  $x$  ( $x > 0.01$ ), which represents the threshold region, the description by FOPT is still superior to the one given by VFNS. This picture changes when  $Q^2 > 10 \text{ (GeV}/c)^2$  (Fig. 13c). In the threshold region ( $x > 0.01$ ) both approaches are equally bad whereas at small  $x$  the VFNS is better than FOPT. The superiority of the VFNS with respect to the FOPT approach becomes even clearer when one looks at Eq. (3.9) plotted at still larger  $Q^2$ -values, which are probably not realizable experimentally, in Figs. 13d-g. This holds for all  $x$ -values including the threshold region. We also notice a considerable improvement when the order  $\alpha_s^2$  corrections are included in  $F_{2,c}^{\text{VFNS}}$ . In particular  $K_{2,c}^{(2),\text{PDF}}$  is much closer to one than  $K_{2,c}^{(1),\text{PDF}}$  at larger  $Q^2$ -values, indicating the rapid convergence of the perturbation series in case of VFNS. From the observations made above we conclude that Eq. (3.9) provides us with a better criterion to determine the predictive power of the perturbation series than the investigation of the stability of the charm structure function under changes in the factorization scale. It shows very clearly that for  $Q^2 > 10 \text{ (GeV}/c)^2$  it is better to use

$F_{2,c}^{\text{VFNS}}$  instead of  $F_{2,c}^{\text{exact}}$  even when  $x$  gets large.

The most important results found in this paper can be summarized as follows. When the charm structure function  $F_{2,c}$  is computed in FOPT for  $Q^2 > 20$  (GeV/c)<sup>2</sup> the results obtained from the exact ( $F_{2,c}^{\text{exact}}$ ) and the asymptotic heavy-quark coefficient functions ( $F_{2,c}^{\text{asympt}}$ ) are indistinguishable. For  $F_{L,c}$  the minimal value of  $Q^2$  becomes larger, say around  $Q^2 = 10^3$  (GeV/c)<sup>2</sup>. Above this minimal value the large logarithms dominate the perturbation series and they can be resummed after having performed mass factorization on the heavy-quark coefficient functions. In this way starting from  $F_{2,c}^{\text{asympt}}$  in the three-flavour scheme one can derive an expression for  $F_{2,c}^{\text{VFNS}}$  valid in the four-flavour scheme. This procedure imposes a relation between the parton density sets parametrized at three and four flavours, which has to be satisfied in the VFNS approach. In the literature the parton density sets (PDF's) do not obey this requirement although in practice this has no serious consequences for the prediction of  $F_{2,c}^{\text{VFNS}}$ , which is almost equal to  $F_{2,c}^{\text{PDF}}$ . Further it turns out that  $F_{2,c}^{\text{VFNS}} > F_{2,c}^{\text{exact}}$  for all  $Q^2$ -values. This can be attributed to the higher-order corrections appearing beyond FOPT which are included in VFNS. Finally we have shown that comparisons between the charm structure functions calculated in different orders in  $\alpha_s$  give better indications about the stability of the perturbation series than a variation in the mass-factorization scale. It turns out that below  $Q^2 = 10$  (GeV/c)<sup>2</sup>,  $F_{2,c}^{\text{exact}}$  (FOPT) gives a better description of the charm structure function whereas above this value it is much better to use  $F_{2,c}^{\text{VFNS}}$ . In particular this holds in the small  $x$ -region under investigation by the HERA experiments.

We stress again that the VFNS is only valid for totally inclusive quantities. At the level of exclusive distributions the large logarithms we have been discussing simply do not exist. If the experimental analysis is carried out on the basis of the photon-gluon fusion model in NLO with three light flavours then we expect that the observed charm contribution  $F_{2,c}(x, Q^2, m^2)$  should agree with the NLO results  $F_{2,c}^{\text{exact}}(x, Q^2, m^2)$  for small  $Q^2$  (say  $Q^2 = 5$  (GeV/c)<sup>2</sup>) and with  $F_{2,c}^{\text{VFNS}}(x, Q^2, m^2)$  for large  $Q^2$  (say  $Q^2 = 100$  (GeV/c)<sup>2</sup>).

Acknowledgements.

W.L. van Neerven enjoyed some discussions about the charm-quark density with A. Vogt. The research of J. Smith and Y. Matiounine was partially supported by the contract NSF 93-09888. J. Smith would like to thank the Alexander von Humbolt Stiftung for an award to allow him to spend his Sabbatical leave at DESY.

## Appendix A

In this appendix we present the unrenormalized operator-matrix elements  $\hat{A}_{gq,H}^{S,(2)}$ ,  $\hat{A}_{gg,H}^{S,(1)}$  and  $\hat{A}_{gg,H}^{S,(2)}$  where  $\hat{A}_{kl,H}^{S,(i)}$  denote the coefficients of  $(\alpha_s/4\pi)^i$  in the perturbation series of the operator-matrix elements (OME's). The corresponding two-loop Feynman graphs are presented in Fig. 3 and Fig. 4 respectively and the calculation proceeds in the same way as is outlined for the other OME's in [10]. Using  $n$ -dimensional regularization for the ultraviolet and collinear divergences the results are given by ( $n = 4 + \epsilon$ )

$$\begin{aligned} \hat{A}_{gq,H}^{S,(2)}\left(\frac{m^2}{\mu^2}, \epsilon\right) &= S_\epsilon^2\left(\frac{m^2}{\mu^2}\right)^\epsilon C_F T_f \left\{ \frac{1}{\epsilon^2} \left[ \frac{64}{3z} - \frac{64}{3} + \frac{32}{3}z \right] \right. \\ &\quad \left. + \frac{1}{\epsilon} \left[ \frac{160}{9z} - \frac{160}{9} + \frac{128}{9}z + \left( \frac{32}{3z} - \frac{32}{3} + \frac{16}{3}z \right) \ln(1-z) \right] \right. \\ &\quad \left. + \frac{4}{3} \left( \frac{2}{z} - 2 + z \right) \ln^2(1-z) + \frac{8}{9} \left( \frac{10}{z} - 10 + 8z \right) \ln(1-z) \right. \\ &\quad \left. + \frac{8}{3} \left( \frac{2}{z} - 2 + z \right) \zeta(2) + \frac{1}{27} \left( \frac{448}{z} - 448 + 344z \right) \right\}. \end{aligned} \quad (\text{A.1})$$

Here  $S_\epsilon$  denotes the spherical factor which is given by

$$S_\epsilon = \exp \left\{ \frac{\epsilon}{2} (\gamma_E - \ln 4\pi) \right\}, \quad (\text{A.2})$$

where  $\gamma_E$  is the Euler constant.

$$\hat{A}_{gg,H}^{S,(1)}\left(\frac{m^2}{\mu^2}, \epsilon\right) = S_\epsilon \left(\frac{m^2}{\mu^2}\right)^{\frac{\epsilon}{2}} \left[ \frac{1}{\epsilon} T_f \left( \frac{8}{3} \delta(1-z) \right) \right], \quad (\text{A.3})$$

$$\begin{aligned} \hat{A}_{gg,H}^{S,(2)}\left(\frac{m^2}{\mu^2}, \epsilon\right) &= S_\epsilon^2\left(\frac{m^2}{\mu^2}\right)^\epsilon \left[ \frac{1}{\epsilon^2} \left\{ C_F T_f \left[ 32(1+z) \ln z + \frac{64}{3z} + 16 \right. \right. \right. \\ &\quad \left. \left. - 16z - \frac{64}{3}z^2 \right] + C_A T_f \left[ \frac{32}{3} \left( \frac{1}{1-z} \right)_+ + \frac{32}{3z} - \frac{64}{3} + \frac{32}{3}z - \frac{32}{3}z^2 \right] \right\} \right. \\ &\quad \left. + \frac{1}{\epsilon} \left\{ C_F T_f \left[ 8(1+z) \ln^2 z + (24 + 40z) \ln z - \frac{16}{3z} + 64 - 32z \right] \right\} \right] \end{aligned}$$

$$\begin{aligned}
& -\frac{80}{3}z^2 + 4\delta(1-z) \Big] + C_A T_f \left[ \frac{16}{3}(1+z) \ln z + \frac{80}{9} \left( \frac{1}{1-z} \right)_+ \right. \\
& \left. + \frac{184}{9z} - \frac{232}{9} + \frac{152}{9}z - \frac{184}{9}z^2 + \frac{16}{3}\delta(1-z) \right] \Big\} + a_{gg,H}^{(2)}(z) \Big], \\
& + \sum_{f=H}^t S_\epsilon^2 \left( \frac{m_f^2}{\mu^2} \right)^{\epsilon/2} \left( \frac{m^2}{\mu^2} \right)^{\epsilon/2} \left[ \frac{1}{\epsilon^2} T_f^2 \left\{ \frac{64}{9} \left( 1 + \frac{\epsilon^2}{4} \zeta(2) \right) \delta(1-z) \right\} \right], \quad (\text{A.4})
\end{aligned}$$

with

$$\begin{aligned}
a_{gg,H}^{(2)}(z) &= C_F T_f \left\{ \frac{4}{3}(1+z) \ln^3 z + (6+10z) \ln^2 z + (32+48z) \ln z \right. \\
& \left. + 8(1+z) \zeta(2) \ln z + \left( \frac{16}{3z} + 4 - 4z - \frac{16}{3}z^2 \right) \zeta(2) \right. \\
& \left. - \frac{8}{z} + 80 - 48z - 24z^2 - 15\delta(1-z) \right\} \\
& + C_A T_f \left\{ \frac{4}{3}(1+z) \ln^2 z + \frac{1}{9}(52+88z) \ln z - \frac{4}{3}z \ln(1-z) \right. \\
& \left. + \frac{8}{3} \left[ \left( \frac{1}{1-z} \right)_+ + \frac{1}{z} - 2 + z - z^2 \right] \zeta(2) \right. \\
& \left. + \frac{1}{27} \left[ 224 \left( \frac{1}{1-z} \right)_+ + \frac{556}{z} - 628 + 548z - 700z^2 \right] \right. \\
& \left. + \frac{10}{9} \delta(1-z) \right\}. \quad (\text{A.5})
\end{aligned}$$

The last term in Eq. (A.4), which is proportional to  $T_f^2$ , is due to the one-loop correction to  $\hat{A}_{gg,H}^{\text{S},(1)}$  in Eq. (A.3). This correction is represented by the heavy quark ( $f$ ) loop contribution to the gluon self energy where  $f$  represents all heavy flavours starting with the quark  $H$  ( $m_H \equiv m$ ) and ending with the top quark  $t$ . The corresponding graph is not shown in Fig. 4. In the next section the renormalization of the OME  $\hat{A}_{gg,H}^{\text{S}}$  will be chosen in such a way that the heavy quarks with  $m_f > m$  decouple from the running coupling constant. This implies that the contributions in the sum of Eq. (A.4) with  $f > H$  completely vanish in the renormalized OME  $\hat{A}_{gg,H}^{\text{S}}$  presented in the next section. However the contribution due to  $f = H$  remains in the renormalized

expressions like those coming from the  $n_f$  light flavours. This renormalization prescription implies that the running coupling constant is presented in the  $\overline{\text{MS}}$ -scheme and it depends on  $n_f + 1$  light flavours including the heavy quark  $H$ .

The  $1/(1 - z)_+$  terms appearing in Eqs. (A.4) and (A.5) have to be understood as distributions, namely

$$\int_0^1 dz \left( \frac{1}{1 - z} \right)_+ f(z) = \int_0^1 dz \frac{1}{1 - z} [f(z) - f(1)]. \quad (\text{A.6})$$

The colour factors in  $SU(N)$  are given by

$$C_F = \frac{N^2 - 1}{2N} \quad C_A = N \quad T_f = \frac{1}{2}, \quad (\text{A.7})$$

with  $N = 3$  for QCD.

## Appendix B

Here we present the renormalized operator-matrix elements (OME's) corresponding to the unrenormalized expressions given in Appendix C of [10] and in Appendix A of this paper. All OME'S have been renormalized in the  $\overline{\text{MS}}$ -scheme. In particular the renormalized coupling constant is presented in the above scheme for  $n_f + 1$  light flavours. Here the heavy quark  $H$  is treated on the same footing as the light flavours and it is not decoupled from the running coupling constant in the VFNS approach. The  $(\alpha_s/4\pi)^2$  coefficient in the heavy-quark OME  $\tilde{A}_{Hq}^{\text{PS}}$  is given by

$$\begin{aligned}
\tilde{A}_{Hq}^{\text{PS},(2)}\left(\frac{m^2}{\mu^2}\right) = C_F T_f \left\{ \left[ -8(1+z) \ln z - \frac{16}{3z} - 4 \right. \right. \\
+ 4z + \frac{16}{3}z^2 \left. \right] \ln^2 \frac{m^2}{\mu^2} + \left[ 8(1+z) \ln^2 z - \left( 8 + 40z + \frac{64}{3}z^2 \right) \ln z \right. \\
\left. - \frac{160}{9z} + 16 - 48z + \frac{448}{9}z^2 \right] \ln \frac{m^2}{\mu^2} \\
+ (1+z) \left[ 32S_{1,2}(1-z) + 16 \ln z \text{Li}_2(1-z) - 16\zeta(2) \ln z \right. \\
\left. - \frac{4}{3} \ln^3 z \right] + \left( \frac{32}{3z} + 8 - 8z - \frac{32}{3}z^2 \right) \text{Li}_2(1-z) \\
+ \left( -\frac{32}{3z} - 8 + 8z + \frac{32}{3}z^2 \right) \zeta(2) + \left( 2 + 10z + \frac{16}{3}z^2 \right) \ln^2 z \\
\left. - \left( \frac{56}{3} + \frac{88}{3}z + \frac{448}{9}z^2 \right) \ln z - \frac{448}{27z} - \frac{4}{3} - \frac{124}{3}z + \frac{1600}{27}z^2 \right\}, \quad (\text{B.1})
\end{aligned}$$

The  $(\alpha_s/4\pi)$  and the  $(\alpha_s/4\pi)^2$  coefficients of the heavy quark OME  $\tilde{A}_{Hg}^{\text{S}}$  are

$$\tilde{A}_{Hg}^{\text{S},(1)}\left(\frac{m^2}{\mu^2}\right) = T_f \left[ -4(z^2 + (1-z)^2) \ln \frac{m^2}{\mu^2} \right], \quad (\text{B.2})$$

and



$$\begin{aligned}
\tilde{A}_{Hg}^{S,(2)}\left(\frac{m^2}{\mu^2}\right) = & \left\{ C_F T_f [(8 - 16z + 16z^2) \ln(1 - z) \right. \\
& - (4 - 8z + 16z^2) \ln z - (2 - 8z)] \\
& + C_A T_f \left[ -(8 - 16z + 16z^2) \ln(1 - z) - (8 + 32z) \ln z \right. \\
& \left. - \frac{16}{3z} - 4 - 32z + \frac{124}{3} z^2 \right] + T_f^2 \left[ -\frac{16}{3} (z^2 + (1 - z)^2) \right] \left. \right\} \ln^2 \frac{m^2}{\mu^2} \\
& + \left\{ C_F T_f \left[ (8 - 16z + 16z^2) [2 \ln z \ln(1 - z) - \ln^2(1 - z) + 2\zeta(2)] \right. \right. \\
& - (4 - 8z + 16z^2) \ln^2 z - 32z(1 - z) \ln(1 - z) \\
& \left. \left. - (12 - 16z + 32z^2) \ln z - 56 + 116z - 80z^2 \right] \right. \\
& + C_A T_f \left[ (16 + 32z + 32z^2) [\text{Li}_2(-z) + \ln z \ln(1 + z)] \right. \\
& + (8 - 16z + 16z^2) \ln^2(1 - z) + (8 + 16z) \ln^2 z \\
& + 32z\zeta(2) + 32z(1 - z) \ln(1 - z) - \left( 8 + 64z + \frac{352}{3} z^2 \right) \ln z \\
& \left. \left. - \frac{160}{9z} + 16 - 200z + \frac{1744}{9} z^2 \right] \right\} \ln \frac{m^2}{\mu^2} \\
& + C_F T_f \left\{ (1 - 2z + 2z^2) [8\zeta(3) + \frac{4}{3} \ln^3(1 - z) \right. \\
& - 8 \ln(1 - z) \text{Li}_2(1 - z) + 8\zeta(2) \ln z - 4 \ln z \ln^2(1 - z) \\
& + \frac{2}{3} \ln^3 z - 8 \ln z \text{Li}_2(1 - z) + 8 \text{Li}_3(1 - z) - 24 \text{S}_{1,2}(1 - z)] \\
& + z^2 \left[ -16\zeta(2) \ln z + \frac{4}{3} \ln^3 z + 16 \ln z \text{Li}_2(1 - z) + 32 \text{S}_{1,2}(1 - z) \right] \\
& - (4 + 96z - 64z^2) \text{Li}_2(1 - z) - (4 - 48z + 40z^2) \zeta(2) \\
& - (8 + 48z - 24z^2) \ln z \ln(1 - z) + (4 + 8z - 12z^2) \ln^2(1 - z) \\
& - (1 + 12z - 20z^2) \ln^2 z - (52z - 48z^2) \ln(1 - z) \\
& \left. \left. - (16 + 18z + 48z^2) \ln z + 26 - 82z + 80z^2 \right\} \right.
\end{aligned}$$

$$\begin{aligned}
& +C_A T_f \left\{ (1 - 2z + 2z^2) \left[ -\frac{4}{3} \ln^3(1 - z) \right. \right. \\
& + 8 \ln(1 - z) \text{Li}_2(1 - z) - 8 \text{Li}_3(1 - z) \left. \right] + (1 + 2z + 2z^2) \\
& \times [-8\zeta(2) \ln(1 + z) - 16 \ln(1 + z) \text{Li}_2(-z) - 8 \ln z \ln^2(1 + z) \\
& + 4 \ln^2 z \ln(1 + z) + 8 \ln z \text{Li}_2(-z) - 8 \text{Li}_3(-z) - 16 \text{S}_{1,2}(-z)] \\
& + (16 + 64z) [2\text{S}_{1,2}(1 - z) + \ln z \text{Li}_2(1 - z)] - \left( \frac{4}{3} + \frac{8}{3} z \right) \ln^3 z \\
& + (8 - 32z + 16z^2) \zeta(3) - (16 + 64z) \zeta(2) \ln z + (16 + 16z^2) \\
& \times [\text{Li}_2(-z) + \ln z \ln(1 + z)] + \left( \frac{32}{3z} + 12 + 64z - \frac{272}{3} z^2 \right) \text{Li}_2(1 - z) \\
& - \left( 12 + 48z - \frac{260}{3} z^2 + \frac{32}{3z} \right) \zeta(2) - 4z^2 \ln z \ln(1 - z) \\
& - (2 + 8z - 10z^2) \ln^2(1 - z) + \left( 2 + 8z + \frac{46}{3} z^2 \right) \ln^2 z \\
& + (4 + 16z - 16z^2) \ln(1 - z) - \left( \frac{56}{3} + \frac{172}{3} z + \frac{1600}{9} z^2 \right) \ln z \\
& \left. - \frac{448}{27z} - \frac{4}{3} - \frac{628}{3} z + \frac{6352}{27} z^2 \right\}, \tag{B.3}
\end{aligned}$$

respectively. Now we present the renormalized expressions for the heavy-quark loop contributions to the light-parton OME's denoted by  $A_{kl,H}$ . The coefficients of the  $(\alpha_s/4\pi)^2$  terms in  $A_{qq,H}$  and  $A_{gq,H}$  are

$$\begin{aligned}
A_{qq,H}^{\text{NS},(2)} \left( \frac{m^2}{\mu^2} \right) &= C_F T_f \left\{ \left[ \frac{8}{3} \left( \frac{1}{1-z} \right)_+ - \frac{4}{3} - \frac{4}{3} z + 2\delta(1-z) \right] \ln^2 \frac{m^2}{\mu^2} \right. \\
& + \left[ \frac{80}{9} \left( \frac{1}{1-z} \right)_+ + \frac{8}{3} \frac{1+z^2}{1-z} \ln z + \frac{8}{9} - \frac{88}{9} z \right. \\
& \left. + \delta(1-z) \left( \frac{16}{3} \zeta(2) + \frac{2}{3} \right) \right] \ln \frac{m^2}{\mu^2} \\
& + \frac{1+z^2}{1-z} \left( \frac{2}{3} \ln^2 z + \frac{20}{9} \ln z \right) \\
& \left. + \frac{8}{3} (1-z) \ln z + \frac{224}{27} \left( \frac{1}{1-z} \right)_+ + \frac{44}{27} - \frac{268}{27} z \right\}
\end{aligned}$$

$$+\delta(1-z)\left(-\frac{8}{3}\zeta(3)+\frac{40}{9}\zeta(2)+\frac{73}{18}\right)\}, \quad (\text{B.4})$$

and

$$\begin{aligned} A_{gq,H}^{\text{S,(2)}}\left(\frac{m^2}{\mu^2}\right) &= C_F T_f \left\{ \left[ \frac{16}{3z} - \frac{16}{3} + \frac{8}{3}z \right] \ln^2 \frac{m^2}{\mu^2} \right. \\ &+ \left[ \frac{160}{9z} - \frac{160}{9} + \frac{128}{9}z + \left( \frac{32}{3z} - \frac{32}{3} + \frac{16}{3}z \right) \ln(1-z) \right] \ln \frac{m^2}{\mu^2} \\ &+ \frac{4}{3} \left( \frac{2}{z} - 2 + z \right) \ln^2(1-z) + \frac{8}{9} \left( \frac{10}{z} - 10 + 8z \right) \ln(1-z) \\ &\left. + \frac{1}{27} \left( \frac{448}{z} - 448 + 344z \right) \right\}. \quad (\text{B.5}) \end{aligned}$$

respectively. The coefficients of the  $\alpha_s/4\pi$  and  $(\alpha_s/4\pi)^2$  terms in  $A_{gg,H}$  are

$$A_{gg,H}^{\text{S,(1)}}\left(\frac{m^2}{\mu^2}\right) = T_f \left[ \frac{4}{3} \delta(1-z) \ln \frac{m^2}{\mu^2} \right], \quad (\text{B.6})$$

and

$$\begin{aligned} A_{gg,H}^{\text{S,(2)}}\left(\frac{m^2}{\mu^2}\right) &= \left\{ C_F T_f \left[ 8(1+z) \ln z + \frac{16}{3z} + 4 - 4z - \frac{16}{3}z^2 \right] \right. \\ &+ C_A T_f \left[ \frac{8}{3} \left( \frac{1}{1-z} \right)_+ + \frac{8}{3z} - \frac{16}{3} + \frac{8}{3}z - \frac{8}{3}z^2 \right] \\ &\left. + T_f^2 \left[ \frac{16}{9} \delta(1-z) \right] \right\} \ln^2 \frac{m^2}{\mu^2} \\ &+ \left\{ C_F T_f \left[ 8(1+z) \ln^2 z + (24 + 40z) \ln z - \frac{16}{3z} + 64 - 32z \right. \right. \\ &- \left. \frac{80}{3}z^2 + 4\delta(1-z) \right] + C_A T_f \left[ \frac{16}{3}(1+z) \ln z + \frac{80}{9} \left( \frac{1}{1-z} \right)_+ \right. \\ &\left. + \frac{184}{9z} - \frac{232}{9} + \frac{152}{9}z - \frac{184}{9}z^2 + \frac{16}{3} \delta(1-z) \right] \right\} \ln \frac{m^2}{\mu^2} \\ &+ C_F T_f \left\{ \frac{4}{3} (1+z) \ln^3 z + (6 + 10z) \ln^2 z + (32 + 48z) \ln z \right. \end{aligned}$$

$$\begin{aligned}
& -\frac{8}{z} + 80 - 48z - 24z^2 - 15\delta(1-z) \Big\} \\
& + C_{AT_f} \Big\{ \frac{4}{3}(1+z) \ln^2 z + \frac{1}{9}(52 + 88z) \ln z - \frac{4}{3}z \ln(1-z) \\
& + \frac{1}{27} \left[ 224 \left( \frac{1}{1-z} \right)_+ + \frac{556}{z} - 628 + 548z - 700z^2 \right] \\
& + \frac{10}{9} \delta(1-z) \Big\}, \tag{B.7}
\end{aligned}$$

respectively.

The definitions for the polylogarithms  $\text{Li}_n(z)$  and the Nielsen functions  $\text{S}_{n,p}(z)$ , which appear in the above expressions, can be found in [25]. We have checked that the renormalized OME's given above satisfy the sum rules presented in Eqs. (2.43) and (2.44). This provides us with a strong check on our results in [10] and in this paper.

## References

- [1] E. Witten, Nucl. Phys. **B104** (1976) 445.  
J. Babcock and D. Sivers, Phys. Rev. **D18** (1978) 2301.  
M.A. Shifman, A.I. Vainstein and V.J. Zakharov, Nucl. Phys. **B136** (1978) 157.  
M. Glück and E. Reya, Phys. Lett. **B83** (1979) 98.  
J.V. Leveille and T. Weiler, Nucl. Phys. **B147** (1979) 147.
- [2] R.K. Ellis and P. Nason, Nucl. Phys. **B312** (1989) 551.  
J. Smith and W.L. van Neerven, Nucl. Phys. **B374** (1992) 36.
- [3] E. Laenen, S. Riemersma, J. Smith and W.L. van Neerven, Nucl. Phys. **B392** (1993) 162.  
S. Riemersma, J. Smith and W.L. van Neerven, Phys. Lett. **B347** (1995) 43.  
B.W. Harris and J. Smith, Nucl. Phys. **B452** (1995) 109.
- [4] S.J. Brodsky, P. Hoyer, A.H. Mueller, W.-K. Tang, Nucl. Phys. **B369** (1992) 519.  
R. Vogt and S.J. Brodsky, Nucl. Phys. **B438**, (1995) 261.
- [5] S. Aid et al. (H1-collaboration), Nucl. Phys. **B472** (1996) 32.
- [6] C. Adloff et al. (H1-collaboration), DESY-96-138, hep-ex/9607012.
- [7] S. Riemersma, J. Smith and W.L. van Neerven, Phys. Lett. **B282** (1992) 171.  
S. Frixione et al. Nucl. Phys. **B412**, (1994) 225; **B431**, (1994) 453.
- [8] M. Glück, E. Hoffmann and E. Reya, Z. Phys. **C13** (1982) 119.  
M. Glück, R.M. Godbole and E. Reya, Z. Phys. **C38** (1988) 441.
- [9] M.A.G. Aivazis, J.C. Collins, F.I. Olness and W.-K. Tung, Phys. Rev. **D50** (1994) 3102.
- [10] M. Buza, Y. Matiounine, J. Smith, R. Migneron and W.L. van Neerven, Nucl. Phys. **B472** (1996) 611.
- [11] M. Glück, E. Reya and M. Stratmann, Nucl. Phys. **B422** (1994) 37.

- [12] A. Vogt, DESY-96-012, hep-ph/9601352.
- [13] F.I. Olness and S.T. Riemersma, Phys. Rev. **D51** (1995) 4746.
- [14] G. Kramer, B. Lampe and H. Spiesberger, Z. Phys. **C72** (1996) 99.
- [15] G. Curci, W. Furmanski and R. Petronzio, Nucl. Phys. **B175** (1980) 27.  
W. Furmanski and R. Petronzio, Phys. Lett. **B97** (1980) 437; Z. Phys. **C11** (1982) 293.
- [16] E.B. Zijlstra and W.L. van Neerven, Nucl. Phys. **B383** (1992) 525.
- [17] M. Glück, E. Reya and A. Vogt, Z. Phys. **C67** (1995) 433.
- [18] P.J. Rijken and W.L. van Neerven, Phys. Rev. **D52** (1995) 149.
- [19] M. Glück, E. Reya and A. Vogt, Z. Phys. **C53** (1992) 127.
- [20] E.B. Zijlstra and W.L. van Neerven, Nucl. Phys. **B417** (1994) 61.
- [21] J. Blümlein, S. Riemersma, W.L. van Neerven and A. Vogt, Nucl. Phys. **B** (Proc. Suppl.) 51. **51C** (1996) 96. J. Blümlein et al. , DESY 96-199, hep-ph/9609400, To appear in the proceedings of the workshop "Future Physics at HERA", DESY, Hamburg, 1996.
- [22] H.L. Lai et al. (CTEQ-collaboration), Phys. Rev. **D51** (1995) 4763.
- [23] A.D. Martin, R.G. Roberts and W.J. Stirling, DTP/96/44, RAL-TR-96-037, hep-ph/9606345.
- [24] B.W. Harris, J. Smith and R. Vogt, Nucl. Phys. **B461** (1996) 181.
- [25] L. Lewin, "Polylogarithms and Associated Functions", North Holland, Amsterdam, 1983.  
R. Barbieri, J.A. Mignaco and E. Remiddi, Nuovo Cimento **11A** (1972) 824.  
A. Devoto and D.W. Duke, Riv. Nuovo. Cimento Vol. 7,N. 6 (1984) 1.

## Figure Captions

- Fig. 1.**  $O(\alpha_s^2)$  contributions to the purely-singlet parton structure function  $\mathcal{F}_{i,q}^{\text{PS}}$  representing the subprocess  $\gamma^* + q \rightarrow q + q' + \bar{q}'$ . Here  $q$  and  $q'$  are represented by the dashed and solid lines respectively. In the case of heavy-quark production  $q' = H$  and these graphs contribute to the heavy-quark coefficient function  $H_{i,q}^{\text{PS}}$ .
- Fig. 2.**  $O(\alpha_s^2)$  contributions to the purely-singlet OME  $A_{q'q}^{\text{PS}}$ . Here  $q$  and  $q'$  are represented by the dashed and solid lines respectively. In the case of  $q' = H$  these graphs contribute to the heavy-quark OME  $A_{Hq}^{\text{PS}}$ .
- Fig. 3.** Two-loop contribution to the OME  $A_{gq,H}^{\text{S}}$ . The dashed and solid lines represent the light quark  $q$  and the heavy quark  $H$  respectively.
- Fig. 4.** Two-loop graphs contributing to the OME  $A_{gg,H}^{\text{S}}$ . The dashed and solid lines represent the Faddeev-Popov ghost and the heavy quark  $H$  respectively. The graph with the external Faddeev-Popov ghost (fig.4g) has to be included if the sum over the gluon polarization states involves the contributions from unphysical polarizations.
- Fig. 5.**  $R_2(NLO)$  (3.1) plotted as a function of  $Q^2$  at fixed  $x$ ;  $x = 10^{-1}$  (dashed-dotted line),  $x = 10^{-2}$  (dotted line),  $x = 10^{-3}$  (dashed line) and  $x = 10^{-4}$  (solid line).
- Fig. 6.**  $R_2(NLO)$  (3.1) plotted as a function of  $x$  at fixed  $Q^2$ ;  $Q^2 = 10$  (GeV/c)<sup>2</sup> (dotted line),  $Q^2 = 50$  (GeV/c)<sup>2</sup> (dashed line),  $Q^2 = 100$  (GeV/c)<sup>2</sup> (solid line).
- Fig. 7.** Same as in Fig. 5 but now for  $R_L(NLO)$ .
- Fig. 8.** Same as in Fig. 6 but now for  $R_L(NLO)$ .
- Fig. 9.** The ratio  $R_{\text{ch}} = f_{c+\bar{c}}^{\text{VFNS}}/f_{c+\bar{c}}^{\text{PDF}}$  (3.5) as a function of  $\mu^2$  at fixed  $x$  in NLO. The charm densities  $f_{c+\bar{c}}^{\text{VFNS}}$  and  $f_{c+\bar{c}}^{\text{PDF}}$  are given by (3.4) and the set GRV92HO [19] respectively;  $x = 10^{-1}$  (dashed-dotted line),  $x = 10^{-2}$  (dotted line),  $x = 10^{-3}$  (dashed line),  $x = 10^{-4}$  (solid line).

**Fig. 10.**  $\Sigma(3, x, \mu^2)$  and  $\Sigma'(4, x, \mu^2)$  (the difference between both singlet combinations of quark densities is unnoticeable in the figure) plotted as functions of  $\mu^2$  at fixed  $x$ ;  $x = 10^{-1}$  (solid line),  $x = 10^{-2}$  (dashed line),  $x = 10^{-3}$  (dotted line),  $x = 10^{-4}$  (dashed-dotted line).

**Fig. 11.**  $G(3, x, \mu^2)$  (lower lines) and  $G(4, x, \mu^2)$  (upper lines) plotted as functions of  $\mu^2$  at fixed  $x$ ;  $x = 10^{-1}$  (dashed-dotted line),  $x = 10^{-2}$  (dotted line),  $x = 10^{-3}$  (dashed line),  $x = 10^{-4}$  (solid line).

**Fig. 12a.** The charm component of the structure function given by  $F_{2,c}$  in NLO as a function of  $x$  at  $Q^2 = 3$  (GeV/c)<sup>2</sup>;  $F_{2,c}^{\text{exact}}(x, Q^2, m^2)$  (solid line),  $F_{2,c}^{\text{VFNS}}(4, x, Q^2)$  (dashed line),  $F_{2,c}^{\text{PDF}}(4, x, Q^2)$  (dotted line) with PDF=GRV92HO.

**Fig. 12b.** The charm component of the structure function given by  $F_{2,c}$  in NLO as a function of  $x$  at  $Q^2 = 5$  (GeV/c)<sup>2</sup>;  $F_{2,c}^{\text{exact}}(x, Q^2, m^2)$  (solid line),  $F_{2,c}^{\text{VFNS}}(4, x, Q^2)$  (dashed line),  $F_{2,c}^{\text{PDF}}(4, x, Q^2)$  (dotted line) with PDF=GRV92HO, and  $F_{2,c}^{\text{asympt}}(x, Q^2, m^2)$  (dashed-dotted line).

**Fig. 12c.** Same as in Fig. 12b but now for  $Q^2 = 10$  (GeV/c)<sup>2</sup>.

**Fig. 12d.** Same as in Fig. 12b but now for  $Q^2 = 50$  (GeV/c)<sup>2</sup>.

**Fig. 12e.** Same as in Fig. 12b but now for  $Q^2 = 100$  (GeV/c)<sup>2</sup>.

**Fig. 13a.** The ratios  $K_{2,c}^{(l)}(x, Q^2)$  (eq.(3.9)) plotted as functions of  $x$  at  $Q^2 = 3$  (GeV/c)<sup>2</sup>;  $K_{2,c}^{(1),\text{exact}}$  (solid line),  $K_{2,c}^{(1),\text{PDF}}$  (dashed line),  $K_{2,c}^{(2),\text{PDF}}$  (dotted line), with PDF=GRV92HO.

**Fig. 13b.** Same as in Fig. 13a but now for  $Q^2 = 5$  (GeV/c)<sup>2</sup>.

**Fig. 13c.** Same as in Fig. 13a but now for  $Q^2 = 10$  (GeV/c)<sup>2</sup>.

**Fig. 13d.** Same as in Fig. 13a but now for  $Q^2 = 50$  (GeV/c)<sup>2</sup>.

**Fig. 13e.** Same as in Fig. 13a but now for  $Q^2 = 100$  (GeV/c)<sup>2</sup>.

**Fig. 13f.** Same as in Fig. 13a but now for  $Q^2 = 10^3$  (GeV/c)<sup>2</sup>.

**Fig. 13g.** Same as in Fig. 13a but now for  $Q^2 = 10^4$  (GeV/c)<sup>2</sup>.



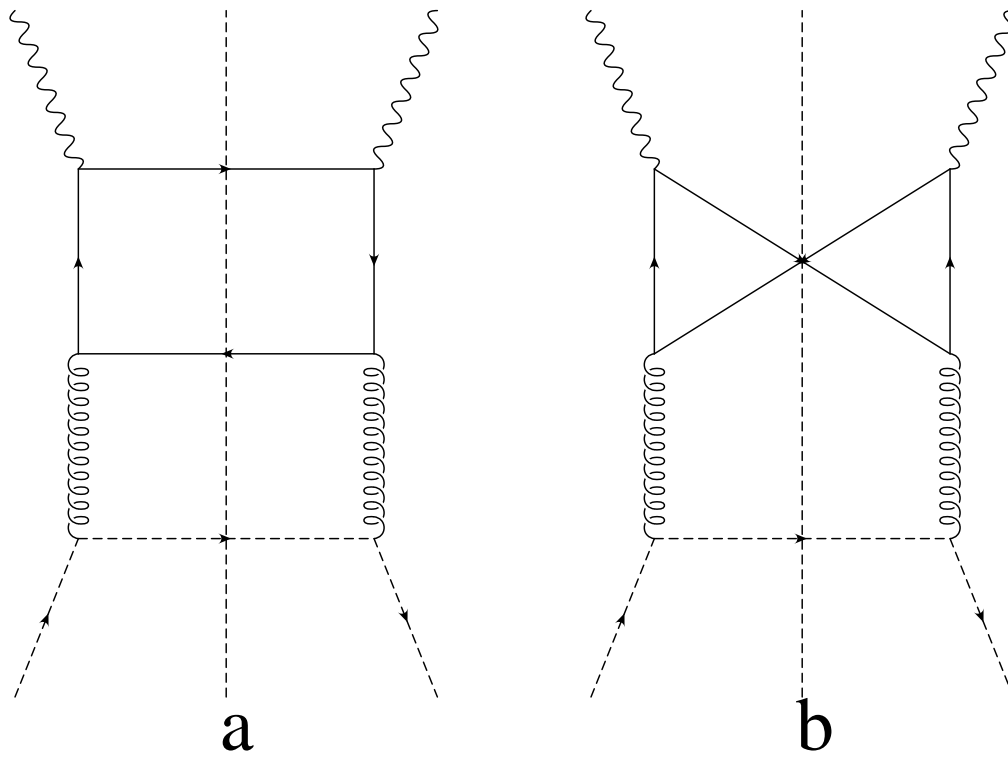


Fig. 1

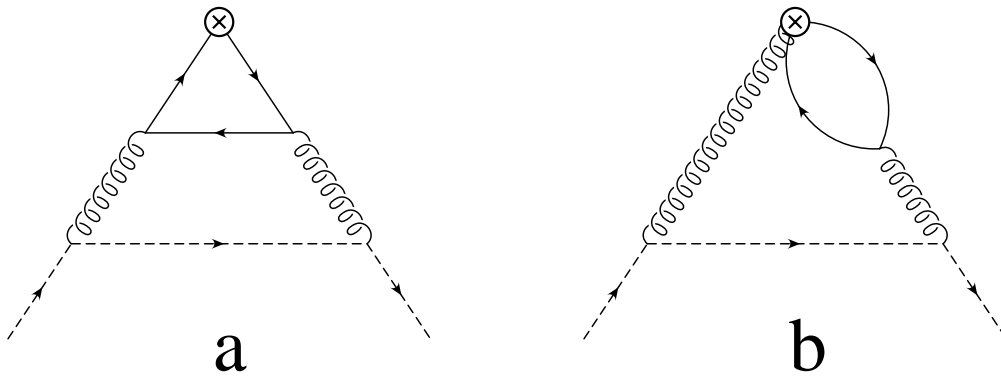


Fig. 2

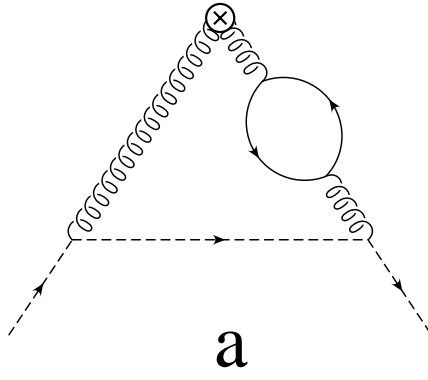
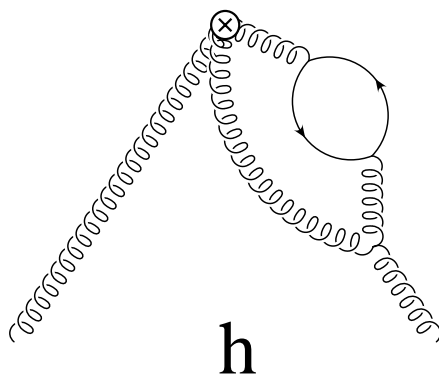
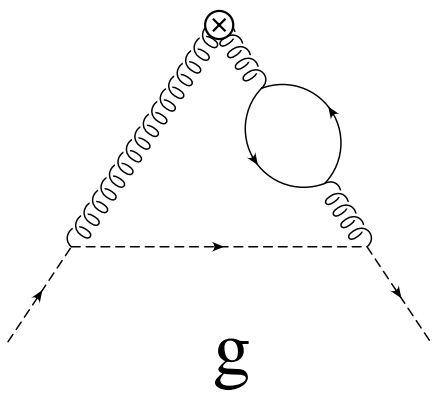
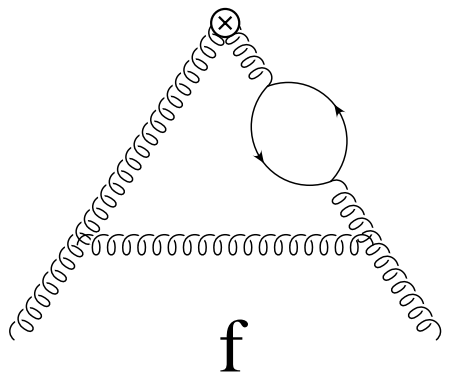
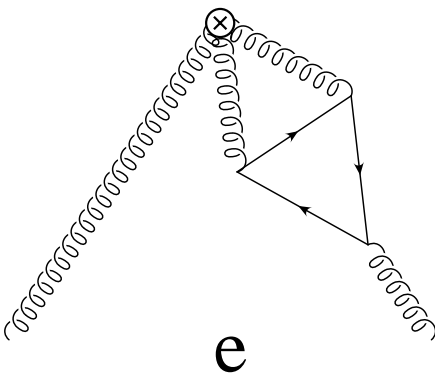
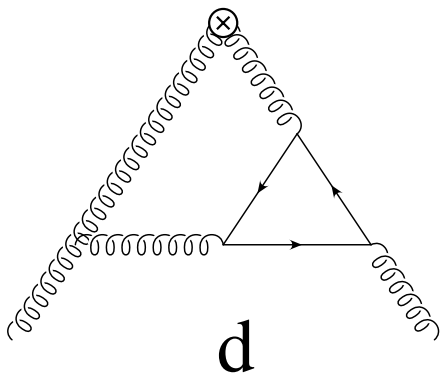
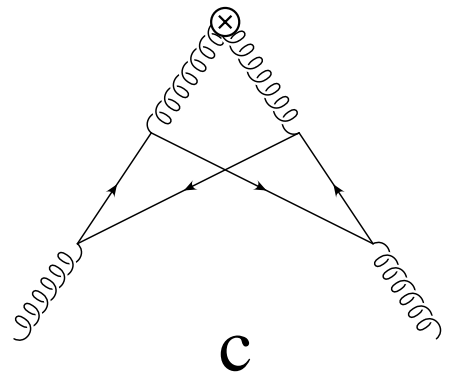
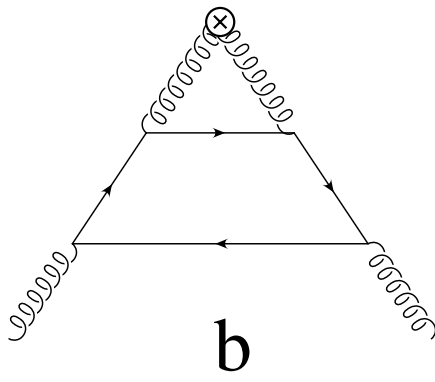
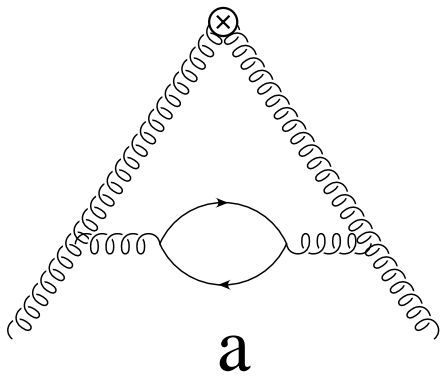


Fig. 3



**Fig. 4**

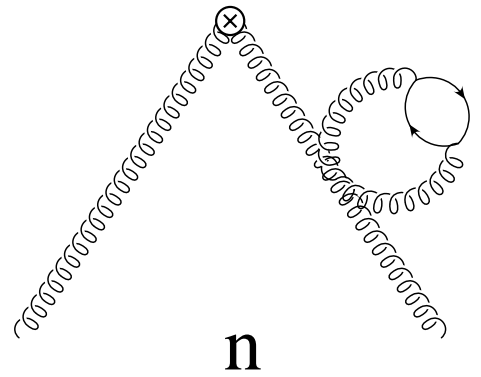
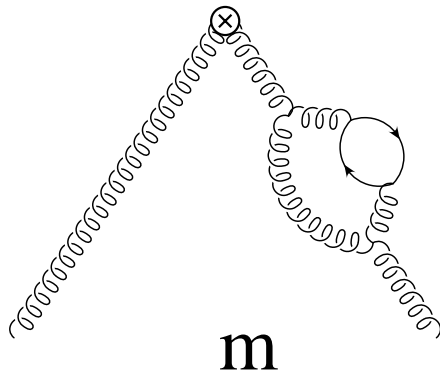
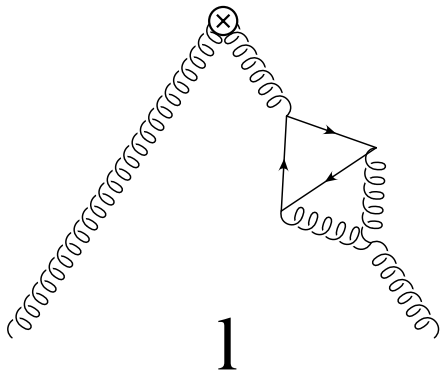
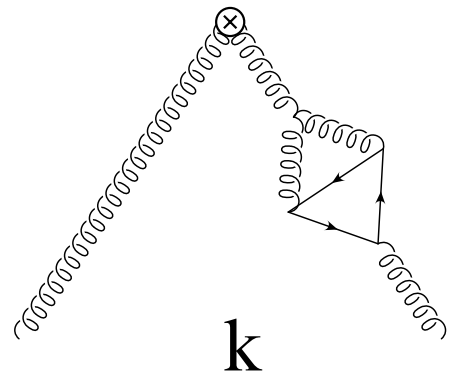
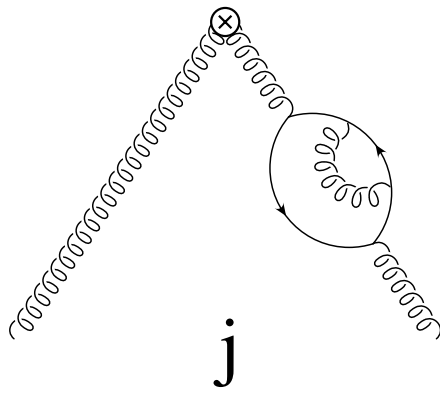
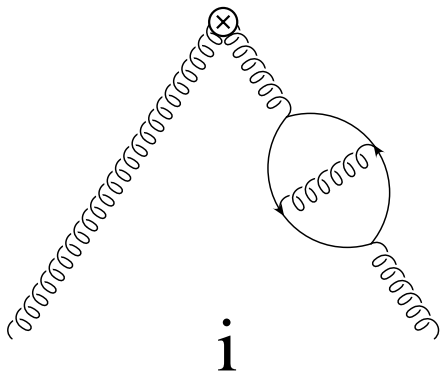


Fig. 4 ( continued )

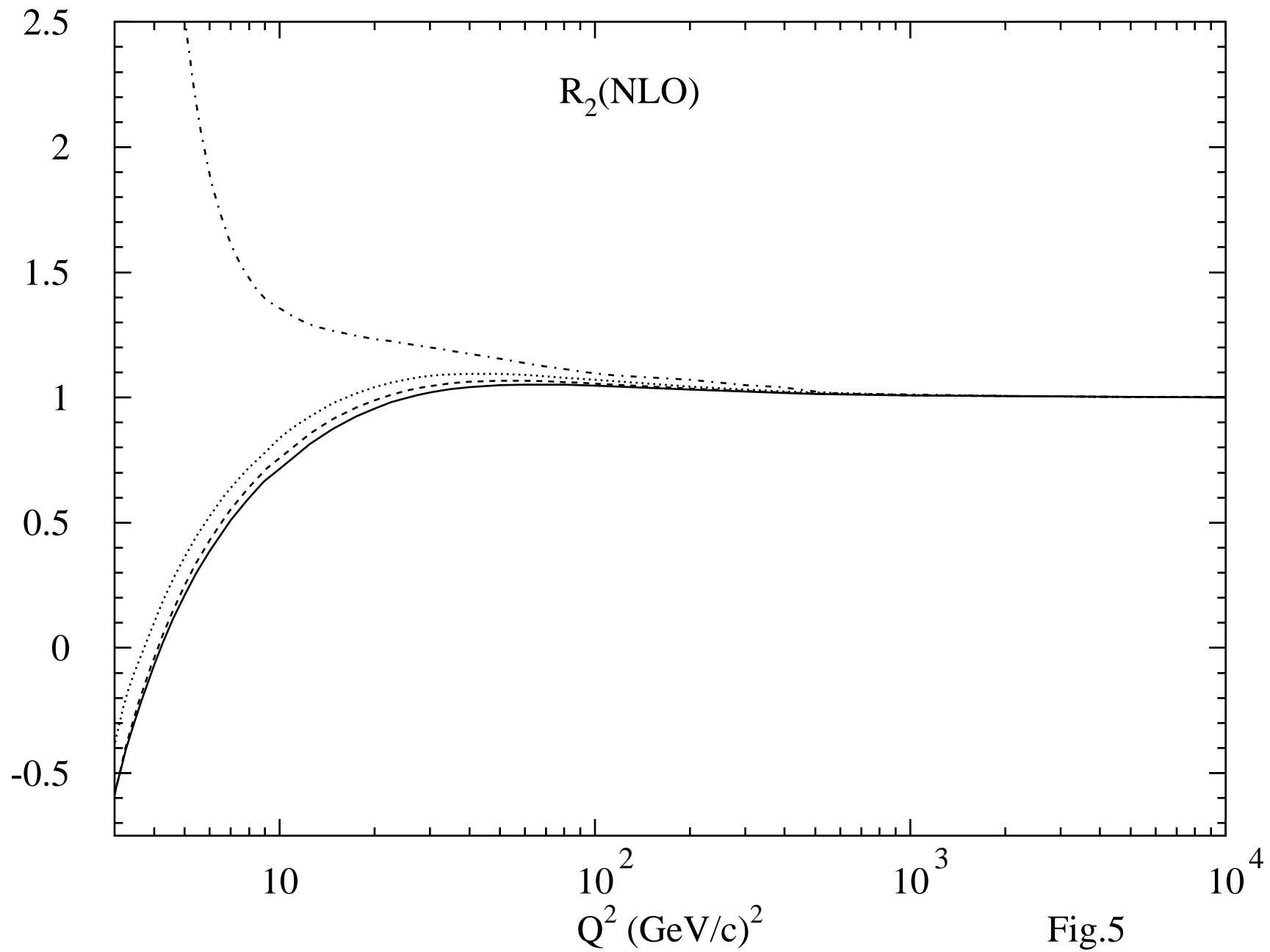
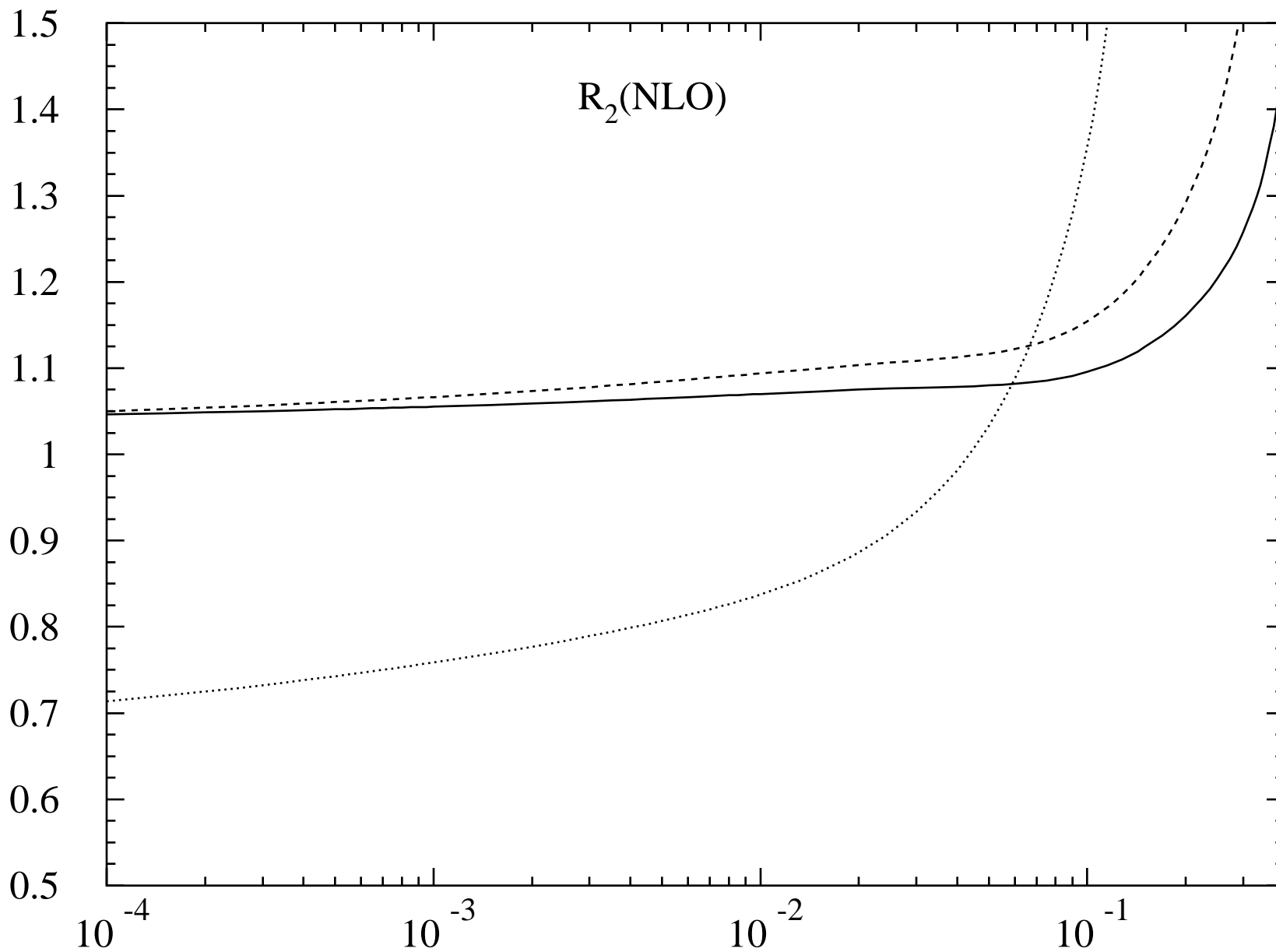


Fig.5



x

Fig.6

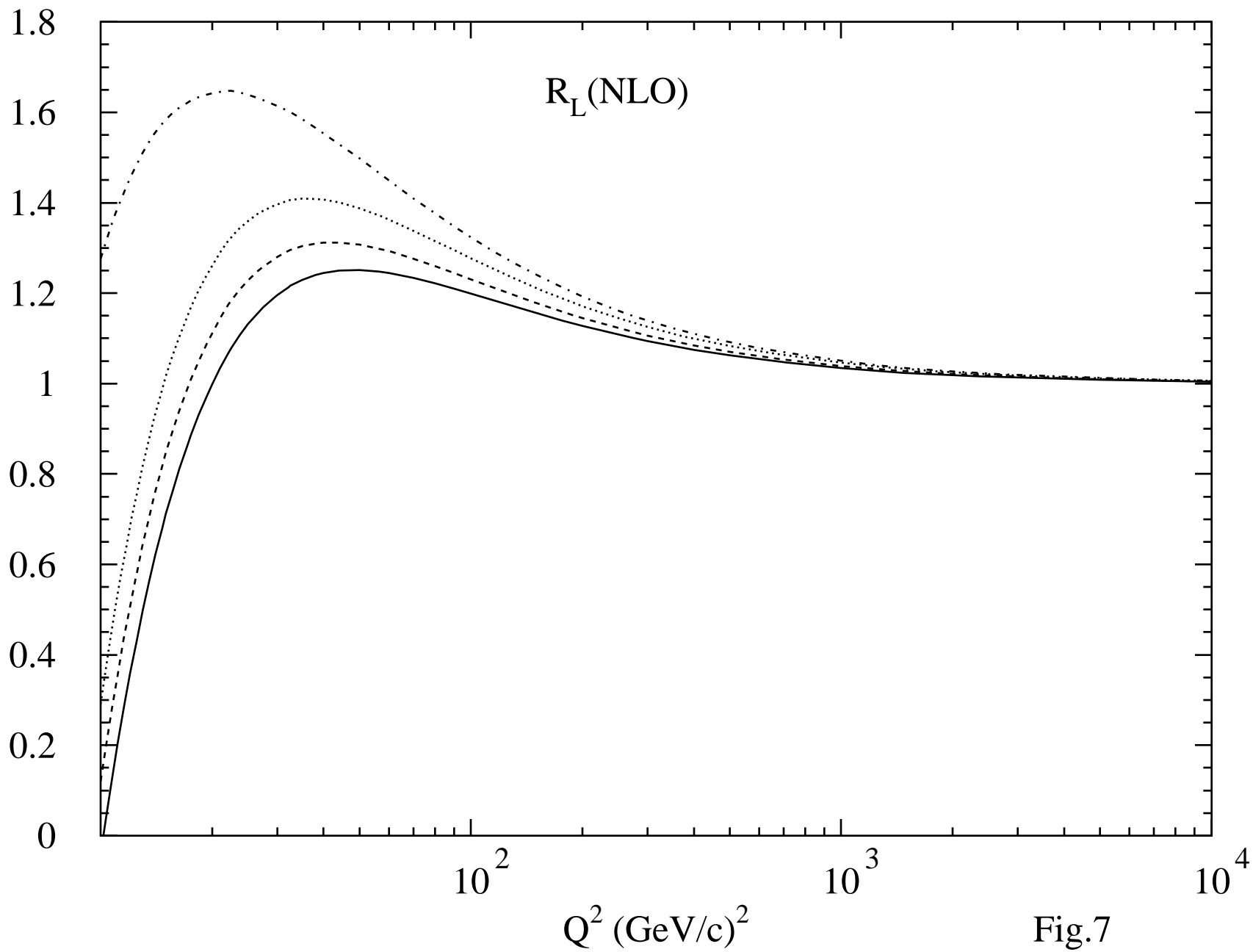


Fig.7



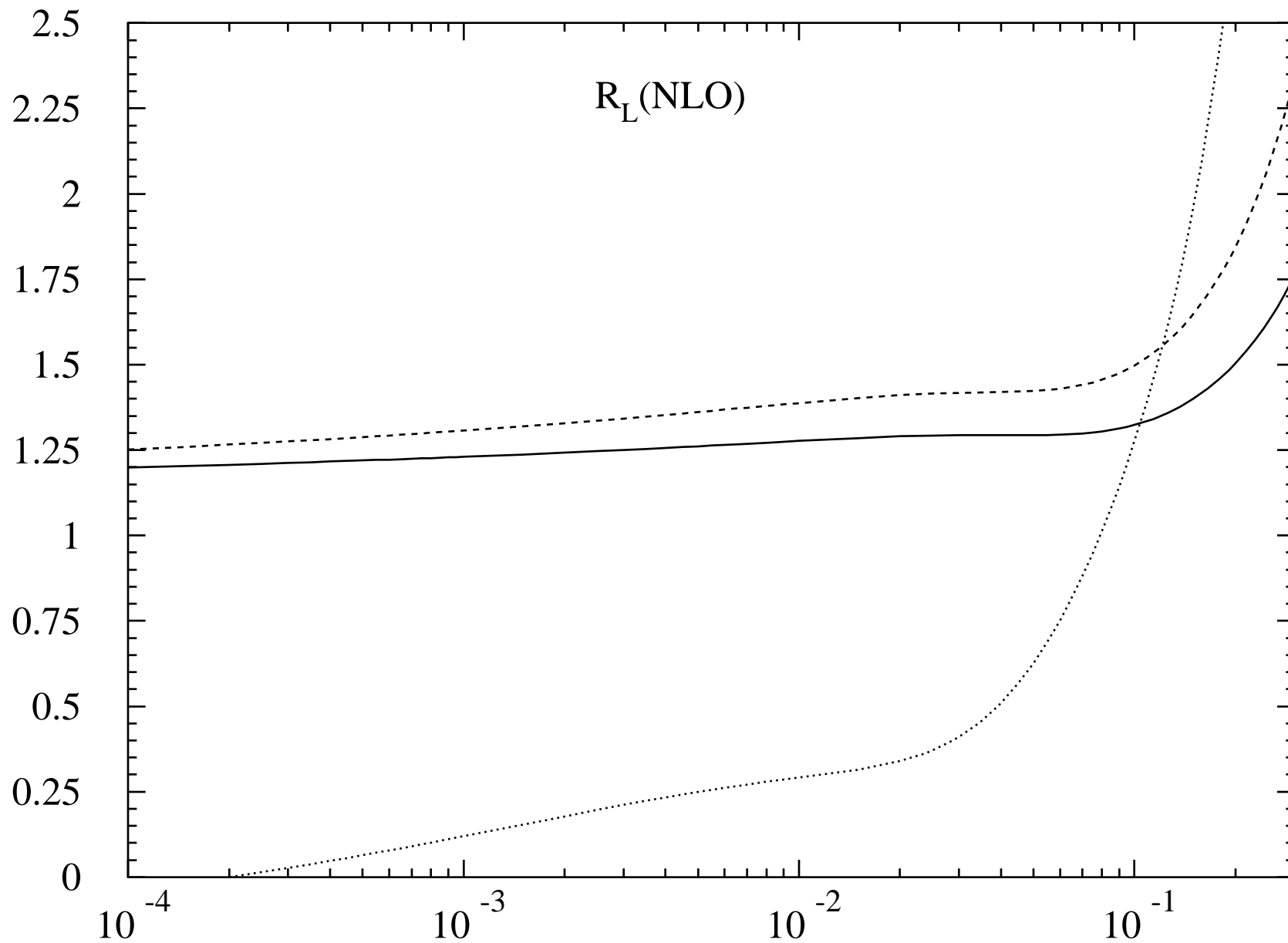


Fig.8

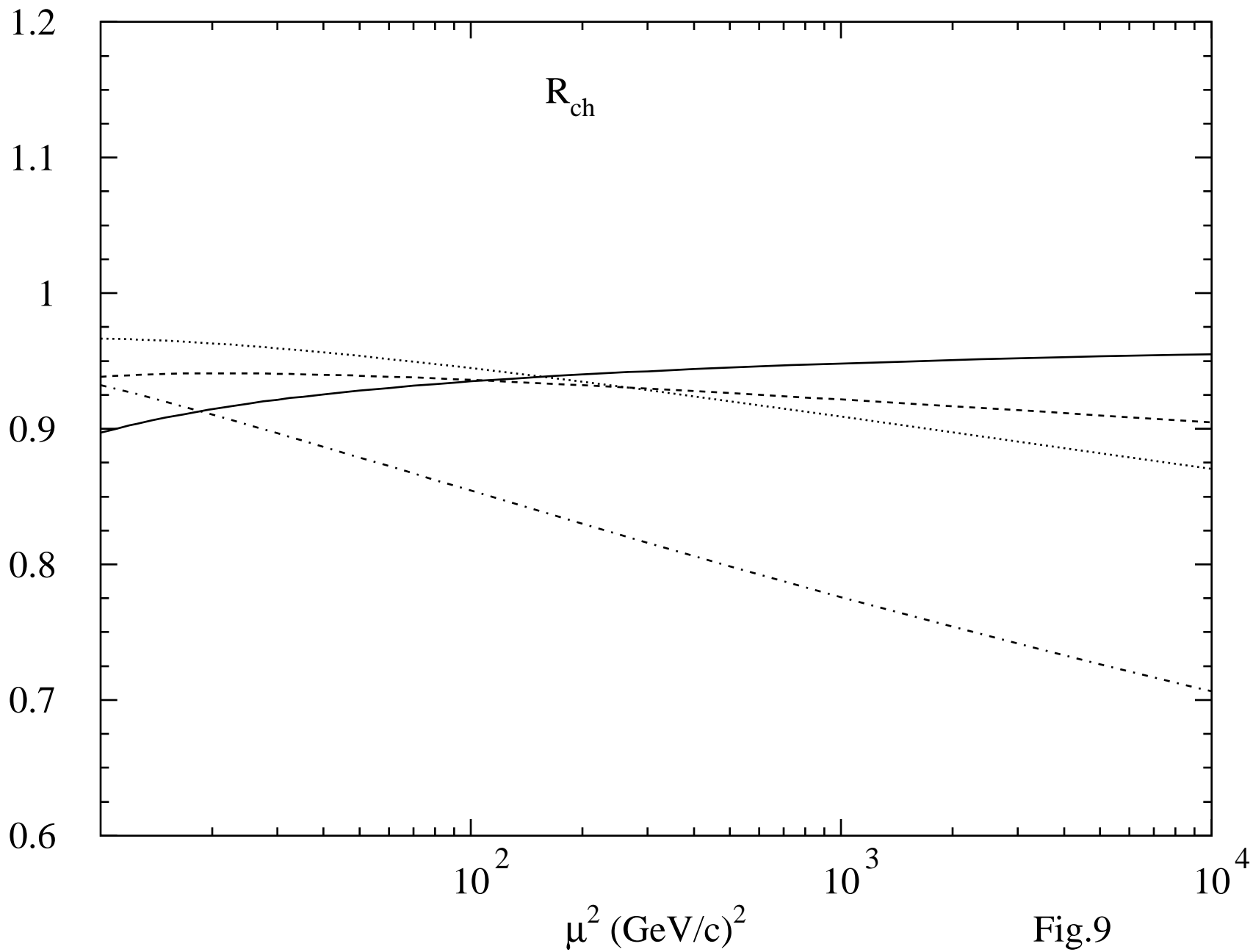


Fig.9

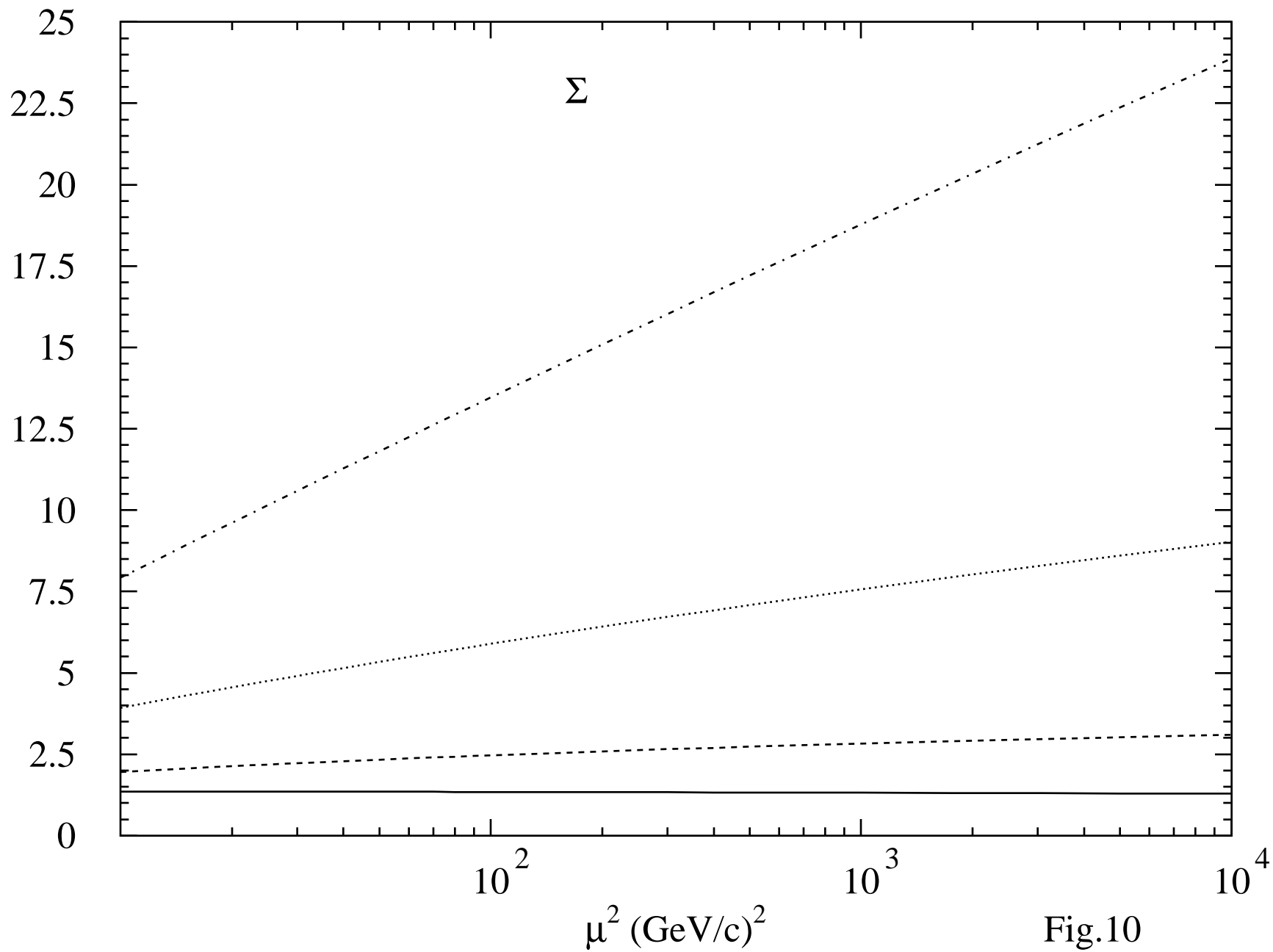


Fig.10

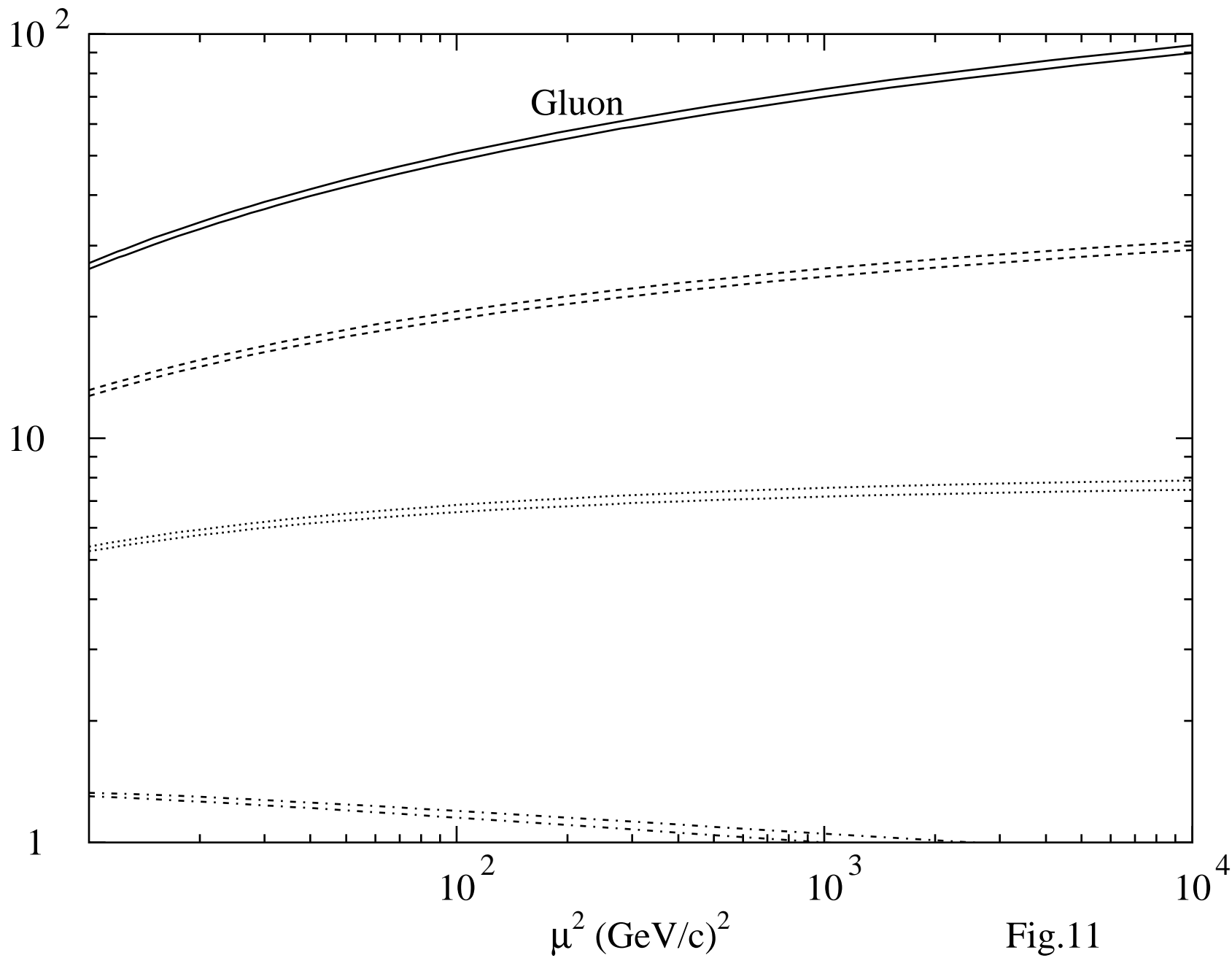
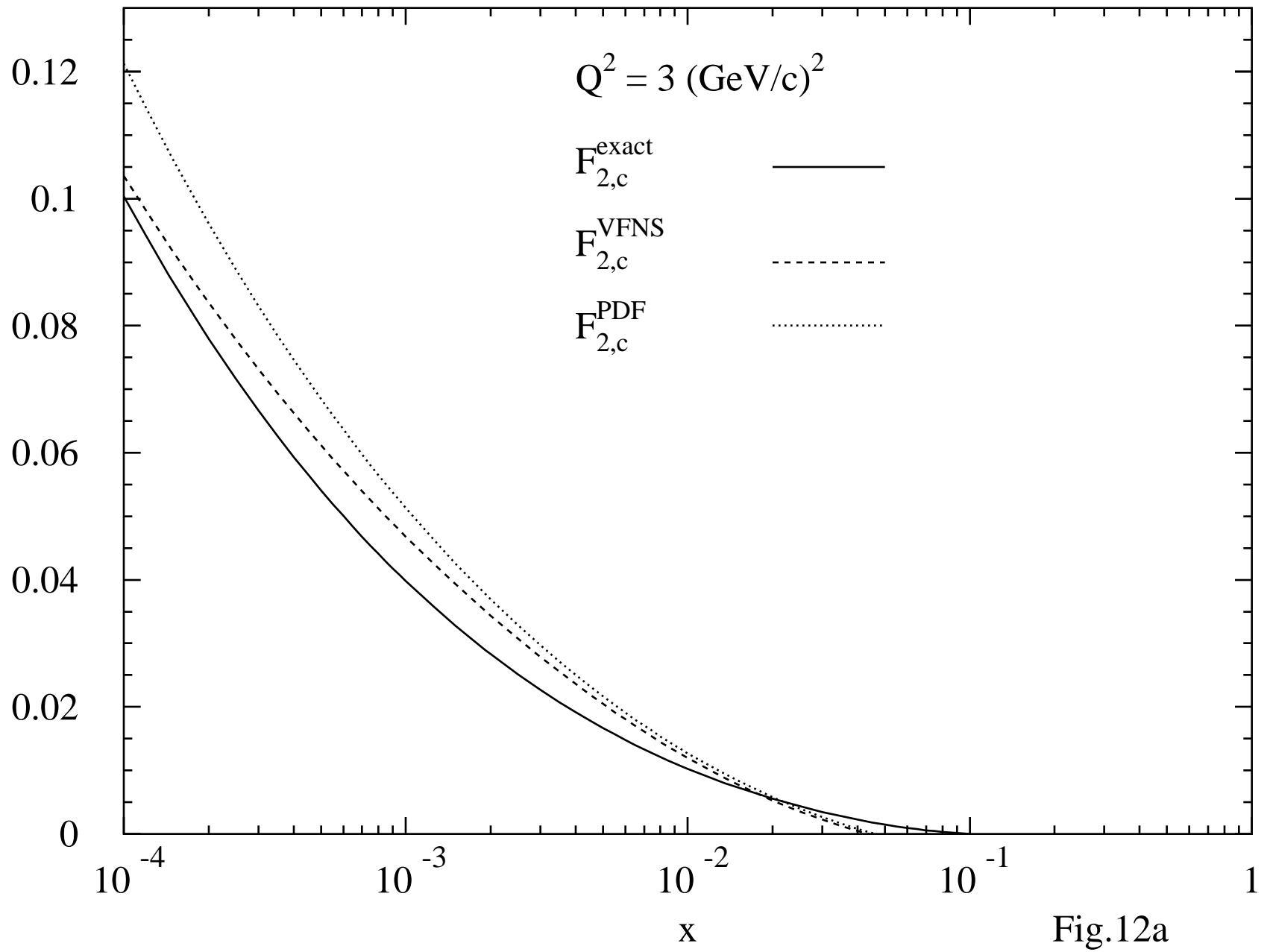


Fig.11



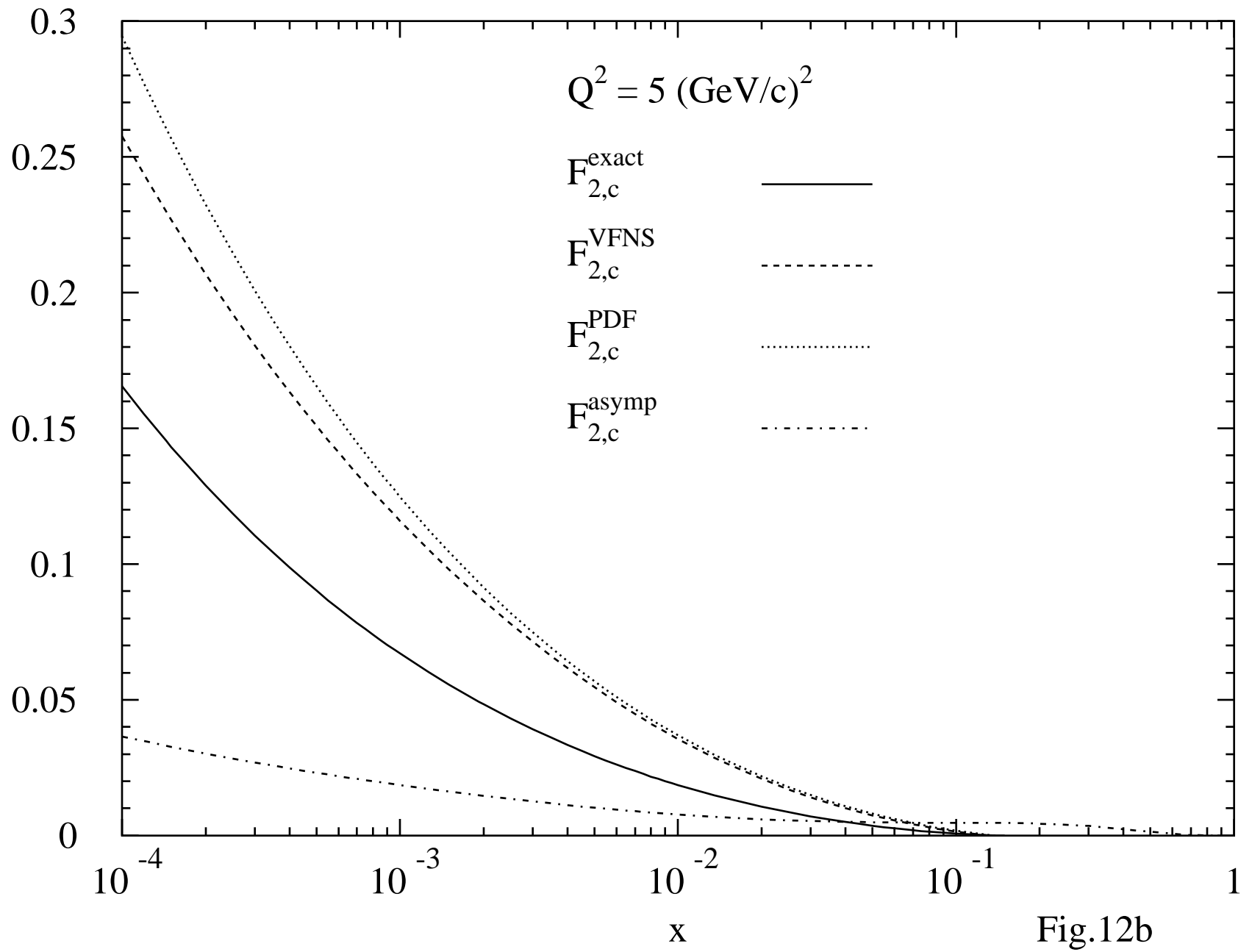


Fig.12b

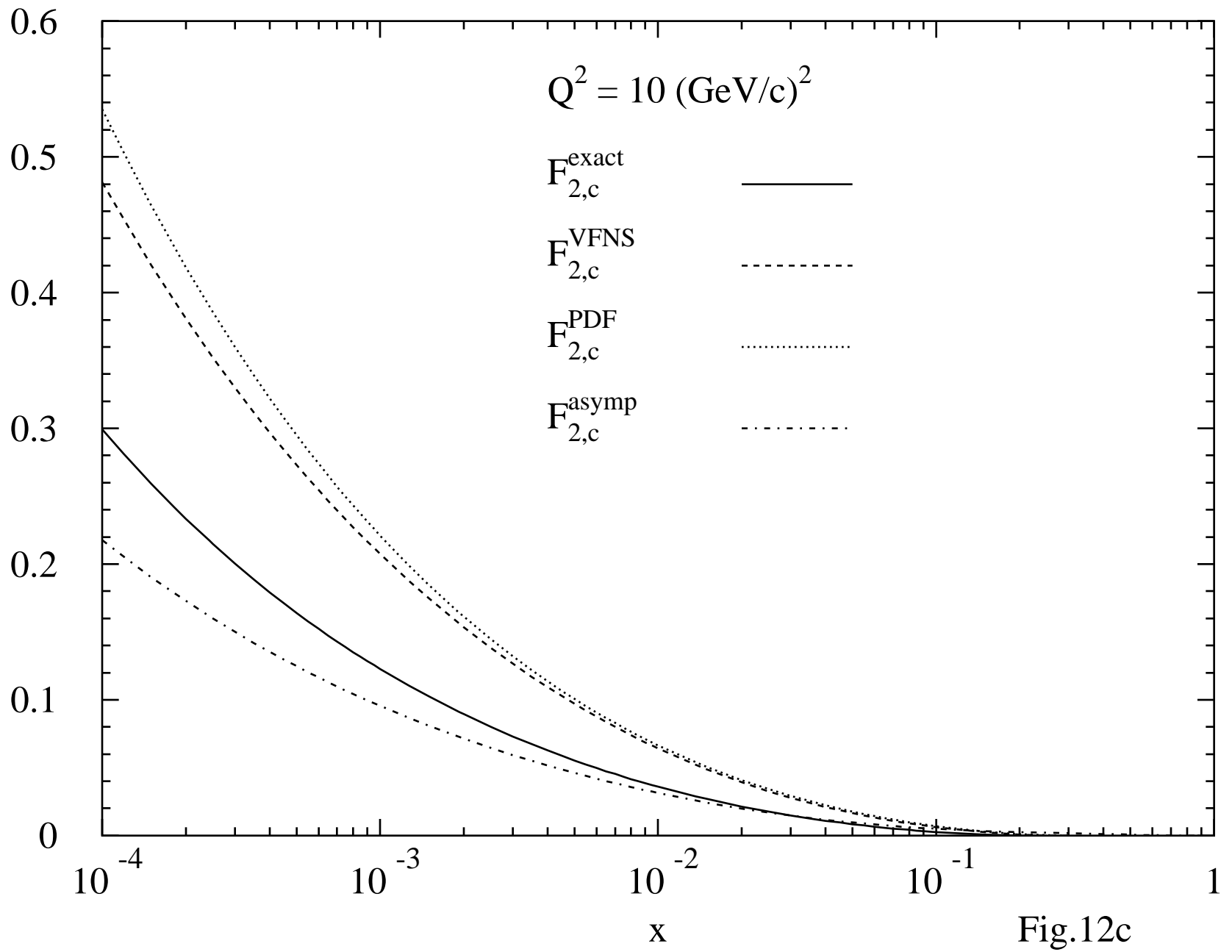


Fig.12c

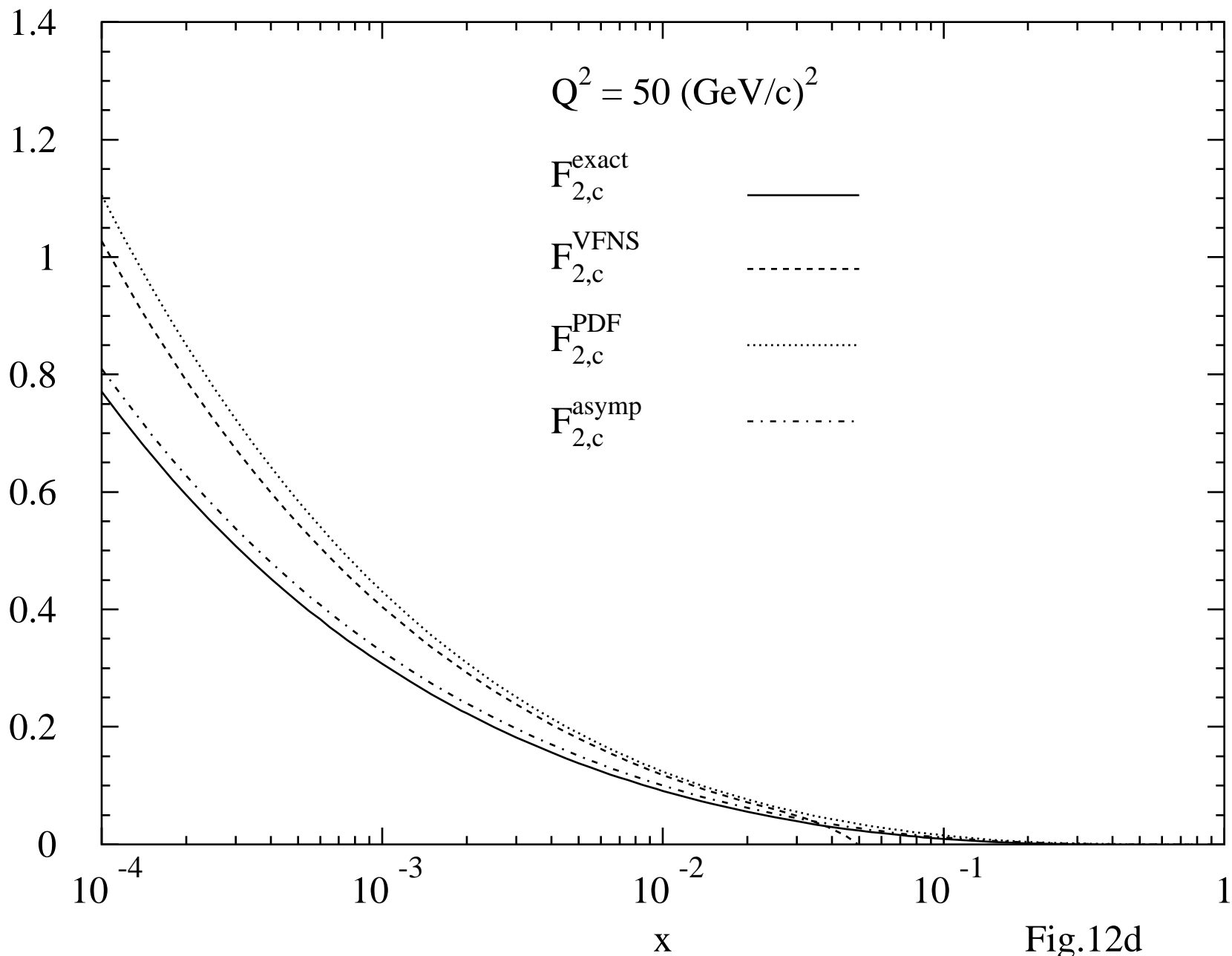


Fig.12d



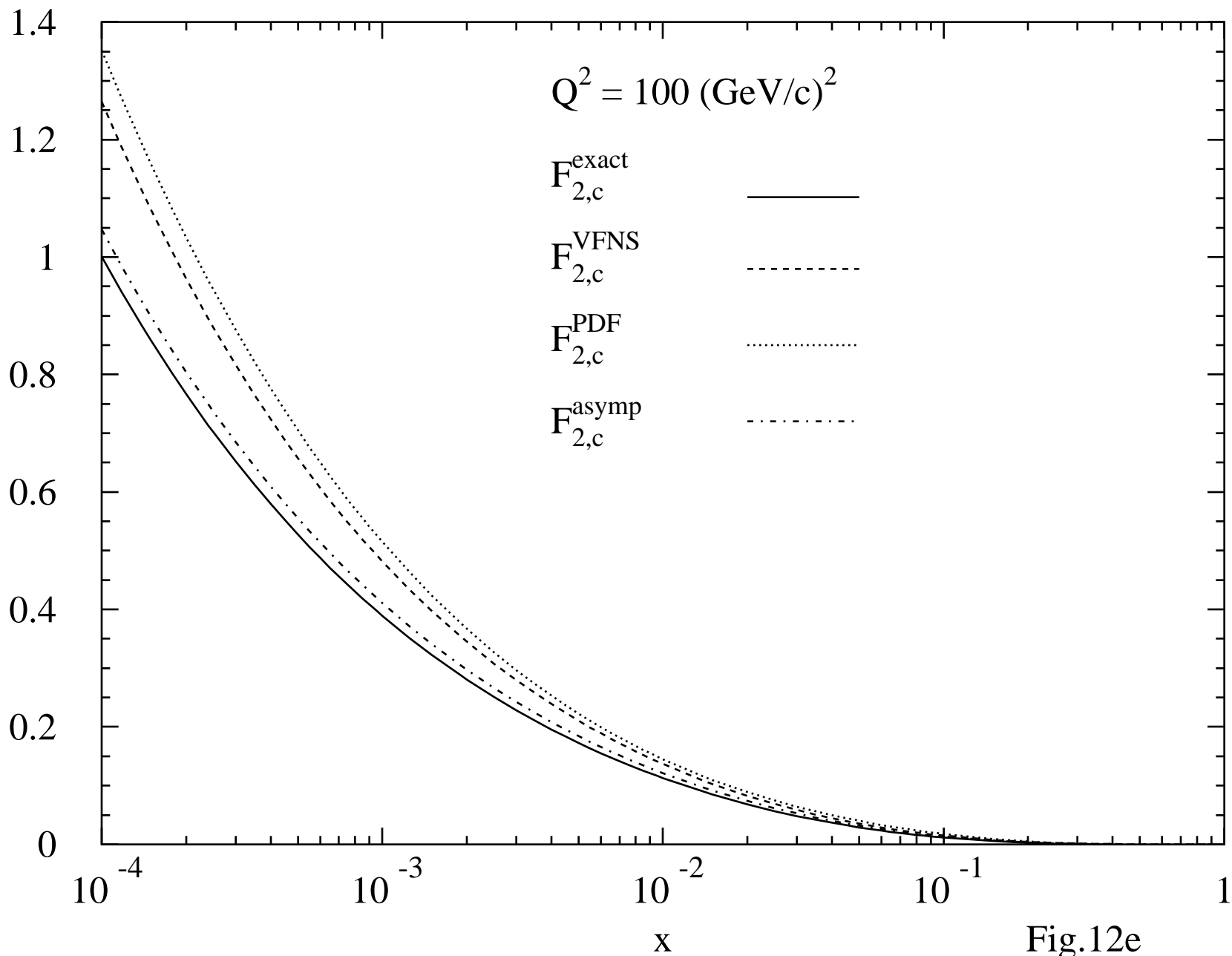


Fig.12e

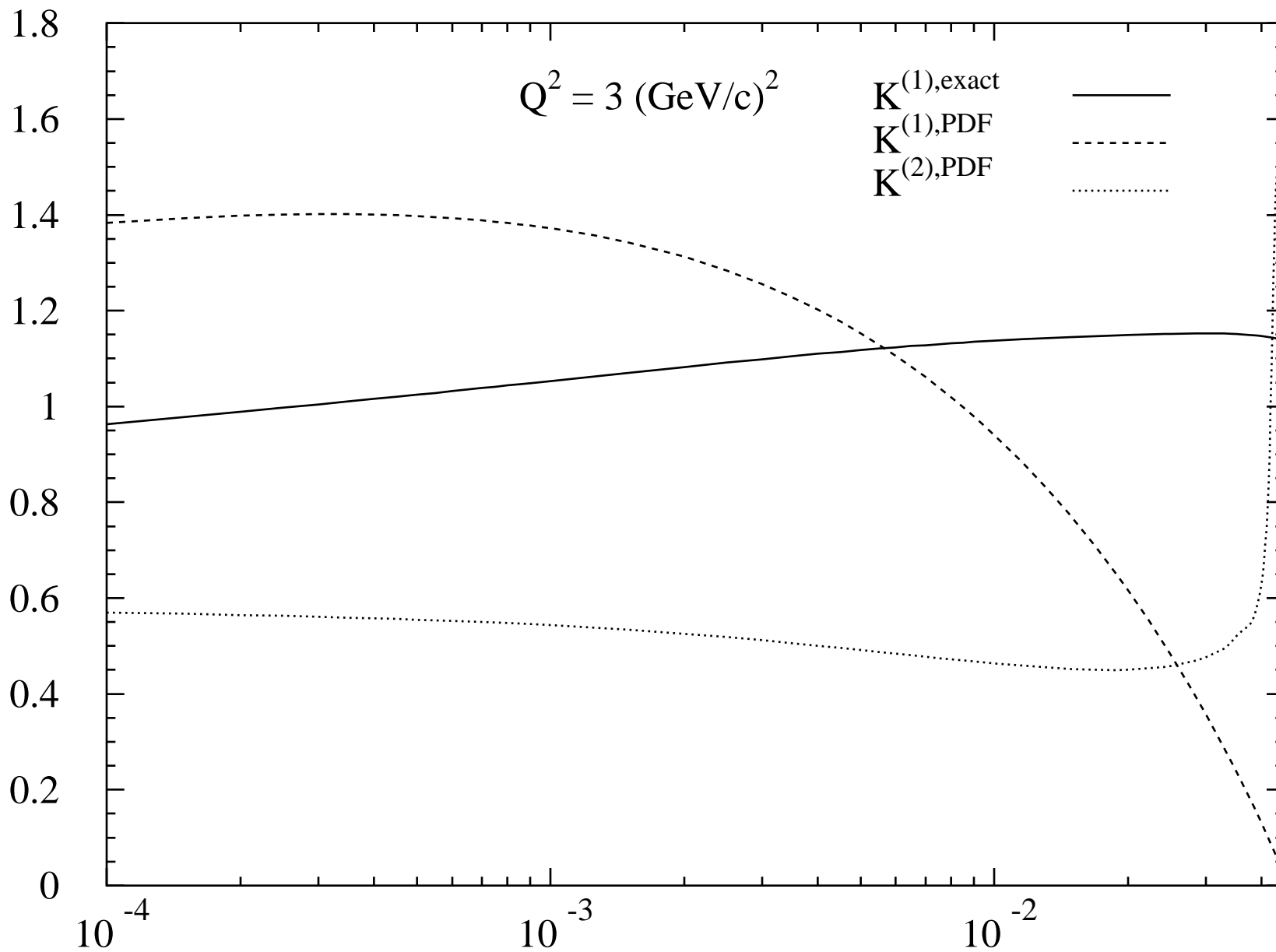


Fig.13a

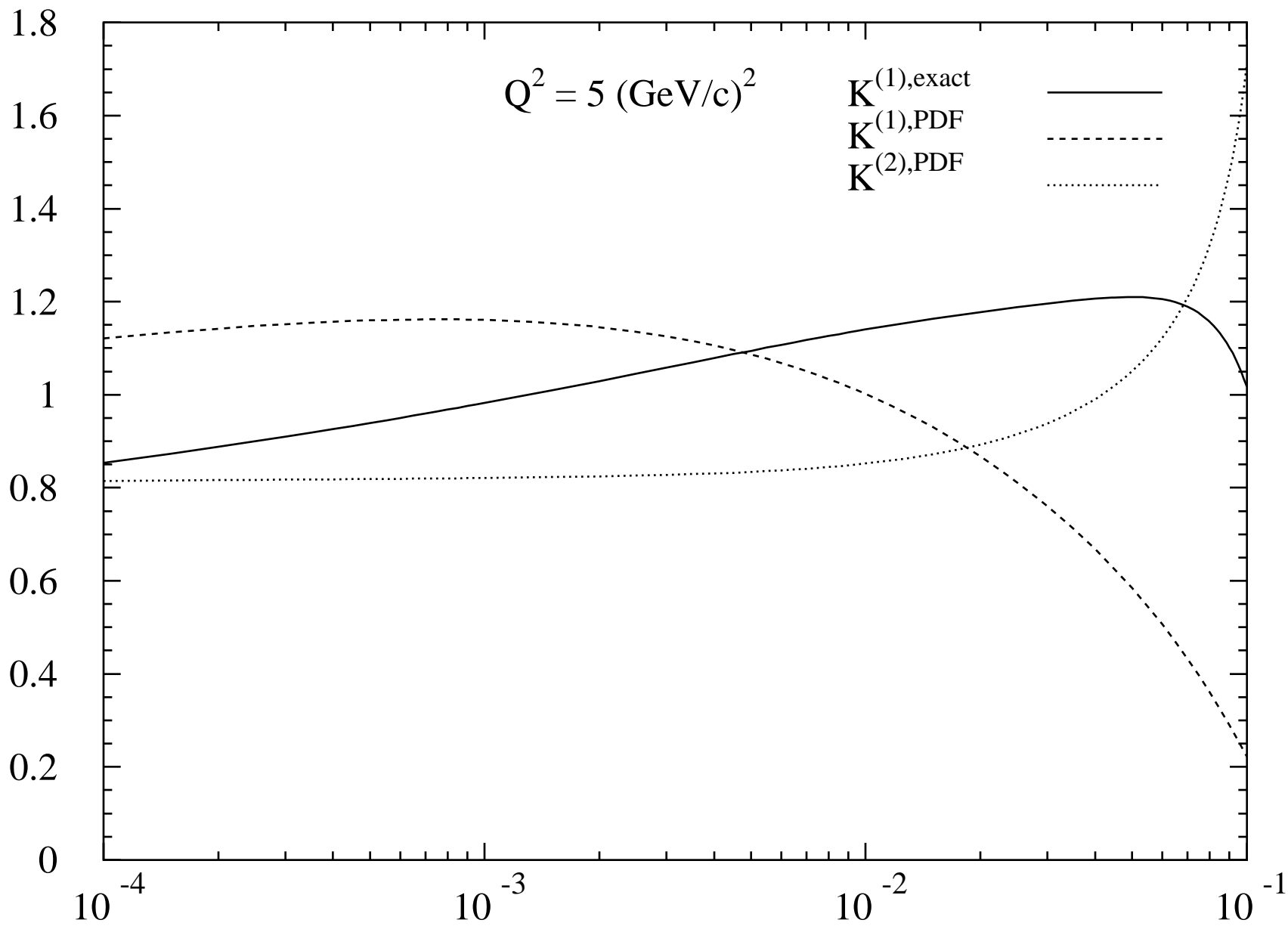
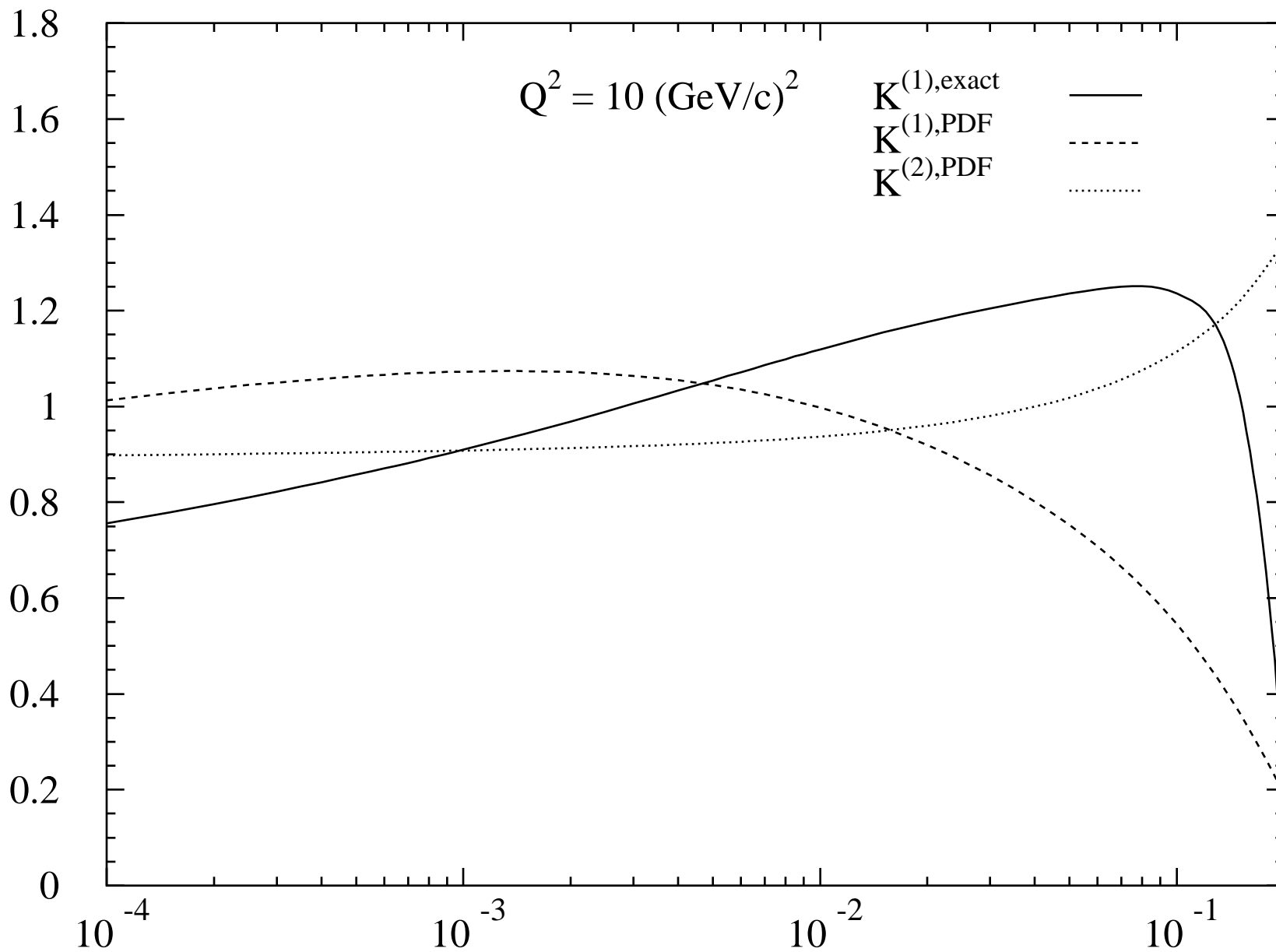
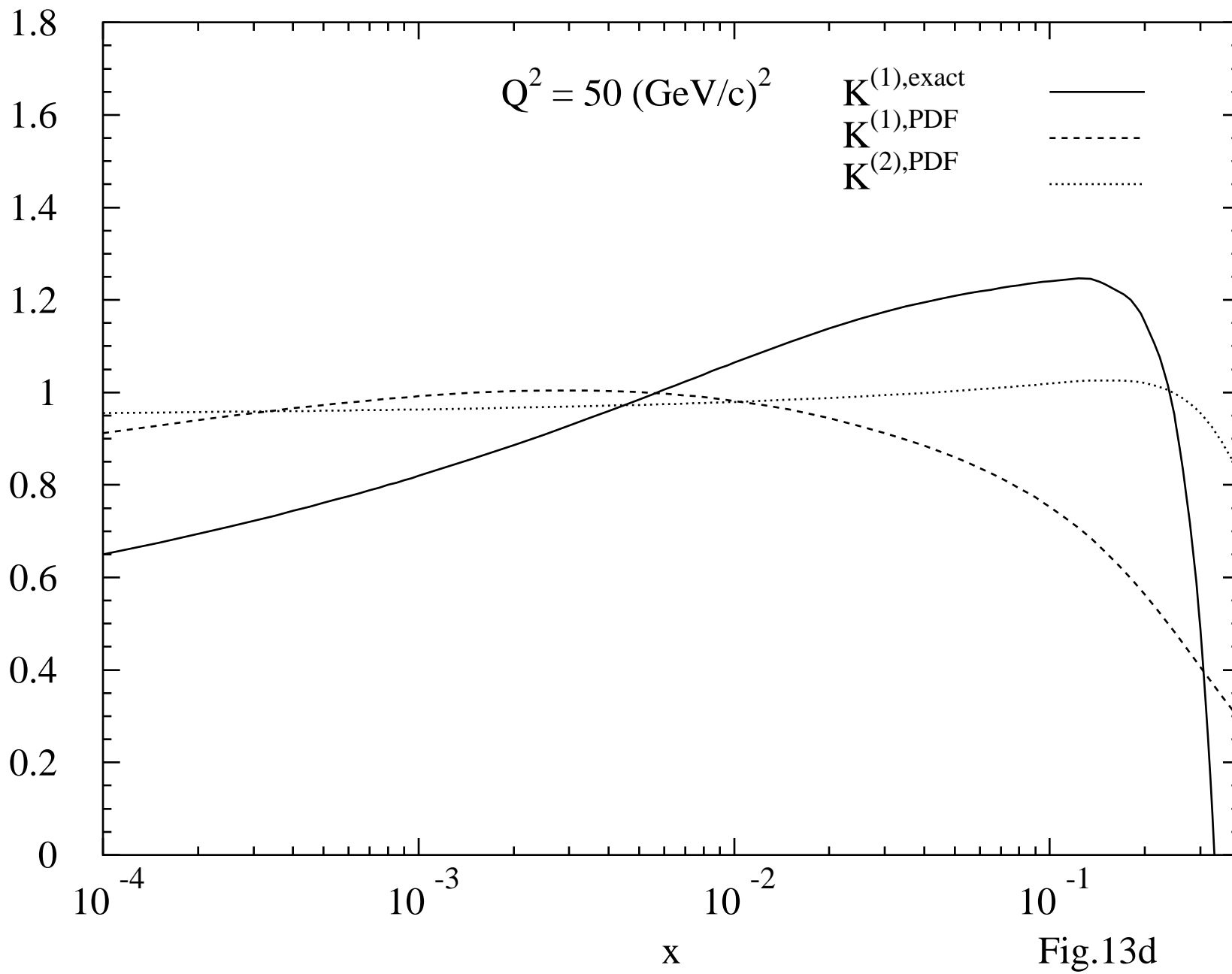


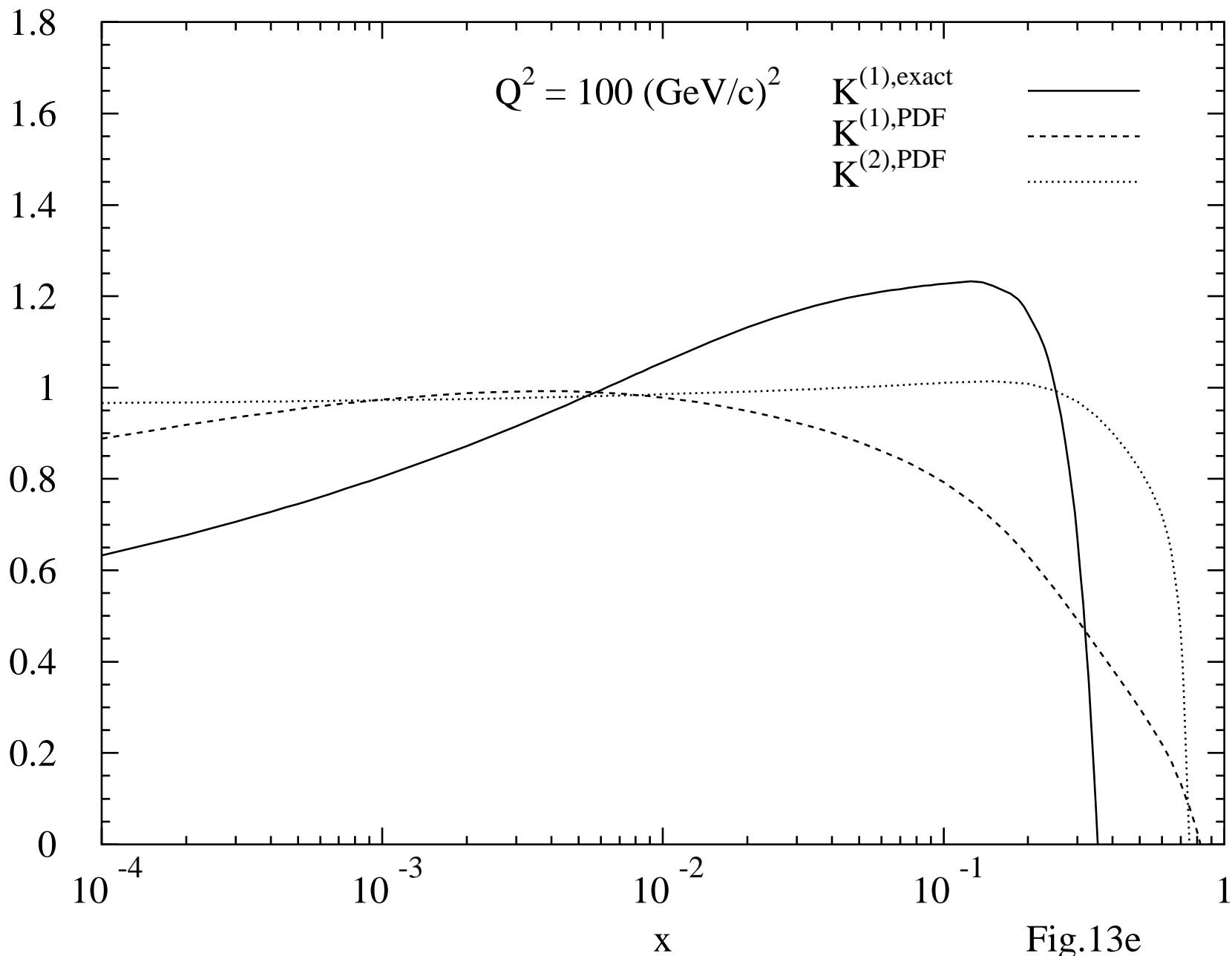
Fig.13b

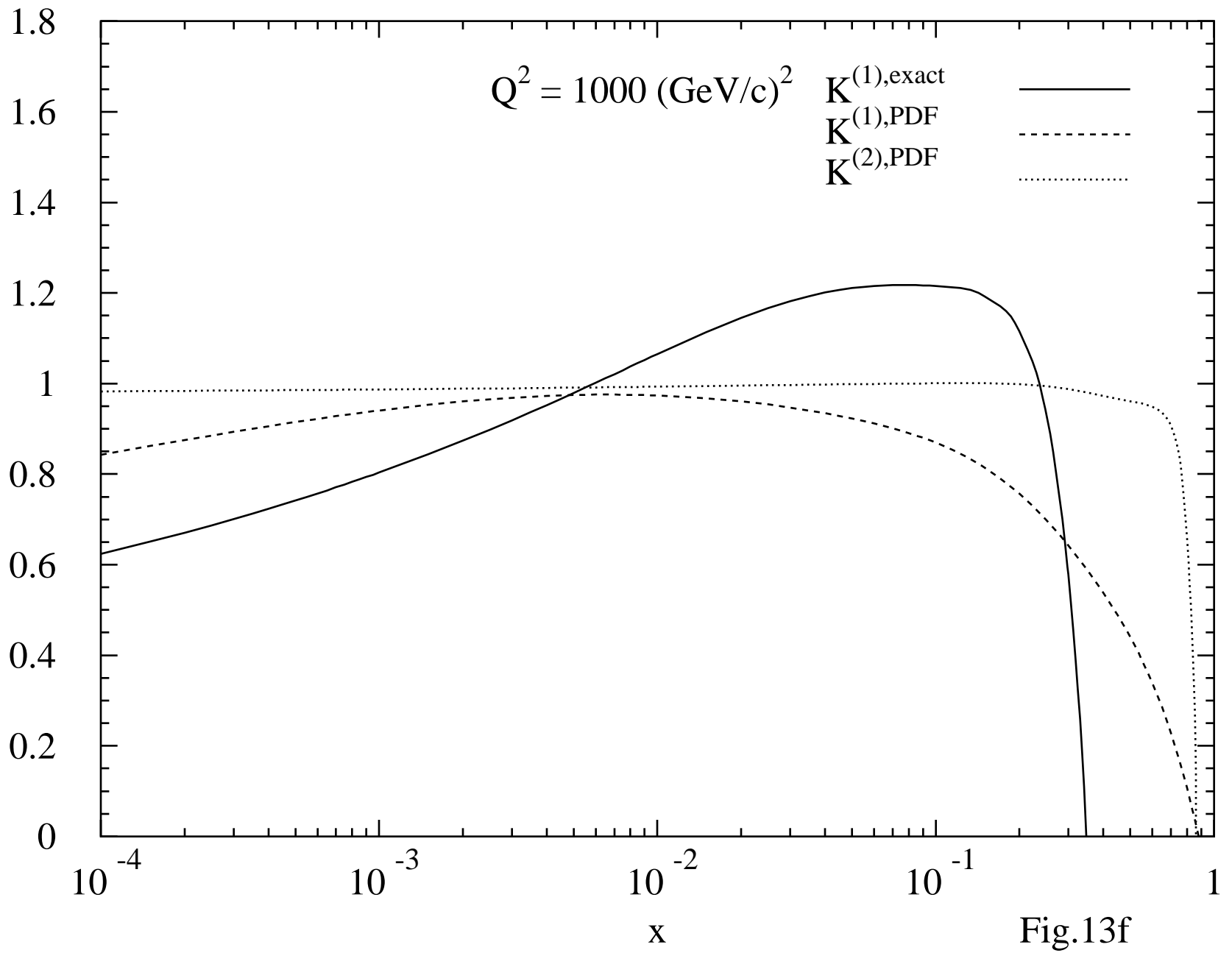


x

Fig.13c







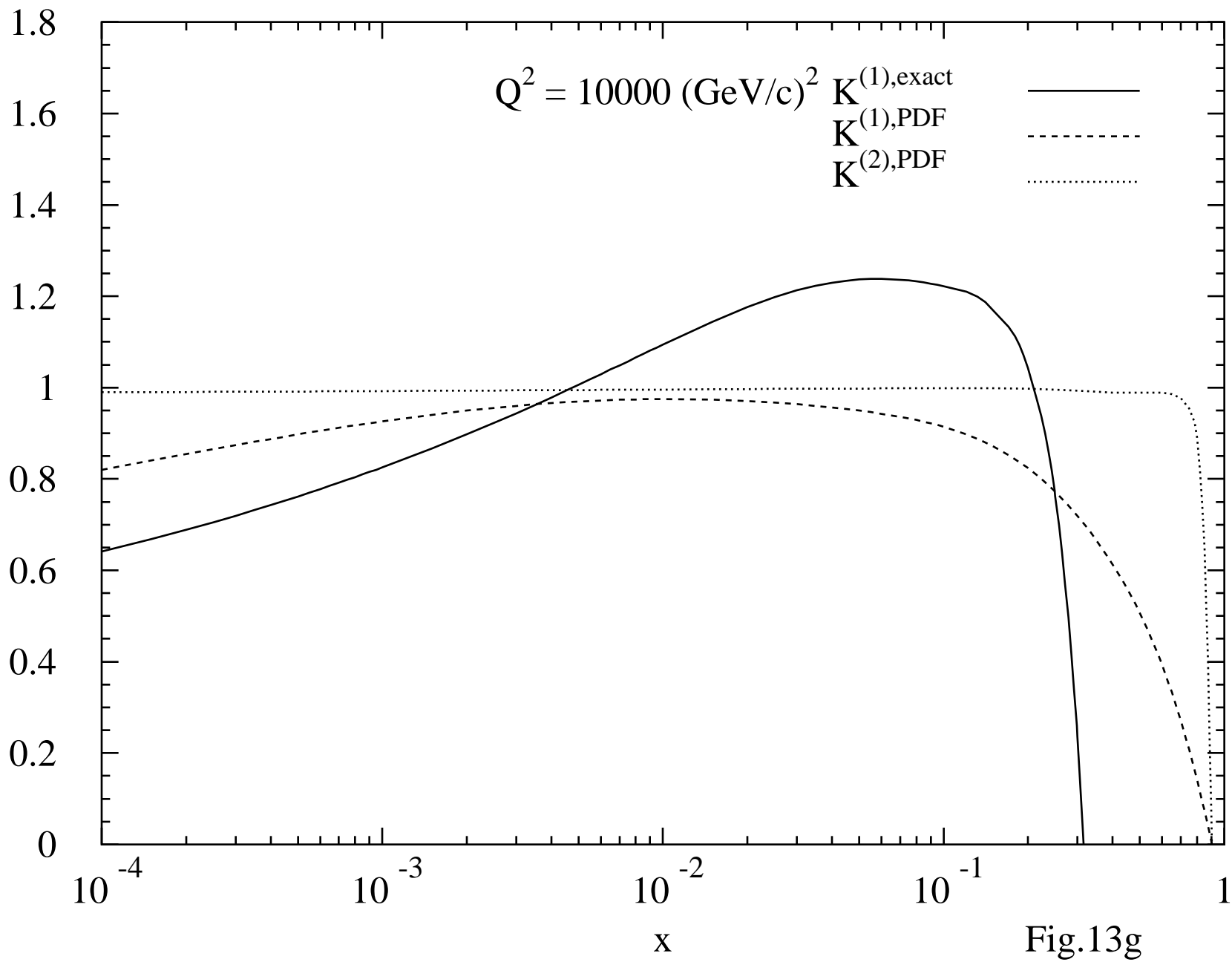


Fig.13g